University of Ioannina, Greece

Department of Physics

"Electrical and optical characterization of Organic LEDs with different Electron Transport Layers"

A Thesis submitted in partial satisfaction of the requirements

for the degree Master of Science

in

Physics with Specialization in Theoretical and Experimental Physics

by

Maskanaki Aikaterini

Supervisor: Assoc. Prof. E. K. Evangelou

Ioannina, 2024

Advisory Committee:

Assoc. Professor E. K. Evangelou (Supervisor)

Professor G. Evangelakis (member)

Professor A. Avgeropoulos (member)

The MSc Thesis is written in compliance with all the Rules of Ethics regarding the avoidance of plagiarism.

Prologue

This master's thesis was completed in the Department of Physics at the University of Ioannina in collaboration with the Institute of Nanoscience and Nanotechnology of the NCSR "Demokritos".

The most significant factor that led me to choose the field of Solid State Physics and Materials Physics is the direct connection of experimental research with the rapid technological development that defines our era. Research on systems already in use or expected to be utilized in the short term is feasible. Consequently, the need for their study is essential. Therefore, aiming at technological advancement, young scientists must combine knowledge and skills from various fields of study, such as solid-state physics, semiconductor physics, organic chemistry, surface physics, and condensed matter physics, etc. The continuous development of a field presupposes thorough study by the scientific community, the future of which lies in our hands.

At this point, I would like to thank all the people who contributed to the successful completion of this work. Firstly, I would like to thank Dr. E. K. Evangelou, Associate Professor of the Department of Physics at the University of Ioannina, for assigning the master's thesis, determining the subject of study, and supervising it throughout its development, as well as for all the knowledge and valuable advice provided. I would also like to thank Professors G. Evangelakis and A. Avgeropoulos, members of the advisory committee for their useful guidance and advice throughout this study.

Next, I would like to thank Dr. M. Vasilopoulou, Researcher A' at NCSR "Demokritos," as well as Dr. A. Soultati and Dr. A. Verykios for fabricating the organic samples studied in this work. Their contribution is of utmost importance, as they made this entire experimental study possible.

Furthermore, I would like to thank my fellow researchers in this study, for our excellent collaboration and all the laboratory members, especially Ms. D. Fotaki and Ms. E.I. Petridou. I would also like to thank Dr. G. Baldoumas and Dr. D. Katsanos for their assistance and support.

Finally, I would like to thank my family, who has supported me at every step throughout all these years.

Contents

Abstract

Organic Light Emitting Diodes (OLEDs) consist of one or more organic layers, polymer or not, which are placed between two electrodes; the anode (usually glass with a thin layer of Indium Tin Oxide, ITO, on top) and the cathode (a metal with low work function, e.g. aluminum). After applying voltage on the electrodes, electrons and holes are injected in the organic layer, and when they get close enough, they form an excited state, the exciton. The exciton's annihilation results in photon emission whose wavelength depends on the energy bandgap of the emissive layer (polymer, small organic molecule or transition metal complex). Choosing the right organic materials and constructing the diode properly are of highest importance in order to create high performance OLEDs.

The technology of constructing OLEDs has progressed a lot during the last years and, as a result, OLEDs are now commercially available by many companies. However, efficiency and stability of those organic LEDs depend on many factors, such as the properties of the used materials and their interfaces with the electrodes. Although the design of organic materials and the construction of efficient OLEDs have advanced, there has not been an equivalent evolution in modifying the interfaces between the electrodes and the organic layers, since the criteria of designing and modifying them remain unclear.

One of the key issues while designing electric contacts in organic optoelectronic devices is the proper band alignment of the energy layers in electrode/organic semiconductor interfaces. In order to achieve efficient charge carrier injection, it is vital to align the electrode's Fermi layer with the charge carrier transfer layers of the organic semiconductor. This is the main reason to include interlayers, thus constructing a multi-layer OLED, which modify the electrode/organic layer interfaces and achieve more efficient exchange of holes and electrons between the electrodes and the organic molecules.

Organic light emitting diodes (OLEDs) are attractive for display applications because of their high brightness, low driving voltage and tunable color. As a result, they are commonly used as a promising technology for solid state lighting and flat panel displays. However, the efficiency and stability of those OLEDs depend on many

factors, such as the properties of the used materials and their interfaces with the electrodes. In order to improve the performance of OLEDs it is vital to incorporate carrier transporting interlayers thus reducing the charge energy barrier at the selected electrode/organic emissive layer. Luminance is severely affected by operation time, as it degrades for reasons yet to be completely understood. An occurring explanation would be that electrical aged OLEDs have generated deep interface states and as a result the interfaces need more time to charge.

The aim of the present work is to study the electrical characteristics of OLEDs with different materials used as an Electron Transport Layer (ETL) and the effects of deep electron traps. Characteristic curves were obtained simultaneously on fresh or electrically stressed devices to investigate both the current conduction mechanisms as well as the evolution of deep electron traps that affect the turn on voltage and the overall quality of the tested OLEDs. Results show that incorporating an ETL improves the device characteristics and eliminates the generated electron traps.

Theoretical Part

1. A Brief History of OLEDs

Exploration of organic semiconductors and their applications started about 50 years ago. The first organic light-emitting diode (OLED) was reported by Williams and Schadt in the late 1960s using an anthracene crystal, structured electrodes and about 100 V as applied bias[1]. It was not until 1987, when the first efficient OLED was reported by Tang and Van Slyke using a bias of only a few volts and incorporated thin films from small molecule materials[2]. Meanwhile Heeger, MacDiarmid, and Shirakawa showed in the years 1977 and 1978 that the electrical conductivity of organic polymers can be increased by doping[3-5]. Eventually, these three scientists received the Nobel prize for chemistry in 2000[6] (interestingly, in the same year Kilby received the prize in physics for the invention of integrated circuits[7], another pioneering step for the electronic world were organic materials are used today). The first polymer OLED has been realized by Burroughes, Bradley, and Friend et al. in 1990[8]. In the meantime, also organic photovoltaic cells (OPVCs) have been fabricated; the first reported with an efficiency of about 1 % again was created by Tang even a year before he published the efficient OLED[9]. Tang's pioneering work started a cascade of studies on organic materials and their applications in OLEDs, OPVCs, and organic field effect transistors (OFETs). Thanks to, among others, advances in material development and processing, the usage of phosphorescent emitters[10], and the controlled doping of organic semiconductors[11,12], OLEDs have developed to very efficient and long living devices[13]. Today, a large number of products have already entered the consumer market in the range of small area displays in mp3-players, cameras, and mobile phones. The first larger OLED screens were already available (Sony XEL-1) while lighting panels are being sold for a few years now. The fast-growing field of organic solar cells has become more and more competitive due to a steady increase of device efficiencies[14-16]. Also, first devices have entered the consumer market in terms of flexible organic solar cells (Konarka). Furthermore, organic transistors[17], memory devices[18,19], and other electronic devices[20,21] have been demonstrated. The realization of an electrically pumped organic laser diode, however, still remains unaccomplished.

References

[1] D. F. Williams and M. Schadt. “A simple organic electroluminescent diode”. Proceedings of the IEEE 58(3) (1970) 476.

[2] C. W. Tang and S. A. VanSlyke. “Organic electroluminescent diodes”. Applied Physics Letters 51(12) (1987) 913–915.

[3] H. Shirakawa, E. J. Louis, A. G. MacDiarmid, C. K. Chiang, and A. J. Heeger. “Synthesis of electrically conducting organic polymers - halogen derivates of polyacetylene, (CH)x”. Journal of the Chemical Society - Chemical Communications 16 (1977) 578–580.

[4] C. K. Chiang, C. R. Fincher, Y. W. Park, A. J. Heeger, H. Shirakawa, E. J. Louis, S. C. Gau, and A. G. MacDiarmid. “Electrical conductivity in doped polyacetylene”. Physical Review Letters 39(17) (1977) 1098–1101.

[5] C. K. Chiang, M. A. Druy, S. C. Gau, A. J. Heeger, E. J. Louis, A. G. MacDiarmid, Y. W. Park, and H. Shirakawa. “Synthesis of highly conducting films of derivates of polyacetylene, (CH)x”. Journal of the American Chemical Society 100(3) (1978) 1013–1015.

[6] http://nobelprize.org/nobel prizes/chemistry/laureates/2000.

[7] http://nobelprize.org/nobel prizes/physics/laureates/2000.

[8] J. H. Burroughes, D. D. C. Bradley, A. R. Brown, R. N. Marks, K. Mackay, R. H. Friend, P. L. Burns, and A. B. Holmes. “Light-emitting diodes based on conjugated polymers”. Nature 347 (1990) 539–541.

[9] C. W. Tang. “Two-layer organic photovoltaic cell”. Applied Physics Letters 48 (1986) 183–185.

[10] M. A. Baldo, D. F. O’Brien, Y. You, A. Shoustikov, S. Sibley, M. E. Thompson, and S. R. Forrest: Highly efficient phosphorescent emission from organic electroluminescent devices. Nature 395, 151–154 (1998).

[11] J. Huang, M. Pfeiffer, A. Werner, J. Blochwitz, K. Leo, and S. Liu: Low voltage organic electroluminescent devices using pin structures. Applied Physics Letters 80, 139–141 (2002).

[12] M. Pfeiffer, K. Leo, X. Zhou, J. S. Huang, M. Hofmann, A. Werner, and J. Blochwitz-Nimoth: Doped organic semiconductors: Physics and application in light emitting diodes. Organic Electronics 4, 89–103 (2003).

[13] K. Walzer, B. Maennig, M. Pfeiffer, and K. Leo: Highly efficient organic devices based on electrically doped transport layers. Chemical reviews 107, 1233–1271 (2007).

[14] B. Kippelen and J.-L. Br´edas: Organic photovoltaics. Energy & Environmental Science 2, 241–332 (2009).

[15] G. Chidichimo and L. Filippelli: Organic Solar Cells: Problems and Perspectives. International Journal of Photoenergy 2010, 1–11 (2010).

[16] M. A. Green, K. Emery, Y. Hishikawa, and W. Warta: Solar cell efficiency tables (version 37). Progress in Photovoltaics: Research and Applications 19, 84–92 (2011).

[17] J. Zaumseil and H. Sirringhaus: Electron and ambipolar transport in organic field-effect transistors. Chemical reviews 107, 1296–1323 (2007).

[18] F. Lindner, K. Walzer, and K. Leo: Organic heterostructure device with nonvolatile memory behavior using electrically doped layers. Applied Physics Letters 93, 233305 (2008).

[19] P. Heremans, G. H. Gelinck, R. Müller, K.-J. Baeg, D.-Y. Kim, and Y.- Y. Noh: Polymer and Organic Nonvolatile Memory Devices. Chemistry of Materials 23, 341–358 (2011).

[20] K. Harada, A. G. Werner, M. Pfeiffer, C. J. Bloom, C. M. Elliott, and K. Leo: Organic Homojunction Diodes with a High Built-in Potential: Interpretation of the Current-Voltage Characteristics by a Generalized Einstein Relation. Physical Review Letters 94, 036601 (2005).

[21] H. Kleemann, R. Gutierrez, F. Lindner, S. Avdoshenko, P. D. Manrique, B. Lüssem, G. Cuniberti, and K. Leo: Organic Zener Diodes: Tunneling across the Gap in Organic Semiconductor Materials. Nano letters 4929– 4934 (2010).

2. Conducting and Semiconducting Polymers

2.1 Organic Semiconductors

In the realm of organic semiconductors, we delve into materials primarily constituted of hydrocarbons, potentially incorporating heteroatoms such as oxygen, nitrogen, and sulfur. These materials manifest properties akin to their inorganic counterparts, exhibiting both electrical conductivity and the absorption/emission of light. Classified into distinct categories[1], these organic solids unfold as follows:

A) Molecular materials: These materials feature amorphous films deposited onto appropriate substrates through methods like evaporation or spin-coating. Their practical applications are notably observed in light-emitting devices (LEDs).

B) Molecular crystals: Distinguished by a high degree of organizational structure, molecular crystals demand relatively thick films to achieve satisfactory morphology and mechanical stability. Although unsuitable for light-emitting diodes (LEDs), they prove valuable in devices where film thickness is subordinate to carrier mobility—a trait particularly pronounced in molecular crystals, exemplified by organic field-effect transistors (OFETs).

C) Polymeric films: Constituted by chains of homopolymerized molecular repeating units (monomers), polymeric films attract technological interest due to their deposition from a solution using cost-effective methods like spin-coating, inkjet printing, and roll-to-roll coating. Their extensive range of applications encompasses all organic electronic devices. Subsequent discourse will delve deeper into this specific category of organic semiconductors as part of our exploration in this master's thesis.

2.2 Conducting Polymers

Polymeric materials are molecules characterized by high molecular weight and composed of numerous repeating units known as monomers. A homopolymer consists of a single type of repeating unit, each connected via covalent bonds to two identical units, except for the polymer chain ends, which are linked to a single unit. Materials composed of different types of monomers are referred to as copolymers. Polymeric materials exhibit a broad spectrum of properties, rendering them suitable for various technological applications.

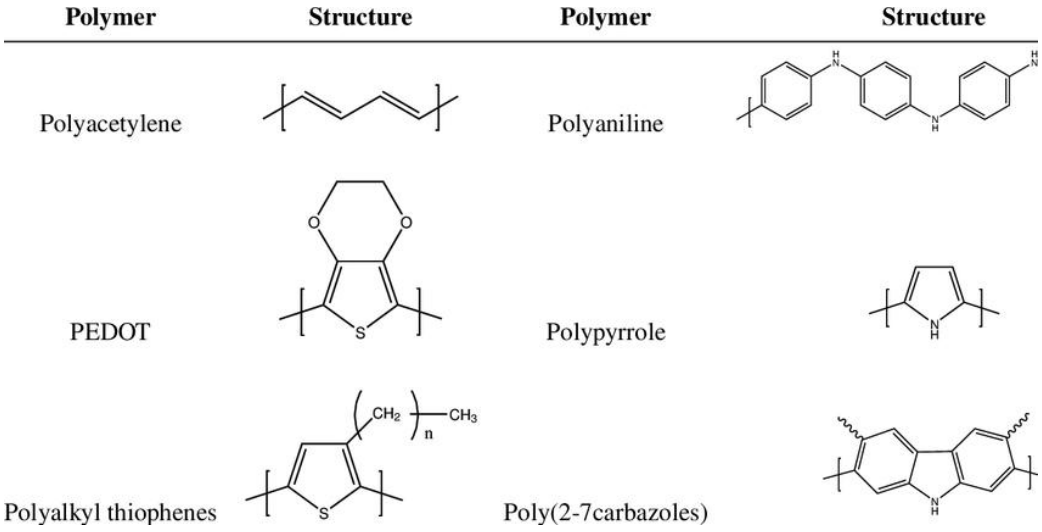

Image 1: Structures of conducting organic polymers.

Some of their key advantages include high resilience, cost-effectiveness in production, easy shaping, electrical and thermal conductivity, temperature-dependent property variations, and resistance to mechanical stress and deformation. Notable examples of polymers include plastics, DNA, and proteins. Conductive polymers represent a new generation of materials that combine the electrical properties of metals and semiconductors with the advantages of plastics. Furthermore, several polymers and polymer derivatives have been discovered, rendering them conductive through the addition of dopants. Generally, all of them consist of carbon and hydrogen atoms arranged in repeating monomeric units connected by homopolar bonds, forming polymer chains. Some repeating units incorporate nitrogen, sulfur, or halogen atoms along with carbon and hydrogen.

2.3 Types of Conducting Polymers

In exploring conductive polymers, we categorize them into four fundamental types, each exhibiting distinct properties and applications. These classifications shed light on the diverse range of conductive materials and their significance in various technological realms. Let's delve into each category for a comprehensive understanding of their characteristics and functionalities.

A) Filled Polymers: Filled polymers become conductive by incorporating materials like graphite, carbon black, metal particles, or metal oxides directly into the polymer matrix. These materials consist of three fundamental components: the polymer matrix, the filler, and the interconnect. Despite challenges such as low reproducibility, complex processing, abrupt conductivity thresholds, and low dielectric constants, they are widely used in electronic devices. Rigorous control over their dispersion is essential for homogeneous synthesis before application.

B) Ionically Conducting Polymers: Also known as ionomers or polymeric electrolytes, these polymers achieve conductivity through ion transport. While they offer easy availability and processing, they are sensitive to humidity, affecting their conductivity. Widely applied in electronic devices like rechargeable batteries, polymeric light-emitting devices, and fuel cells, their functionality relies on the release, transport, and binding of ions within the polymer structure.

C) Conjugated Polymers: Conjugated polymers are organic macromolecules characterized by a strong chain of alternating single or double bonds. Their high conductivity levels are achieved through the doping process. Due to their unique structure, they exhibit intriguing optical and electromagnetic properties, making them suitable for applications such as light-emitting diodes (LEDs), plastic electronics, corrosion protection for metals, sensors, and nonlinear optical devices. However, their structure can make them fragile and sensitive under ambient conditions.

D) Charge Transport Polymers: These polymers derive their conductivity from charge transport. Most in this category are p-type, and their conductivity arises from aggregates formed between electron donor and acceptor moieties, enabling partial charge transfer. Despite possessing a crystalline structure for optimal conductivity,

these materials are often challenging to handle due to their fragility. Efforts have been made to attach donor and acceptor groups to the polymer backbone, producing easily processable polymers with improved chemical properties. Widely used in electrophotographic receivers, they, along with conjugated polymers, constitute the two most significant categories of semiconducting organic materials.

2.4 Electrical Conductivity of Polymers

The classification of solids into good and poor conductors, or insulators, is based on their ability to conduct electric current. Good conductors include metals, which facilitate the flow of current with ease, and semiconductors. Electrical conductivity results from the movement of electrons within a material and is determined by the number of electrons in the outermost shell. These valence electrons, responsible for the material's electrical, magnetic, and optical properties, exhibit weak binding forces.

In metals, valence electrons move freely within the crystalline lattice. In contrast, semiconductors and insulators retain strong atomic bonds, resulting in significantly higher specific electrical resistance. The categorization of solids into metals, semiconductors, and insulators reveals the prevailing conditions in the occupied highest energy bands. The uppermost band, where electrons move freely, is termed the conduction band, while the one immediately below it is known as the valence band.

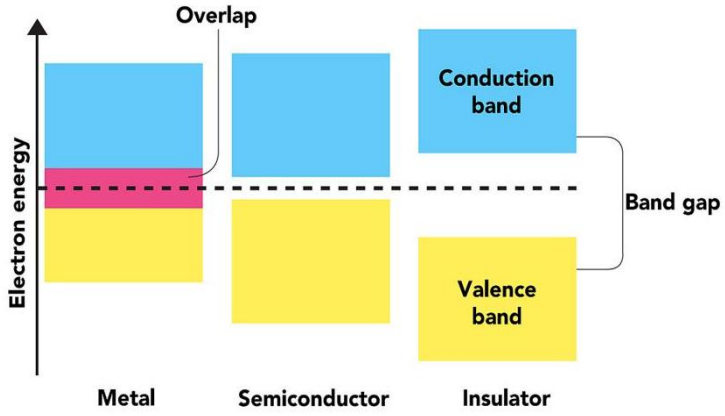

Image 2: Energy diagram for metal, semiconductor, and insulator.

Specifically, as illustrated in Image 2, a solid behaves as an insulator if it has such a number of electrons that all allowed energy bands are either fully occupied or completely "empty" of electrons. Consequently, when an electric field is applied, there are no “free” electrons available to move. In contrast, a solid behaves as a metal if it contains one or more energy bands that are partially occupied/filled by electrons. Finally, a solid exhibits semiconducting behavior if all its bands are almost fully occupied, i.e., one or two bands are slightly "empty" of electrons. In insulators, the energy gap between the upper stations is very large (on the order of 10 eV), while in semiconductors, it is very small, allowing it to be overcome by thermal excitation of electrons.

The electrical conductivity of polymers results from the creation of energy bands similar to those in inorganic systems. In other words, for a polymer to be electrically conductive, its electrons must move freely without being bound to the atoms. A necessary condition for this is the presence of alternating single and double bonds (conjugated double bonds). The electronic structure of all organic semiconductors is described by conjugated π-electrons. A conjugated organic structure is, as mentioned earlier, based on alternating single and double bonds between carbon atoms forming a carbon chain. The single bonds are commonly known as σ-bonds, while the double bonds consist of a σ-bond and a π-bond. π-electrons are much more mobile than σ-

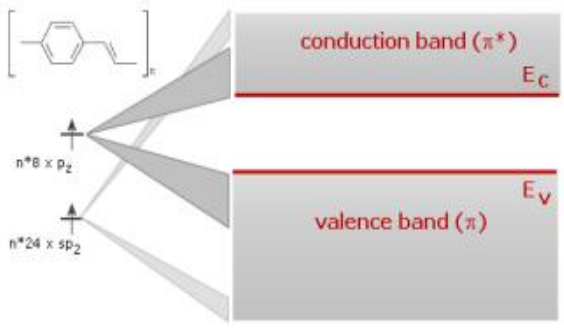

Image 3: Formation of π and π* orbitals in polymers.

electrons and have the ability to migrate between carbon atoms due to the overlap of π-orbitals. The overlap of p_z orbitals separates them, resulting in the existence of two "new" orbitals: a lower-energy bonding π-orbital (π-bond) and a higher-energy antibonding π-orbital (π*-bond), as illustrated in Image 3. Analogous to the valence and conduction bands in inorganic semiconductors, it is observed in organic

semiconductors that the occupied π-band corresponds to the Highest Occupied Molecular Orbital (HOMO), and the unoccupied π*-band corresponds to the Lowest Unoccupied Molecular Orbital (LUMO) of the polymer[2].

As the overlap between adjacent p_z orbitals and the number of electrons participating in the π-system increase, the widths of the bands broaden, and the energy gap (E_g) between them decreases. π-electron systems possess all the necessary characteristics and properties required for photovoltaic applications, such as the generation and transport of electric charges, and the ability to conduct electrical current and absorb light, both in the visible and ultraviolet spectra of solar radiation.

A crucial criterion for selecting a potentially conductive polymer is how easily it can be oxidized or reduced along its chain. Conjugated polymers become conductive due to the presence of unsaturated π-bonds along their chains. These unsaturated bonds can easily lose or gain an electron, transforming the chain into a polymeric ion. Saturated σ-bonds are hardly affected, maintaining the polymer's structure and being responsible for its mechanical properties.

An intriguing characteristic of conductive polymers is that the oxidation or reduction of their chain is accompanied by the disturbance of the chemical bonds surrounding the resulting hole or extra electron from the doping. These disturbances are responsible for the appearance of additional energy states within the energy gap (Image 4), affecting the optical and magnetic properties of the polymer.

Despite this, the presence of extensive conjugation in these molecules does not directly imply their electrical conductivity, as the energy gap is usually greater than 1.5-2 eV, making thermal excitation of electrons in the vacant orbitals impossible (note that $kT \approx 0.026$ eV at room temperature). This means that these materials are initially semiconductors or insulators, but they can easily become conductors once carriers are introduced into them, or through some form of doping. In that case, extensive conjugation allows for the rapid movement of carriers along the chain and between chains, resulting in three-dimensional mobility and rendering them practically conductive. The mobility of carriers is generally limited by the disorder of the material, which is why molecular crystals with a high degree of organization exhibit much higher mobilities than polymeric materials.

Doping of the conjugated polymers can occur through (a) chemical means, (b) electrochemical means, (c) optical excitation (photon absorption), or (d) electrical excitation (direct injection of electrons/holes from electrodes)[3]. Doping introduces mobile carriers into the π-system. For relatively low levels of doping, charges are localized and give rise to non-linear excitations (solitons, polarons, bipolarons), which are consequences of the electrostatic interactions of charges both among themselves and with the lattice. These excitations are directly dependent on the geometry of the material. Thus, we can distinguish two fundamental cases for the ground state accompanied by corresponding excitations[4-8]:

1) Doubly Degenerate: Doubly degenerate refers to a polymer composed of two isoenergetic and perfectly equivalent isomeric forms, with the characteristic example being trans-polyacetylene. The excitations can be:

- Solitons: Topological excitations representing a segment of the polymer that separates one isomeric structure from another and can extend up to 14 structural units. Solitons are non-linear excitations that move freely and are created or annihilated in pairs. They are spectroscopically characterized by a new state in the middle of the energy gap and exhibit an inverse spin-charge relationship compared to electrons and holes.

- Polarons: Non-topological excitations resulting from the injection of an electron or hole, equivalent to a bound pair of soliton-antisoliton (a neutral and a charged soliton). They are spectroscopically characterized by two new states in the energy gap, equidistant from the Fermi level (bonding and antibonding states within the gap corresponding to the bound pair of soliton and antisoliton forming the polaron), while the spin-charge relationship for polarons is the same as that for electrons and holes.

- Bipolarons: Arise from adding a second electron or a second hole to the lattice but are not stable when the ground state is degenerate, breaking into pairs of negatively or positively charged solitons. Charge transfer in these polymers occurs through electron hopping between soliton states in the middle of the gap (intersoliton hopping), making conductivity significantly increase with the proper

arrangement of polymer chains during synthesis due to the topological constraint of solitons.

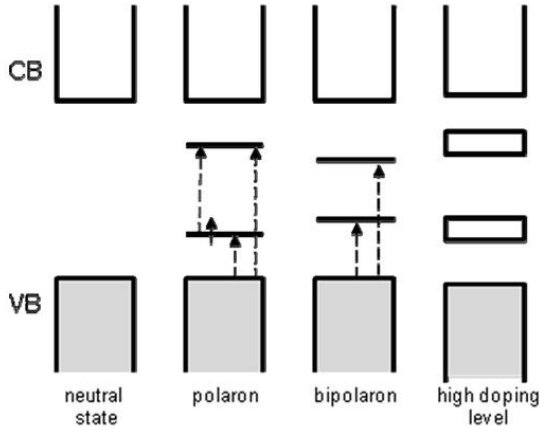

Image 4: Energy diagram for doubly degenerate polymers.

2) Non-degenerate: Non-degenerate refers to polymers with two isomeric forms having slightly different energies. Characteristic examples include polyphenylene and polythiophene, where the aromatic structure is more stable than the helical one. In this case, the energy gap arises not only from Peierls instability but also from the dynamics of a single electron (contributions also from the σ electrons). Excitations in these polymers do not take the form of solitons; due to the absence of degeneracy, soliton-antisoliton pairs are more localized and form bipolarons or polarons. Charge transfer occurs through electron hopping from low-energy polaronic states to corresponding higher-energy states within the gap. Due to the absence of topological constraints in polarons and bipolarons, the transfer of charge between chains (three-dimensional transport) is feasible.

It is worth mentioning that the ability for reversible doping also plays a significant role in the conductivity of polymers, stemming from weak interactions between macromolecular chains. Consequently, diffusion of molecules in the blend is allowed, and the robust forces constituting each chain ensure the integrity of the polymer, ensuring the reversibility of the addition of dopants. Therefore, it is possible to increase or decrease the percentage of additives in a polymer sample through chemical or electrochemical methods without needing to destroy or reconstruct the material. The electrical conductivity of most semiconducting polymers ranges from

10^{-1} to 10^{5} S/cm. This broad conductivity range depends on the production process and the degree of oxidation or reduction.

2.5 Applications of Conductive Polymers

The wide range of properties and ease of processing of conductive polymers make them suitable for use in a broad spectrum of applications. Due to their low density and mechanical flexibility, these materials can be employed in various electronic, optoelectronic, and electrochemical applications. Specifically, they can serve as conductive elements for absorbing ultraviolet rays in microelectronics and in fluorescent and electrochromic devices when the redox process is accompanied by absorption in the optical spectrum.

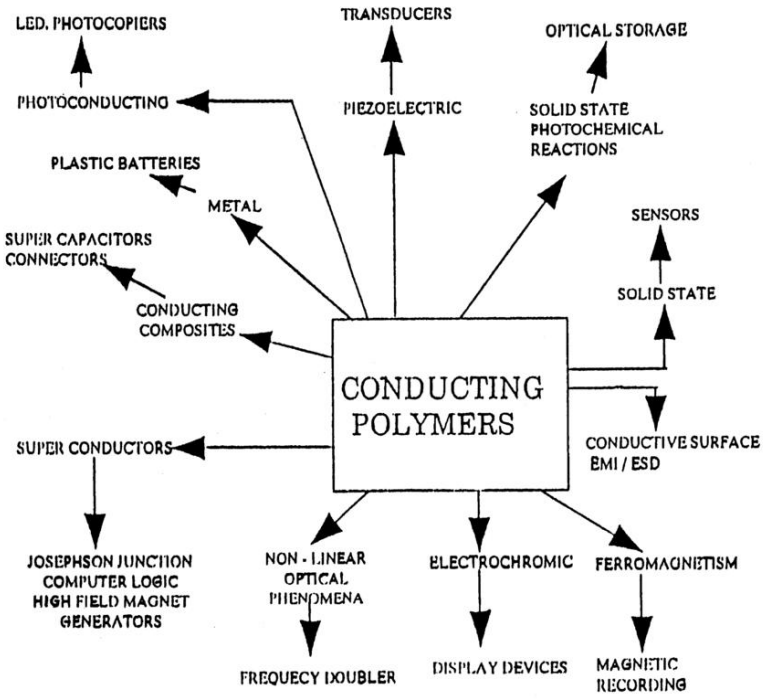

Image 5: Various applications of conducting polymers.

Conductive polymers can also be utilized as membranes due to their porous nature and as ion exchangers owing to their selectivity for certain ions. Furthermore, they can be deposited as protective coatings against corrosion, replacing traditional chromate coatings that are toxic, with environmentally friendly materials promoting

human health. Lastly, they find applications in gas, chemical, biochemical, or thermal detectors, as well as in rechargeable batteries.

References

[1] A. Köhler and H. Bässler, Materials Science & Engineering R-Reports 66, 71 (2009).

[2] P. Argitis, "Πολυμερή στη Μικροηλεκτρονική", (2003).

[3] A. G. MacDiarmid, Reviews of Modern Physics 73, 701 (2001).4.

[4] A. Brazovskii and N. N. Kirova, JETP Letters 33, 4 (1981).

[5] J. L. Bredas, R. R. Chance, and R. Silbey, Physical Review B 26, 5843 (1982)

[6] J. L. Bredas, B. Themans, J. G. Fripiat, J. M. Andre, and R. R. Chance, Physical Review B 29, 6761 (1984).

[7] A. J. Heeger, S. Kivelson, J. R. Schrieffer, and W. P. Su, Reviews of Modern Physics 60, 781 (1988).

[8] A. J. Heeger, Reviews of Modern Physics 73, 681 (2001).

3. Organic Light Emitting Diodes

3.1 What is an OLED?

The Organic Light Emitting Diode (OLED) is a device that converts electrical energy into light. In contrast to common incandescent bulbs, where light is emitted by passing an electric current through a tungsten filament (thermionic emission) or fluorescent lamps, where the electric current passes through a gas (usually noble gases like neon, argon, krypton, xenon, or low-pressure mercury vapor), OLEDs generate light from the current passing through one or more thin organic layers. Concerning inorganic Light Emitting Diodes (LEDs), they differ from organic ones in terms of materials, construction methods, emitted light type, and their potential applications. Specifically, inorganic LEDs are based on the inorganic semiconductors of groups III-V, such as GaAs, GaN, GaAsP, etc., and usually require relatively energy-intensive and expensive manufacturing processes (using robotic systems and one-by-one placement of electrical contacts). They are point sources of high-brightness light with beam alignment capabilities, finding applications in flat screens, signage, and lighting. On the other hand, organic LEDs are based on small organic molecules or polymeric materials, which can be deposited on glass or polymeric -thus flexible- substrates either from a solution using methods like inkjet printing or from solid material in powder form through vacuum evaporation. They emit diffuse light, with the ability to emit in many different colors, including white light, expanding their application field beyond screens to lighting products[1,2].

The multitude of advantages presented by OLEDs (Table 1), both compared to inorganic LEDs and other devices predominantly used in screens (liquid crystals, Liquid Crystal Displays - LCDs), as well as for small and large area lighting (compared to incandescent lamps and fluorescent lamps), make OLEDs a highly competitive technology expected to play a leading role in the global market in the coming years. The specifications for OLEDs vary depending on the application.

Table 1: Advantages of OLED-based displays compared to conventional LCDs.

• Lower energy consumption
• Faster rate of image refreshing (order of μs)
• Greater contrast (up to 2,000,000 :1)
• Greater brightness
• Maximum possible viewing angle
• Ability to manufacture new types of screens (superthin, flexible, transparent)
• Greater thermal resistance (they function in bigger temperature range)
• Very light weighted (they can be printed on thin surfaces)

While a long lifetime of the diode (40,000-50,000 hours) is desirable for economic reasons, as well as the high-power efficiency (60-80 lm/W), which ensures low energy consumption, the required brightness varies significantly, for example, for use on a computer screen (100 cd/m^2) and for space lighting applications (1,000-100,000 cd/m^2). Additionally, in lighting fixtures, high resolution is not required as in screen pixels, but homogeneous illumination of the illuminated surface is needed. Further material development and optimization of arrangements to achieve higher performance and longer life, as well as reducing the deposition and manufacturing costs of OLEDs in the coming years, are expected to drive the wider commercialization of related products. Despite the numerous advantages and applications of OLEDs in everyday electronic devices, they still have some drawbacks. Specifically, the lifespan of devices emitting wavelengths near the ultraviolet spectrum is quite limited (approximately 14,000 hours), unlike devices emitting near red or green, which have much longer lifespans (60,000 to 225,000 hours of

operation). Additionally, the manufacturing processes of OLEDs are costly, and finally, OLEDs are highly sensitive to water and can be easily damaged by it[3-10].

3.2 Principles of Operation of Organic Light-Emitting Diodes (OLEDs)

The simplest structure of an organic light-emitting diode consists of a thin organic layer, serving as the emissive layer of the device, deposited between two electrodes, the anode and the cathode. When a potential difference is applied to the two electrodes, electrons and holes are injected into the organic emissive layer from the cathode and anode, respectively. A polymer LED is, therefore, a charge carrier double-injection device. Electrons are injected from the cathode and transported to the LUMO level of the organic layer, while holes are injected from the anode of the device and transported to the HOMO level of the organic semiconductor. The recombination of these carriers leads to the emission of radiation[11-13].

The intricacies of charge carrier injection within organic light-emitting diodes (OLEDs) are pivotal to their operational dynamics. This process is closely tied to the energy barrier existing at the interface between the electrode and the organic material. Upon the application of a potential difference across the anode and cathode, electrons are injected from the cathode, while holes are injected from the anode. The subsequent transport of these injected charge carriers within the organic layer is a critical step toward their recombination and subsequent light emission. This journey is significantly influenced by the mobility of carriers within the organic material. Notably, the mobility of carriers in organic materials tends to be comparatively lower

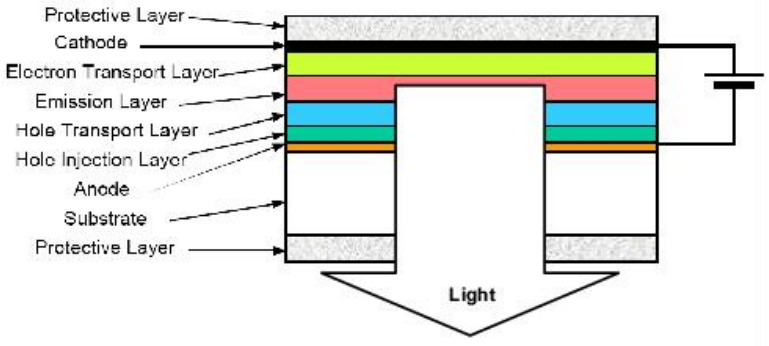

Image 6: Schematic representation of a typical structure of an organic light-emitting diode (OLED).

than in their inorganic counterparts, potentially impacting the efficiency of exciton generation and overall OLED performance[14,15].

An intriguing observation is the inherent imbalance of carriers within the organic layer. The mobility of holes, as positively charged carriers, is lower compared to that of electrons, the negatively charged carriers. This intrinsic imbalance may result in a non-uniform distribution of carriers within the organic layer, thereby influencing the recombination dynamics. Furthermore, two principal mechanisms governing charge carrier injection are introduced—tunneling injection and thermionic emission. Tunneling injection involves carriers traversing the energy barrier through a quantum tunneling process, while thermionic emission entails carriers overcoming the energy barrier through thermal excitation. These mechanisms constitute foundational elements for comprehending the intricate pathways that charge carriers navigate within the OLED structure[16,17].

3.3 Characterization Parameters of OLEDs

Parameters crucial for the comprehensive characterization of an OLED include the following:

1) Luminance (L) - [cd/m²]:

Luminance refers to the intensity of emitted light from a source in relation to the

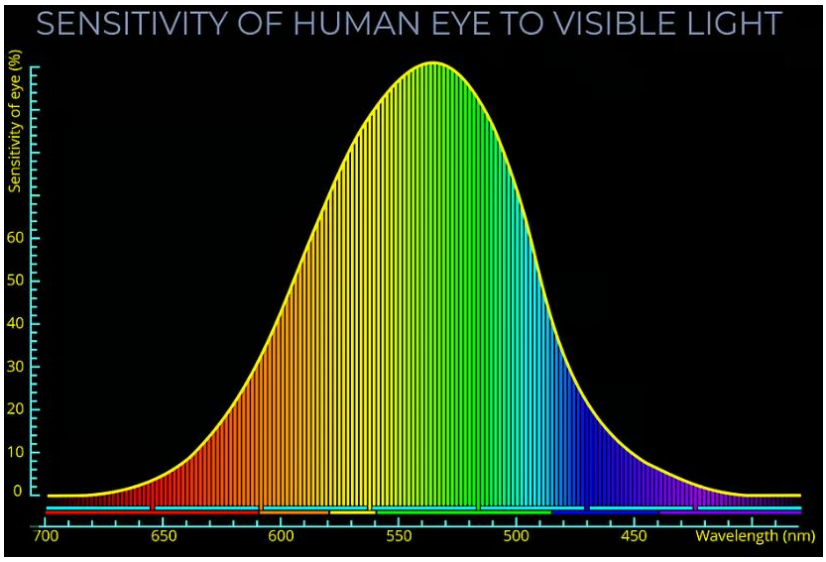

Image 7: Sensitivity of human eye to visible light curve.

human eye's sensitivity to each wavelength, as represented by the photopic response curve shown in Image 7[18].

This curve exhibits an almost Gaussian shape, with its peak corresponding to the green-yellow segment of the spectrum, where human vision is most sensitive. The sensitivity sharply decreases towards the red or blue regions of the spectrum. The significance of this curve in diode design lies in its correlation with photon emission. For a green light emitter, a specific number of photons are emitted with a specific number of optical or electrical excitations, corresponding to a particular luminance value. However, for a red-light emitter, a significantly higher number of excitations within the same timeframe is required to achieve the same luminance value as green. Thus, for materials with similar quantum efficiency of fluorescence, more emitted photons imply higher currents, achievable at increased operating voltages. Consequently, to maintain similar functional characteristics and luminance levels, materials must exhibit different quantum efficiencies (e.g., red and blue materials with higher efficiencies than green).

Additionally, light emission occurs across the entire surface rather than from a single point, as seen in incandescent bulbs. Hence, luminance intensity is expressed in cd/m² rather than in cd. Generally, it is conventionally assumed that OLED emission is Lambertian, meaning isotropic, indicating that the intensity of emitted light is the same regardless of the measurement/viewing angle, forming a perfect hemisphere. However, this assumption is not entirely accurate, as discussed below, phenomena of contribution disturb the Lambertian profile of the diode. Finally, for the characterization of an OLED, the maximum luminance value is of interest, along with specific luminance values used as reference points when providing operational voltage, efficiency, and lifespan values (e.g., 100 cd/m², 1,000 cd/m², 10,000 cd/m², 100,000 cd/m², etc.).

2) Characteristic Voltages (V) - [V]:

A. Turn-On Voltage (V_{on}): The turn-on voltage is a critical parameter denoting the voltage at which light emission initiates. In an ideal scenario, this voltage aligns with $V_{on} = E_g$, where E_g represents the energy gap of the light-emitting material in electronvolts (eV), and e symbolizes the elementary charge of an electron. However,

practical considerations, such as potential barriers at electrode/organic interfaces and limitations imposed by the light measurement system, often result in a higher recorded turn-on voltage. Consequently, V_{on} is practically defined as the voltage corresponding to a luminance of 1 cd/m². It's noteworthy that in specific scenarios, V_{on} may be referenced at luminance levels of 0.1 cd/m² for low-light systems or when highly sensitive photodiodes are employed, and at 10 cd/m² in high-brightness systems.

B. Operating Voltage (V_{op}): The operating voltage holds paramount technological significance and is once again defined based on luminance, tailored to the application and diode type. For low-brightness configurations, it signifies the voltage necessary to achieve the typically required luminance in flat-panel displays (100 cd/m²). Conversely, in high-brightness devices designed for lighting applications, elevated reference values (1,000 cd/m² or 10,000 cd/m²) are chosen to capture the device's performance under more demanding conditions.

3) Efficiency

Organic Light-Emitting Diodes (OLEDs) are at the forefront of display and lighting technologies due to their unique properties, offering thin, flexible, and energy-efficient solutions. To comprehensively assess the performance of OLEDs, several efficiency metrics are employed, each shedding light on different aspects of their functionality. In this section, we delve into three key efficiency parameters: Luminance Efficiency (η_L), Power Luminous Efficiency (η_p), and Quantum Efficiency[19].

A. Luminance Efficiency, η_L [cd/A]: Luminance efficiency is a crucial parameter that assesses how effectively an OLED converts electrical current into visible light. A higher η_L indicates a more efficient device. However, practical considerations such as voltage drop across electrodes and measurement limitations might cause the actual turn-on voltage to be higher. Therefore, η_L serves as a valuable benchmark for comparing the performance of OLEDs across different conditions.

$$\eta_l = \frac{L}{J} \quad (1)$$

B. Power Luminous Efficiency, η_p [lm/W]: Power luminous efficiency, derived from luminance efficiency, provides insights into how effectively the OLED transforms electrical power into visible light. This metric is crucial for applications where power consumption is a critical factor, such as in portable devices or energy-efficient lighting solutions. The inclusion of the correction factor π ensures that the conversion from luminance to luminous flux aligns with Lambertian emission characteristics (1 cd = π lumens).

$$\eta_p = \pi \frac{\eta_l}{V} \quad (2)$$

C. Quantum Efficiency (%):

C1. Internal Quantum Efficiency, η_{int}: Internal quantum efficiency is a measure of the efficiency with which electrons and holes recombine to produce excitons and subsequently emit photons. This parameter is influenced by the choice of materials, device architecture, and exciton management strategies. Improving η_{int} contributes to enhancing overall device efficiency, especially in phosphorescent OLEDs, where the spin statistics play a crucial role[20].

$$\eta_{int} = \eta_{PL}\eta_{s/t}n_{rec} \quad (3)$$

Where:

- η_{PL} is the quantum efficiency of the phosphorescent emitter.
- $\eta_{s/t}$ is the probability of forming a singlet or triplet exciton.
- n_{rec} is the probability of electron-hole recombination.

C2. External Quantum Efficiency, η_{ext}: External quantum efficiency is a key metric for assessing the practical light-emitting performance of an OLED. It takes into account not only the internal processes of exciton formation and recombination but also factors affecting light extraction efficiency. Challenges such as light trapping and waveguiding within the device layers can reduce η_{ext}. Strategies like employing microcavity structures or advanced outcoupling techniques are explored to enhance

external quantum efficiency, making the emitted light more accessible for various applications, from displays to lighting.

Defined as the ratio of the number of photons that ultimately exit the transparent electrode to the number of electrons flowing through the circuit. Essentially, it is the internal quantum efficiency multiplied by a factor accounting for light waveguiding, internal reflections, and other optical phenomena that typically reduce the percentage of emitted light compared to what was generated by the material. In the calculation, adjustments are made based on the eye's response, and it can also be experimentally measured using an integrating sphere, ensuring that only photons leaving in the vertical direction are recorded:

$$\eta_{ext} = \eta_{int}\eta_c = \eta_{PL}\eta_{s/t}n_{rec}\eta_c \quad (4)$$

Where, η_c is the light outcoupling efficiency of the diode in the vertical viewing direction.

In summary, these performance metrics collectively provide a comprehensive evaluation of OLED devices, reflecting their efficiency, power consumption, and practical luminous output characteristics, essential for optimizing their application in diverse technological domains.

4) Emission Color

A. The determination of emission color is based on chromatic coordinates (x, y), as defined by the Commission Internationale de l'Eclairage (CIE coordinates), representing the position of the emitted light color in the chromaticity triangle (Image 8). These coordinates result from integrating the emission spectrum with respect to the wavelength in relation to the eye's sensitivity to each wavelength (color)[18].

B. Color Rendering Index (CRI): It relates to the "color appearance," indicating the color perceived when an object is illuminated with a white light source compared to the color of the same object when illuminated with a standard source (e.g., blackbody radiation source). It serves as an indicator of the quality of white light and takes values on a scale from 0 to 100, where the standard source receives a value of 100.

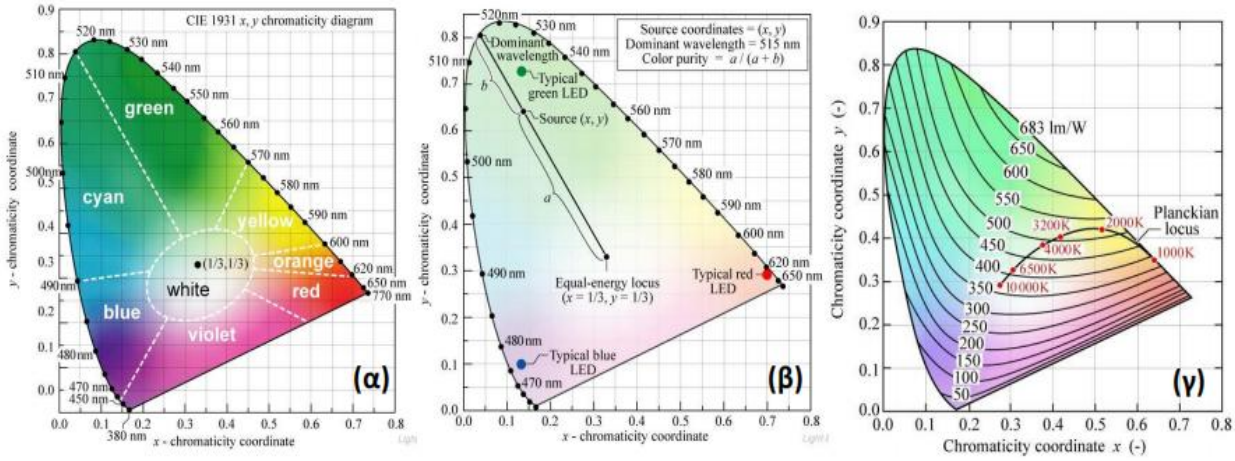

Image 8: Color triangles based on coordinates (x, y) according to CIE 1931[21]. The coordinates of the "pure" colors, which correspond to specific wavelengths, belong to the perimeter of the triangle, while white is located at the center of the triangle, as a combination of all colors (0.33, 0.33). (a) The areas of the seven basic colors are distinguished. (b) The typical coordinates for the basic colors red – green – blue (RGB) are distinguished, as well as the method for determining the "dominant emission color" and the "purity of the color" based on the white point. (c) Correlation of maximum theoretical luminous power output with chromatic coordinates.

5) Lifetime [hours, h]

Lifetime of an OLED is usually defined as the time elapsed until the initial brightness of a diode decreases by 50% under the application of constant current density. Alternatively, it can be attributed to the time required for the power efficiency to drop to half its initial value while maintaining constant brightness with a gradual increase in voltage (and consequently, the current flowing through the diode). In industrial terminology, it is common to calculate lifetime with respect to 70% of the initial value.

Understanding the factors that contribute to the longevity of OLEDs is essential for ensuring reliable performance over time. OLEDs utilize organic compounds in their emissive layers, and the degradation of these materials is a key determinant of their lifespan. Exposure to environmental factors such as moisture, oxygen, and light can

lead to material breakdown. To counteract this, advanced encapsulation techniques, including the use of barrier films and hermetic sealing, are employed to shield OLEDs from these influences. The operating conditions of OLEDs play a crucial role in their lifespan. Current density and voltage are significant factors, with higher values accelerating degradation processes. Efficient thermal management is also essential, as elevated temperatures during operation can contribute to material breakdown. Careful optimization of operating parameters is necessary to strike a balance between performance and longevity. The overall design of OLED devices, particularly encapsulation strategies, directly influences their lifetime. Aging mechanisms, such as luminance decay and color shift, are inherent to OLEDs. Luminance decay, a gradual reduction in brightness, is a common aging factor influenced by material stability and device design. Addressing color stability through material selection and manufacturing processes is crucial for maintaining accurate and consistent colors over time.

Manufacturers conduct rigorous accelerated aging tests to simulate long-term operation within a shorter timeframe. These tests help estimate the device's lifetime under normal operating conditions. International standards, established by bodies like the International Electrotechnical Commission (IEC), provide guidelines for OLED lifetime testing and characterization, ensuring consistency and reliability in the assessment process. Ongoing research endeavors focus on improving the lifetime of OLEDs. This includes the development of stable organic materials with enhanced resistance to degradation. Technological advancements, such as new device architectures and encapsulation methods, contribute to extending the operational lifespan of OLED devices. In conclusion, the lifetime of OLEDs is a multifaceted consideration involving material properties, operational conditions, device architecture, and aging mechanisms. As OLED technology continues to evolve, efforts in research and development are dedicated to addressing these factors, paving the way for widespread and durable applications in the realm of displays and lighting.

3.4 Efficiency Optimization

As mentioned earlier, the external quantum efficiency of an organic light-emitting diode (OLED) is given by the relationship:

$$\eta_{ext} = \eta_{PL} \cdot \eta_{s/t} \cdot n_{rec} \cdot \eta_c \quad (5)$$

Therefore, maximizing performance requires the individual optimization of each factor. Before discussing how this can be achieved, it is relevant to address the fundamental physical processes that take place during the operation of an OLED, which are as follows[22]:

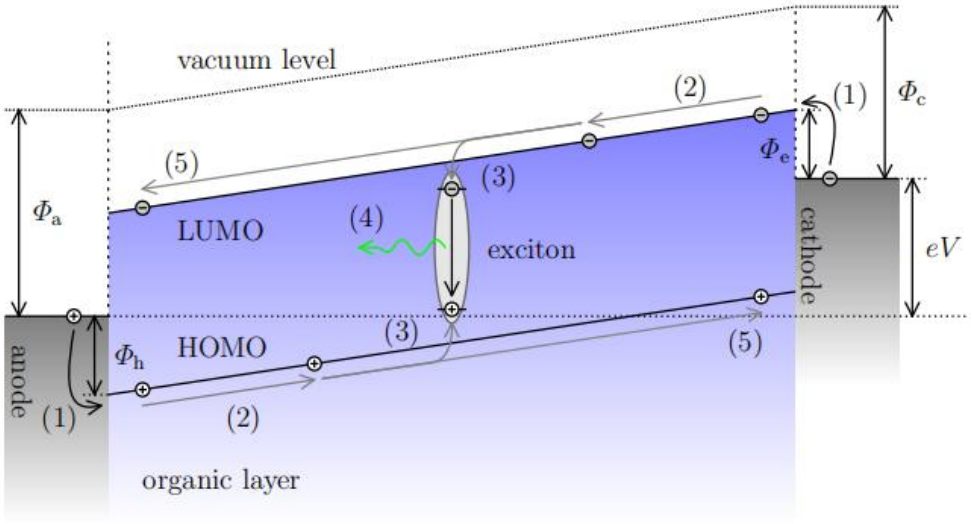

Image 9: Simplified energy level diagram for an OLED consisting of only one organic layer. (1) charge carrier injection, (2) charge carrier transport, (3) exciton formation, (4) exciton decay / radiative recombination, (5) leakage current.

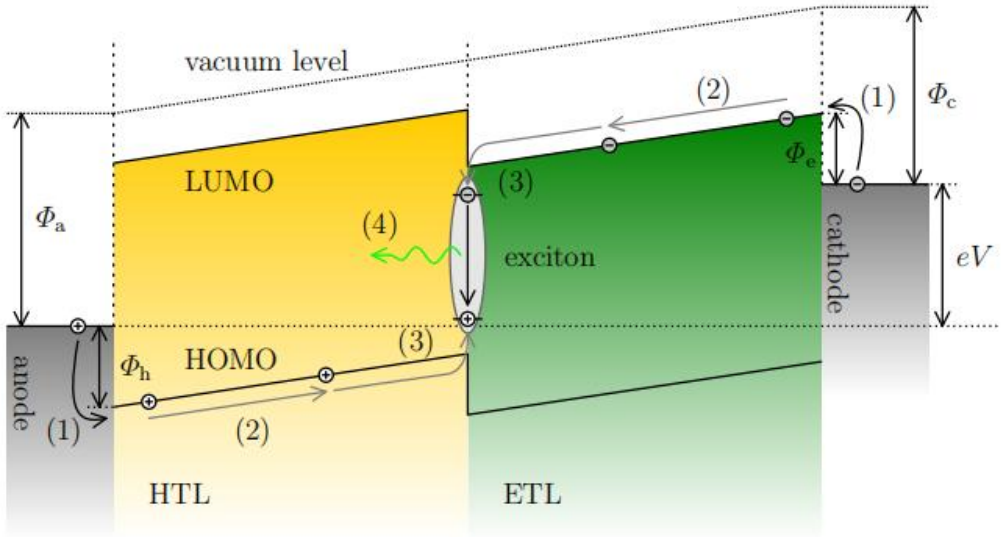

Image 10: Simplified energy level diagram for an OLED consisting of two organic layers, e.g., a diamine as hole transporting layer (HTL) and Alq3 as electron transporting layer (ETL) as in reported by Tang et al. (1) charge carrier injection, (2) charge carrier transport, (3) exciton formation, (4) exciton decay / radiative recombination. Charge carriers are blocked at the HTL/ETL interface due to barriers as a result of differences in the HOMOs (for holes) and LUMOs (for electrons).

- Injection of carriers from both electrodes
- Their transport to the emissive layer
- Recombination of carriers – exciton formation
- Annihilation of exciton with light emission

The first three processes are related to the electrical characteristics of the materials, while the last one pertains to the optical characteristics of the photo-emitting organic material. Subsequently, we will analyze how each of these stages can be separately optimized to maximize the efficiency of the device.

3.4.1 Injection and Carrier Transport to the Emission Zone

The injection of carriers from the electrodes is associated with the energy barriers at the interfaces, while the transport of carriers relies on their mobility within the respective organic material. Due to the generally low mobility of carriers in organic materials compared to inorganic ones, the mechanisms of carrier injection and transport to the emission layer are interrelated concerning their contribution to exciton formation efficiency. Moreover, the mobilities of carriers are unequal, with hole mobility typically exceeding that of electrons in most cases of organic materials.

Carrier injection can occur through various mechanisms, which can be categorized based on whether there is a significant energy barrier at the electrode/organic interface for carrier injection. The energy barrier for hole or electron injection (Δ_h, Δ_e) is defined as the difference between the work function of the anode (Φ_{an}) or cathode (Φ_{cat}) and the ionization potential (IP) or electron affinity (EA), respectively, of the organic molecule:

$$\Delta_h = |IP - \Phi_{an}| \; and \; \Delta_e = |EA - \Phi_{cat}| \quad (6)$$

A. Δ_h and/or $\Delta_e < 0.1$ eV

In this case, the contacts are ohmic, as there is no significant energy barrier for carrier injection. Therefore, the electrodes provide more carriers per unit time than can be transported along the organic layer. In the ohmic electrode, the electric field is nullified due to the shielding caused by the space charge generated by the continuous flow of carriers of the same sign. Subsequently, a "virtual" electrode forms near the ohmic electrode, acting as a charge reservoir. The current generated is restricted by the created space charge (Space Charge Limited Current, SCLC), and its dependence on the field follows Child's Law:

$$j^{SCL} = \frac{9}{8}\varepsilon\varepsilon_0\mu\frac{E^2}{L} \quad (7)$$

Where ε is the dielectric constant of the organic material, ε₀ is the dielectric constant in vacuum, μ is the mobility of the carrier, E is the electric field, and L is the thickness of the organic layer. The above relationship is modified accordingly if there are charge traps in the system, considering the type of energy distribution of these traps (exponential, Gaussian, etc.).

In general, the current varies proportionally to the square of the field and inversely proportional to the thickness of the organic layer for the same value of the electric field, while the mobility of the carriers is considered independent of the field. However, this is not true in systems where charge transport occurs through a hopping mechanism, as is the case in many conjugated polymers.

B. Δh and Δe >0.1 eV

This case is more common in diodes composed of commonly used electrodes, such as ITO anodes and aluminum cathodes. The current flowing through the diode is significantly limited by the carrier injection rate (injection-limited current), and the size of the potential barrier at each interface determines the type of majority and minority carriers. In most organic polymer materials, the potential barrier is larger for electron injection than for hole injection, making holes the majority carriers.

The injection of carriers can follow the following mechanisms:

B1. *Richardson–Schottky (RS) thermionic emission*, where the current is an exponential function of the square root of the applied field and exhibits temperature dependence according to the formula:

$$j \sim e^{\beta\sqrt{E}} \quad (8)$$

Where β:

$$\beta = \frac{\sqrt{\frac{e^3}{4\pi\varepsilon\varepsilon_0}}}{kT} \quad (9)$$

where e is the electron charge, k is the Boltzmann constant, and T is the temperature. This mechanism does not take into account the scattering that carriers may undergo in the polymer chain lattice. It is more applicable to inorganic semiconductor systems where the average carrier mobility is significantly higher due to longer mean free paths.

B2. *Fowler-Nordheim (FN) tunneling injection*, where the current variation with the field does not show temperature dependence, and the slope of the logarithmic neperian $\ln(j/E^2) = f(E^{-1})$ can provide information directly about the magnitude of the potential barrier at the corresponding electrode, as shown by the formula:

$$j \sim E^2 exp\left(\frac{-4\sqrt{m_{eff}}\sqrt[3]{\Delta_{h/e}}}{\hbar eE}\right) \quad (10)$$

Where m_{eff} is the effective mass of the charge carrier passing through the tunnel, and $\hbar$ is the Planck constant divided by 2π. In practice, it has been demonstrated that both mechanisms occur: thermionic emission at low applied field values and tunneling injection at higher fields.

3.4.2 Recombination of Charge Carriers - Formation of Excitons

Recombination of charge carriers i.e., the recombination of electrons and holes leading to exciton formation, is described as a bimolecular chemical reaction. The rate

of this chemical reaction is related to the diffusion of carriers in the emissive layer and is called Langevin-type recombination. According to this model, the average free path of carriers is smaller than the critical Coulomb radius, r_c, which represents the action distance of Coulomb electrostatic attraction between an electron and a hole and is given by the relationship:

$$r_c = \frac{q^2}{4\pi\varepsilon\varepsilon_0 kT} \quad (11)$$

Where q is the electric charge of the electron, ε is the dielectric constant of the material, ε_0 is the vacuum dielectric constant, k is the Boltzmann constant, and T is the temperature. Therefore, substituting into the above equation T=300K, which is the ambient temperature, and ε=3, which is the dielectric constant for most π-conjugated polymers, we get r_c=185 Å, a value much larger than the distance between coupled segments of a polymer chain, which is usually on the order of 10 Å. Thus, the stage determining the rate of the bimolecular reaction is the diffusion of electrons and holes within their mutual electrostatic field. The recombination of electrons with holes is determined by the Langevin recombination constant given by the equation:

$$\gamma = \frac{e(\mu_e + \mu_h)}{\varepsilon\varepsilon_0} \quad (12)$$

Where e is the electric charge of the electron, μ_e is the electron mobility, and μ_h is the hole mobility. This relationship arises from the relation $\gamma=4\pi r_c D$ and Einstein's equation $D = (\mu_e+\mu_h)kT$, where D is the carrier diffusion coefficient, indicating the temporal spread of transported charge carriers. Furthermore, the ratio γ/μ is derived, expressing the equilibrium between recombination and the transport of carriers due to their electrostatic field. The mobility, μ, of carriers depends on the electrostatic field, unlike the Langevin constant, γ, which is independent of it.

Finally, the recombination yield, n_{rec}, is the ratio of the Langevin current density, J_L, to the total current density flowing through the OLED device. The Langevin current density is given by $J_L = \gamma np/d$, where n and p are the electron and hole concentration densities, respectively, and d is the thickness of the recombination zone, which is much smaller than the thickness of the organic layer.

In conclusion, we have:

$$n_{rec} = \frac{J_L}{J_{tot}} \quad (13)$$

The recombination efficiency is maximum when the concentration of carriers in the organic emission layer is both maximum and balanced. This balance implies that the concentration of electrons equals that of holes. As a result, leakage current is zero and does not contribute to the overall current flowing through the device. This phenomenon is achieved when the contacts between the electrodes and the emission layer are ohmic, and the mobilities of electrons and holes are equal. When, for example, the mobility of holes is greater than that of electrons, the efficiency will still be maximum, but the recombination zone will shift closer to the electrodes, carrying the slower carriers. However, in this case, at the cathode, there is an increased likelihood of exciton destruction or non-radiative deactivation due to potential interaction with the cathode metal.

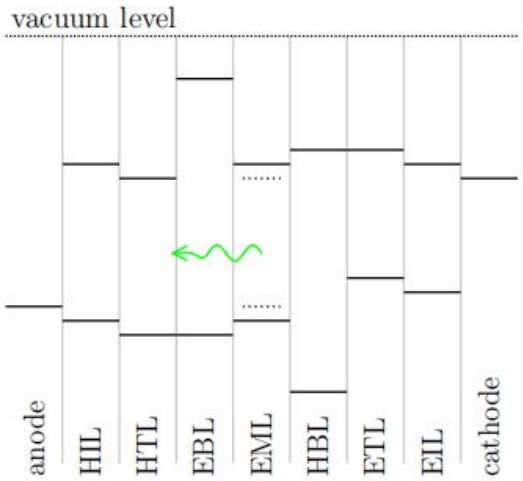

Image 11: Schematic HOMO and LUMO energy levels. Energy levels of the dye in the EML indicated with dashed lines.

When at least one contact (e.g., corresponding to majority carriers, say the anode) is ohmic, and in the other (cathode) there is a potential barrier, the probability of their recombination and, therefore, the performance of this particular arrangement is maximized when the mobility of majority carriers (holes) is smaller than that of

minority carriers (electrons). Obviously, the same logic will apply in the case of two contacts with asymmetric energy barriers.

3.4.3 OLED Architecture

Since the absolute matching of the output levels of the electrodes with the energy levels of various organic materials (especially those with a large energy gap emitting blue light) is rare, especially when it is desirable to avoid reactive metals in the cathode, such as calcium, in favor of a more inert but higher work function aluminum, bilayer and multilayer structures are required (Image 11). Thus, for example, at the surface of the organic layer with the cathode, an electron-injecting/transporting/hole-blocking layer (EIL/ETL/HBL) is interposed. The material that will play this role will primarily be selected based on its energy levels, i.e., it should have a relatively high electron affinity (LUMO level) and a high ionization energy (HOMO level). In this way, indirect enhancement of the electron injection rate at the cathode can be achieved: majority carriers (holes) will accumulate at the surface of the active emitting layer (EML)/HBL (similar to the accumulation of charge on the plates of a capacitor) since they will not be able to pass the new potential barrier imposed due to

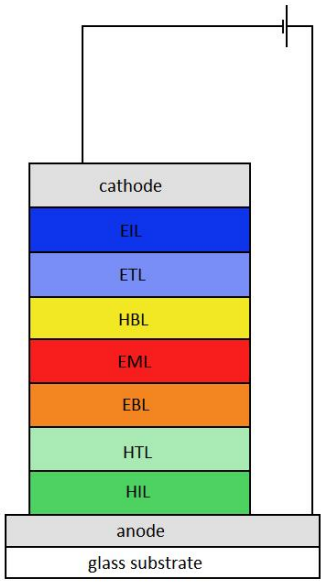

Image 12: Highly efficient OLED stack composed of various layers, each having its specific purpose: hole injection layer (HIL), hole transporting layer (HTL), electron blocking layer (EBL), emission layer (EML, usually a dye as dopant in a matrix), hole blocking layer (HBL), electron transporting layer (ETL), electron injection layer (EIL).

the large difference between the HOMO of the HBL and the Fermi level of the cathode metal.

This will result in a spatial redistribution of the electric field and reinforcement near the cathode, resulting in easier electron injection and a simultaneous significant reduction in leakage current, as majority carriers will no longer reach the cathode to discharge. Similarly, hole injection can be enhanced using an intermediate hole-injecting/transporting/electron-blocking layer (HIL/HTL/EBL). The properties of injecting one carrier and blocking the other may not coexist in the same chemical compound but may be deposited as separate successive layers. Therefore, multilayer arrangements (Image 12) that have high efficiencies, but extremely complex construction (stacked OLEDs) are created. They usually consist of low molecular weight molecules, which are easily deposited by evaporation, allowing their thickness to be easily adjusted (usually in the tens of nm range), and, more importantly, not to disturb the previous layer with the deposition of the next one. Thus, it is understandable that optimizing recombination efficiency is a complex task and depends on the correlation and control of the mutual interaction of the charge of the added interfaces, the redistribution of the electric field, and the passage of carriers through energy barriers that depend on the field and thickness of each interfacial membrane.

3.4.4 Exciton Excitation with Light Emission

The recombination of an electron and a hole, leads to the creation of a neutral excited state: the exciton. The exciton can be in a singlet or triplet state, depending on whether the orientation of the spins is antiparallel or parallel, respectively. In general, the ratio of singlet to triplet states for an exciton is 1:3, meaning that there is a 25% chance of finding an exciton in a singlet state and a 75% chance of finding it in a triplet state. In most organic molecules, the excitation of a singlet exciton leads to the emission of radiation, while triplet excitons are thermally excited without radiation emission.

It is also worth noting that when the photoemissive material is a transition metal complex, usually of the 5th or 6th period of the Periodic Table, then triplet excitons can be excited by radiation. Radiation emission due to the excitation of triplet excitons is generally prohibited. However, it is possible through the coupling of orbital angular momentum with spin angular momentum (spin-orbit coupling, SOC/l-s coupling), where the conservation of total angular momentum applies. Transition metal complexes exhibit particularly high l-s coupling, mainly due to their large atomic number, such as palladium (Pd, Z=46), iridium (Ir, Z=77), and platinum (Pt, Z=78).

Finally, another factor that determines the performance of the device is the quantum efficiency of the photo-photogeneration of the photoemissive substance. This is largely influenced by the presence of impurities in the organic material that can act as electron or hole receptors and lead to the quenching of excitations with radiation emission. The issue of material purity is more pronounced in polymers, as low molecular weight organic molecules are usually deposited by evaporation, which is generally a "cleaner" process and excludes environmental contamination from factors such as oxygen and humidity. It should also be noted that the quantum efficiency of a material is different in its sparse solution (usually higher) than in its solid state. This is because additional non-radiative processes occur in the solid state, such as interactions between chains (e.g., exciton annihilation) and quenching of exciton radiation due to external factors (e.g., metal electrodes) and imperfections in polymer arrangement. Measuring the absolute efficiency of photophotogeneration in the deposited membrane is useful for material characterization and can only be done using an integrating sphere[23,24].

3.4.5 Decoupling Efficiency

Even if 100% internal quantum efficiency is achieved (e.g., using phosphorescent metal complexes[25]), the final external quantum efficiency in the direction of the surface from which light exits in typical OLEDs with an ITO anode and Al cathode does not exceed 20-30%. This is because the majority of the generated light:

1) Gets trapped within the arrangement. The difference in refractive indices on the surfaces of various materials composing an OLED (Table 2) results in a portion of the generated light undergoing successive total reflections and being trapped through waveguide modes inside the arrangement.

Table 2: Refractive indices of OLED materials

Material	Refractive index (n)
Air	1.0
Glass	1.5
Plastic (PET, PC)	1.6
ITO	1.8
Organic Materials	1.6-1.8

2) Emerges from the horizontal surface through a cone with an angle of approximately 40° and not from the entire surface; hence, it depends on the viewing angle (Image 13).

A typical OLED consists of several different layers, both organic and inorganic, each with a different refractive index, forming a weak microcavity. This structure introduces significant contributions from interference phenomena to the efficiency and emission spectrum, causing it to deviate from that of an ideal Lambertian emitter (i.e., the perception of brightness by the human eye being independent of the viewing angle). Consequently, the emission intensity exhibits a strong dependence on the viewing angle relative to the light wavelength.

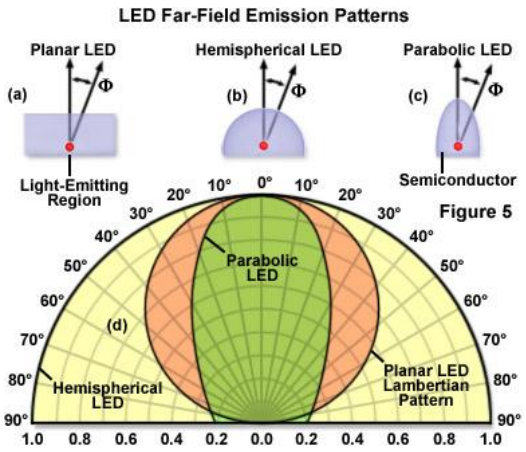

Image 13: Correlation of emission intensity with viewing angle for (a) flat (Lambertian), (b) hemispherical, and (c) parabolic photovoltaic diode. Normalization was performed with maximum intensity at a 0-degree angle.

Furthermore, given that light is emitted only towards the side of the exit where the transparent electrode is located, a large portion of the emitted light can be waveguided through the substrate and organic layers, eventually exiting from the edges of the glass (or plastic) substrate. Usually, as the light generated inside an OLED has to be coupled out through one of the electrodes, ITO (indium tin oxide) is used as transparent, conductive oxide, having a high work function. This is usually used in the so called 'bottom-emitting OLED' (Image 14), consisting of a transparent substrate, usually glass, ITO, organic layers, and a reflecting metal cathode: the generated light leaves the device through ITO and the substrate on the 'bottom' side. 'Top-emitting OLEDs' (Image 14) are not so common as a transparent, yet conductive layer has to be deposited on top of the organic layers. This can be achieved by thin metal films or the use of ITO, however, the latter is deposited using sputtering techniques, damaging the organic layers. However, the substrate in this case is rather arbitrary. Both OLED types can be designed as 'microcavity OLEDs', i.e., both electrodes consist of metals (one actually being thin enough to be semi-transparent).

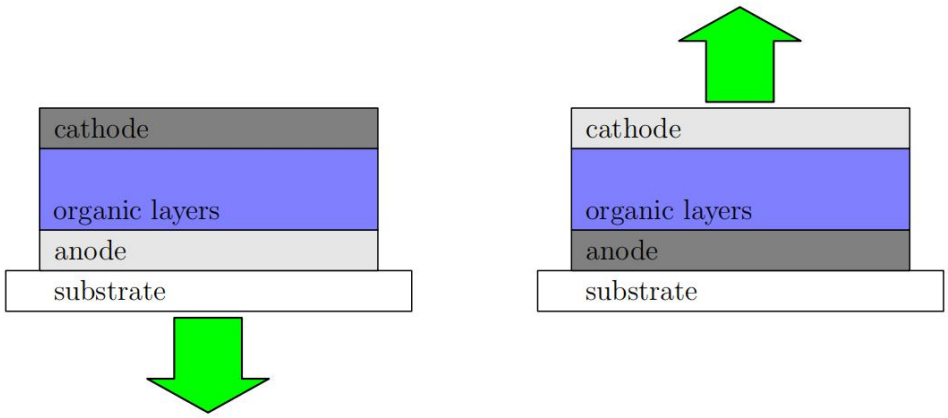

Image 14: Bottom-emitting OLED with transparent anode and opaque cathode (left). Top-emitting OLED with opaque anode and semi-transparent cathode (right).

In the context of light-emitting diode technology, it has been determined that, as a general rule, only about 20% of the generated light exits vertically from the diode surface ($n_c = 1/2n^2$). Various efforts have been made to enhance this percentage, as outlined in literature[26].

One approach involves replacing the glass substrate with a material of higher refractive index ($n > 1.8$). This modification aims to create an optical structure where the substrate, indium tin oxide (ITO), and organic layers collectively form a thick film, thereby limiting total reflections. However, a drawback of this method lies in the fact that materials with such high refractive indices are often fragile, expensive, and potentially toxic. Another strategy focuses on the creation of microcavities using a translucent material on the anode, such as an ultra-thin metal. This design encourages various radiation diffusion mechanisms (photon modes) to propagate towards the forward direction. Nevertheless, disadvantages of this approach include its inherent wavelength-dependency, rendering it unsuitable for applications requiring white light, and introducing color emission variation based on the viewing angle. A third avenue explores the structuring of organic materials to effectively disperse light. However, this process proves to be practically demanding, considering the need to account for the inherent roughness of the substrate. Additionally, there is a proposal to replace ITO with a structure consisting of oxide/metal/oxide. Lastly, employing micro lenses on the substrate surface is suggested to improve the coupling of light and ensure uniform diffusion. This approach aims to make the performance independent of the viewing angle, enhancing the overall efficiency of light emission from the diode.

3.4.6 Stability Issues and Lifetime of OLEDs

The lifetime of an OLED device, defined as the time (in hours) until the initial brightness is reduced by half while maintaining constant current density, represents a fundamental obstacle to the widespread dissemination and commercialization of OLEDs. The failure of an OLED device may be attributed to the occurrence of one or more of the following factors[27]:

- Formation of dark spots on the surface of the cathode.
- Reduction in the efficiency of photo- and electroluminescence.
- Increase in the operating voltage to maintain constant brightness or current density (reducing power efficiency). The causes leading to these outcomes may include[28,29]:

1. Photochemical reactions that certain polymers may undergo, such as the photooxidation of poly(phenylene vinylene) and poly(fluorene).
2. Reactions negatively affecting the electrode surfaces with organic materials, involving either diffusion of atoms from the electrodes, e.g., indium from ITO, or corrosion of low work function reactive metals used in the cathode.
3. Thermal instability of organic layers leading to crystallization and a dramatic change in their morphology.
4. Electrochemical instability and decomposition of certain organic materials.

It is evident that exposure of the OLED device to environmental conditions, particularly oxygen and humidity, accelerates its degradation, especially in the case of phosphorescent emitters. Therefore, the construction of devices in a controlled environment and their encapsulation using protective layers are essential for achieving long lifetimes.[18,30]

Image 15 illustrates the increased demands for OLED isolation from the environment. In Images 15b and c, two methods of encapsulating OLEDs are depicted, with thin film encapsulation (TFE) technology (Image 15c) being the most prevalent today.

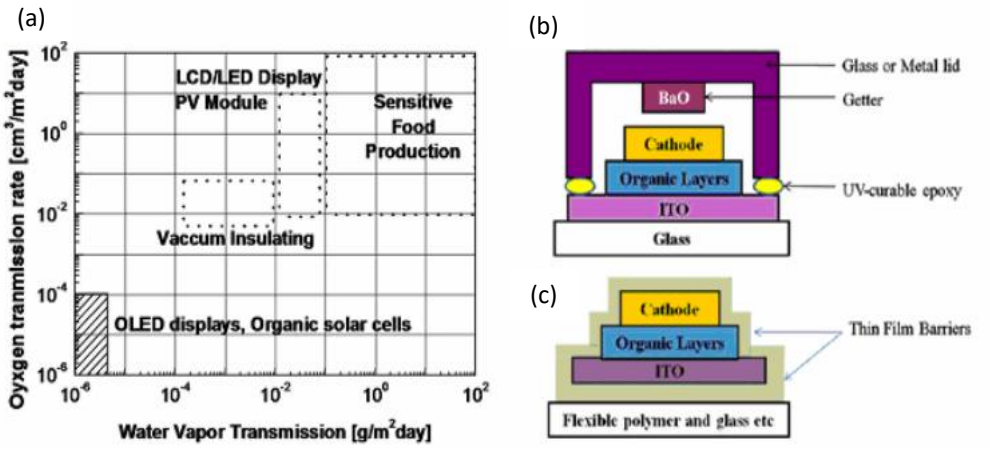

Image 15: (a) Specifications for permeability to oxygen and moisture for various types of arrangements, and (b), (c) schematic representation of different encapsulation methods for OLEDs.

3.5 Types of Organic Light-Emitting Diodes (OLEDs)

The field of organic light-emitting diodes (OLEDs) is characterized by a rich variety of technologies, each designed to cater to specific applications and performance requirements. The types of light-emitting diodes are distinguished based on the type of materials used in their construction. Thus, OLED devices are categorized into the following classes:

Small molecule organic light-emitting diodes (small molecule OLEDs, sm-OLEDs) have an emissive layer composed of organic molecules with small molecular weight. The deposition of the organic layers primarily occurs through vacuum evaporation; however, there are cases where organic molecules can be deposited using solution processes. The advantages of these configurations include good quality and control over the thickness of the organic layer, achieved through vacuum deposition. Nonetheless, the deposition processes increase the complexity and manufacturing cost of sm-OLEDs. Despite this, the best performances for OLED configurations reported to date involve structures based on small organic molecules, with their layers deposited through vacuum evaporation.[31,32]

Polymer light-emitting diodes (Polymer LEDs, PLEDs) are based on polymer layers as emissive layers, deposited through solutions, such as inkjet printing, spin coating,

etc. The thickness of the polymer layers depends on the polymer composition, its concentration in the solution, and the deposition conditions. The performance of PLEDs is limited by the injection of electrons and holes into the electrodes. Achieving balanced injection and carrier transport relies on introducing a conductive polymer layer between the electrode and the polymer material to facilitate carrier transport. For the anode of a PLED, a transparent conductive oxide with a high work function is chosen, such as Indium Tin Oxide (ITO), to be close to the Highest Occupied Molecular Orbital (HOMO) level of most polymers (approximately 5 eV). For the cathode, metals with low work function are preferred, such as aluminum and silver, to match the Lowest Unoccupied Molecular Orbital (LUMO) level of most conjugated polymers (approximately 3.5 eV).[2]

Phosphorescent OLEDs (PHOLEDs) represent a significant advancement in OLED technology by incorporating phosphorescent emitters. Unlike traditional fluorescent OLEDs, phosphorescent emitters can harvest both singlet and triplet excitons, leading to a more efficient use of charge carriers. PHOLEDs exhibit higher external quantum efficiencies and improved power efficiency, making them ideal for applications requiring high-performance displays and lighting systems. The use of phosphorescent materials enhances the overall efficiency of OLED devices, contributing to their widespread adoption in various industries.[8]

Tandem OLEDs present an innovative approach to addressing the stability and efficiency challenges associated with traditional OLED configurations. In a tandem structure, multiple OLED units are stacked, each optimized for specific emission colors. This design helps minimize efficiency losses and extends the overall device lifespan. Tandem OLEDs are particularly advantageous for large-scale displays and lighting applications. By carefully engineering each OLED unit in the tandem stack, manufacturers can achieve improved performance and reliability, paving the way for the development of more durable and efficient OLED devices.[33]

White OLEDs (WOLEDs) are a versatile category designed to emit white light efficiently. There are two primary approaches to achieve white emission: using multiple emissive layers with different colors or employing a blue OLED with color-converting layers. WOLEDs find widespread applications in general lighting and

display technologies due to their ability to produce high-quality white light, offering a broad color gamut and improved color rendering. As the demand for energy-efficient and aesthetically pleasing lighting solutions grows, WOLED technology continues to play a pivotal role in meeting these diverse needs across residential, automotive, and commercial sectors.[3,4]

Hybrid Light-Emitting Diodes (HyLEDs) stand out with their unique structure in the realm of light-emitting diodes (LEDs). The emissive layer in HyLEDs is composed of organic material, distinguishing it from the inorganic films typically used for carrier injection and transport. These inorganic films, deposited through methods like solution processing or vacuum deposition, contribute to enhanced carrier injection and transport within the device. Transition Metal Oxides (TMOs), a significant category of inorganic materials serving as Interfacial Layers (ILs), offer a blend of high transparency in the visible spectrum, electronic conductivity, and controllable morphology. This allows for their economical deposition over large surfaces.[34]

Expanding the discussion to other display technologies, *Quantum Dot LEDs (QLEDs)* have gained prominence by utilizing semiconductor nanocrystals known as quantum dots, providing precise control over emitted colors. Organic LEDs (OLEDs), on the other hand, leverage organic materials to generate light, offering flexibility in design and applications such as flexible displays. In addition to these technologies, *Organic-Inorganic Hybrid LEDs (OIHLs)* integrate both organic and inorganic materials within their structure. This hybrid approach aims to capitalize on the unique benefits of each material class, optimizing performance, efficiency, and cost-effectiveness. *Perovskite LEDs*, another noteworthy development, involve the use of perovskite materials as the emissive layer. Perovskite LEDs have shown promise for their high efficiency and ease of fabrication, making them a subject of considerable research interest in the field of optoelectronics. In the dynamic landscape of LED technologies, these diverse approaches, including HyLEDs, OIHLs, QLEDs, OLEDs, and perovskite LEDs, contribute to the ongoing evolution and innovation in display and lighting applications.[35-38]

References

[1] Tang, C. W., & VanSlyke, S. A. (1987). Organic electroluminescent diodes. Applied Physics Letters, 51(12), 913-915.

[2] Burroughes, J. H., Bradley, D. D. C., Brown, A. R., Marks, R. N., Mackay, K., Friend, R. H., Burns, P. L., & Holmes, A. B. (1990). Light-emitting diodes based on conjugated polymers. Nature, 347(6293), 539-541.

[3] Reineke, S., Lindner, F., Schwartz, G., Seidler, N., Walzer, K., Lüssem, B., & Leo, K. (2009). White organic light-emitting diodes with fluorescent tube efficiency. Nature, 459(7244), 234-238.

[4] Kido, J., Kimura, M., & Nagai, K. (1995). Multilayer white light-emitting organic electroluminescent device. Science, 267(5202), 1332-1334.

[5] Kondakov, D. Y., & Sandifer, J. R. (2007). Degradation of organic materials for organic light-emitting diodes. Journal of Applied Physics, 102(5), 054509.

[6] Gather, M. C., & Reineke, S. (2013). Recent advances in light outcoupling from white organic light-emitting diodes. The Journal of Physical Chemistry Letters, 4(9), 1532-1543.

[7] Burrows, P. E., Forrest, S. R., & Sapochak, L. S. (1995). Single layer organic electroluminescent devices and displays. Science, 269(5220), 963-966.

[8] Baldo, M. A., O'Brien, D. F., You, Y., Shoustikov, A., Sibley, S., Thompson, M. E., & Forrest, S. R. (1998). Highly efficient phosphorescent emission from organic electroluminescent devices. Nature, 395(6698), 151-154.

[9] Cao, Y., Parker, I. D., Yu, G., Zhang, C., Heeger, A. J., & Stucky, G. D. (1999). Light-emitting diodes based on conjugated polymers. Nature, 397(6715), 414-417.

[10] Sasabe, H., & Kido, J. (2013). Development of high performance OLEDs for general lighting. The Journal of Materials Chemistry C, 1(9), 1699-1707.

[11] Forrest, S. R., & Thompson, M. E. (2004). Introduction: The physics of organic semiconductors. Chemistry of Materials, 16(23), 4574-4583.

[12] Pope, M., & Swenberg, C. E. (1999). Electronic processes in organic crystals and polymers. Oxford University Press.

[13] Kondakov, D. Y., Sandifer, J. R., Tang, C. W., & Young, R. H. (2007). Nonradiative recombination centers and electrical aging of organic light-emitting diodes: Direct connection between accumulation of trapped charge and luminance loss. Journal of Applied Physics, 101(2), 024512.

[14] Riede, M., & Leo, K. (2006). Limits for the efficiency of organic light-emitting diodes. Physical Review B, 74(12), 125328.

[15] Popovic, Z. D. (1998). Carrier injection and transport in organic light-emitting devices. Optical Engineering, 37(2), 549-559.

[16] So, F., & Forrest, S. R. (1999). Charge transport and photoluminescence of organic thin films. Physical Review B, 59(18), 12964.

[17] Kalinowski, J., Cocchi, M., Virgili, D., Ulanski, J., Grzegorczyk, W., & Zassowski, P. (2007). Charge transport and recombination in organic light-emitting diodes. Journal of Physics D: Applied Physics, 40(2), R1.

[18] M. T. Bernius, M. Inbasekaran, J. O'Brien, and W. S. Wu, Advanced Materials 12, 1737 (2000).

[19] S. R. Forrest, D. D. C. Bradley, and M. E. Thompson, Advanced Materials 15, 1043 (2003).

[20] R. H. Friend, R. W. Gymer, A. B. Holmes, J. H. Burroughes, R. N. Marks, C. Taliani, D. D. C. Bradley, D. A. Dos Santos, J. L. Bredas, M. Logdlund, and W. R. Salaneck, Nature 397, 121 (1999).

[21] www.LightEmittingDiodes.org.

[22] W. Brütting, S. Berleb, and A. G. Mückl, Organic Electronics 2, 1 (2001).

[23] N. C. Greenham, I. D. W. Samuel, G. R. Hayes, R. T. Phillips, Y. Kessener, S. C. Moratti, A. B. Holmes, and R. H. Friend, Chemical Physics Letters 241, 89 (1995).

[24] J. C. deMello, H. F. Wittmann, and R. H. Friend, Advanced Materials 9, 230 (1997).

[25] C. Adachi, M. A. Baldo, M. E. Thompson, and S. R. Forrest, Journal of Applied Physics 90, 5048 (2001).

[26] K. Leo, Nature Photonics 5, 716 (2011).

[27] Y. Sato, S. Ichinosawa, and H. Kanai, IEEE Journal of Selected Topics in Quantum Electronics 4, 40 (1998).

[28] J. R. Sheats and D. B. Roitman, Synthetic Metals 95, 79 (1998).

[29] F. So and D. Kondakov, Advanced Materials 22, 3762 (2010).

[30] J. S. Park, H. Chae, H. K. Chung, and S. I. Lee, Semiconductor Science and Technology 26, 34001 (2011).

[31] X. Y. Deng, International Journal of Molecular Sciences 12, 1575 (2011).

[32] H. B. Michaelson, IBM Journal of Research and Development 22, 72 (1978).

[33] Kim, Y. H., & Moon, C. K. (2007). Tandem organic light-emitting diodes: A review. Energy & Environmental Science, 1(5), 504-520.

[34] Zhao, Q., Kim, B. J., Hillhouse, H. W., & Pyun, J. (2008). Fabrication of hybrid organic-inorganic light-emitting diodes through layer-by-layer assembly. Nano Letters, 8(4), 1129-1134.

[35] Jeon, N. J., Noh, J. H., Kim, Y. C., Yang, W. S., Ryu, S., Seo, J., & Seok, S. I. (2015). Compositional engineering of perovskite materials for high-performance solar cells. Nature, 517(7535), 476-480.

[36] Lee, J., Lee, K., Jeong, S., Joo, J., & Park, S. (2017). Recent progress on flexible and transparent electronic devices: From materials to devices. Advanced Materials, 29(29), 1700363.

[37] Shirasaki, Y., Supran, G. J., Bawendi, M. G., & Bulović, V. (2013). Emergence of colloidal quantum-dot light-emitting technologies. Nature Photonics, 7(1), 13-23.

[38] Yang, Y., You, J., Chen, C. C., Hong, Z., Song, T. B., Chen, H., ... & Li, G. (2015). High-performance multiple metal halide perovskite light-emitting diodes through morphology control of perovskite films. Advanced Materials, 27(25), 6363-6370.

4. Luminescent Processes

4.1 Introductory Concepts of Photophysical Processes

Luminescence can be characterized primarily based on the type of excitation that induces it, namely photoluminescence (PL - optical excitation), electroluminescence (EL - electrical excitation) or chemiluminescence (CL - chemical reaction). Additionally, depending on the energy level from which the emission occurs, it is classified as fluorescence (fl - simple state, singlet) or phosphorescence (ph - triplet state). Fluorescence and phosphorescence are two examples of electronic transitions between different energy states of a molecule. These transitions are schematically described using Jablonski diagrams and are characterized by the rate constant, k, the lifetime, τ, and the quantum yield, Φ.

In Image 16, all possible transitions following the absorption of a photon by a molecule and the subsequent transfer of an electron from the fundamental state, S_0, to the first or second excited energy level, S_1 or S_2, are illustrated.[1] Radiative transitions involving the absorption or emission of radiation are represented by vertical solid

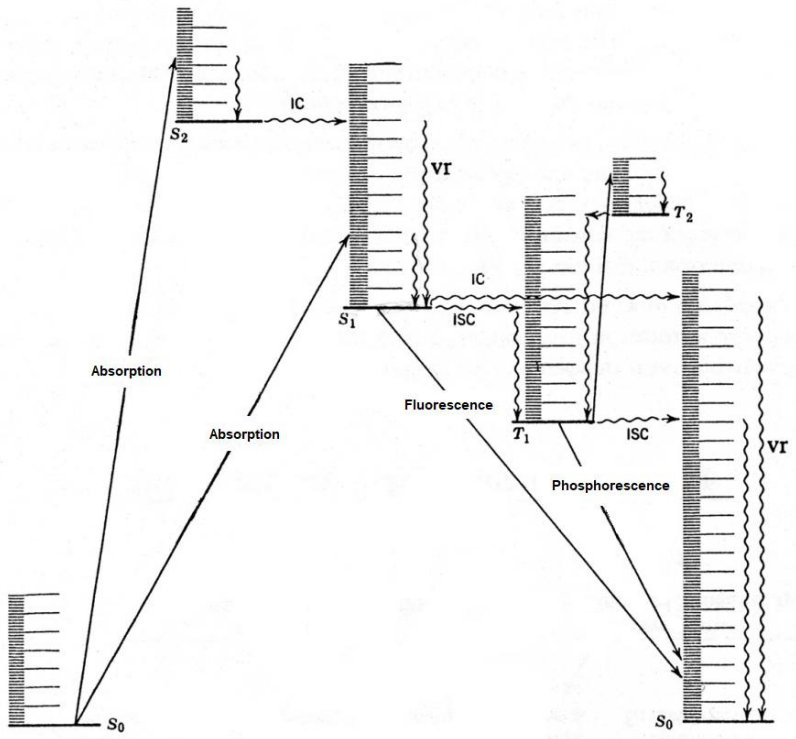

Image 16: Simplified Jablonski diagram of a coupled organic molecule (e.g., anthracene), representing the basic optical transitions.

lines, while non-radiative transitions are indicated by wavy lines. Non-radiative transitions include internal conversion (IC), an isoenergetic transition between states of the same multiplicity ($S_2 \rightarrow S_1$, $S_1 \rightarrow S_0$, $T_2 \rightarrow T_1$, etc.), and intersystem crossing (ISC), an isoenergetic transition from a singlet excited state to a triplet state (e.g., $S_1 \rightarrow T_1$). Vibrational relaxations (vr) are also distinguished, representing transitions from higher-energy vibrational levels (ν=1,2,3...) to the corresponding lower-energy levels (ν=0).

Table 3: Lifetimes of optical transitions.

Type of Transition	**Lifetime [sec]**
Absorption	10^{-15}
Vibrational Relaxation	10^{-12}-10^{-10}
Fluorescence	10^{-10}-10^{-7}
Intersystem Crossing (ISC)	10^{-10}-10^{-8}
Internal Conversion (IC)	10^{-11}-10^{-9}
Phosphorescence	10^{-6}-1

A special case of radiative deactivation is the so-called delayed fluorescence, which can occur in various ways, such as the transfer of energy from the triplet state back to the singlet state (triplet-singlet back transfer) or the mutual annihilation of two triplet states (triplet-triplet annihilation, TTA). In the latter case, the energy is shared in a non-radiative transition to the fundamental state and simultaneous energy transfer to the nearest higher-energy singlet state (e.g., $T_1 + T_1 \rightarrow S_0 + S_1$). It is called delayed fluorescence because, although the radiation emission ultimately occurs from the singlet state S_1 (fluorescence), the lifetime is longer than usual and sometimes approaches the phosphorescence lifetime (see Table 3 for the lifetimes of the mentioned processes).

Each electronic transition is characterized by a probability corresponding to the square of the transition dipole moment. This probability must be non-zero for the transition to occur. Forbidden and allowed electronic transitions are commonly

discussed, even though theoretically even forbidden transitions are characterized by a very small, non-zero probability under certain conditions that will be mentioned below. The "allowability" of a transition can be quantified in absorption through the absorptivity coefficient, ε, and in radiative deactivation transitions through the rate constant, k. The larger these values, the more permissible the transition. For example, allowed radiative transitions such as fluorescence are characterized by a short lifetime and a large rate constant k, while the opposite holds true for phosphorescence.

For a transition to be allowed, the principles of conservation of energy and conservation of momentum must not be violated. Therefore, in quantum mechanical calculations of the transition dipole moment, selection rules related to the following should be taken into account[2]:

1) Linear nuclear motion

It can be considered - without significant error - that the movement of the nucleus is much slower than the movement of the electrons around it, so the nucleus does not significantly shift during an electronic transition (Franck-Condon Principle). Thus, for radiative transitions, the geometry of the nuclei does not change during the absorption of a photon and the subsequent movement of an electron to a higher-energy orbital, while for non-radiative transitions, the motion of the nucleus remains unchanged during the movement of the electron to a different orbital. This principle applies to vibrational transitions/relaxations, which usually follow a vertical Franck-Condon transition. Such transitions, while sometimes symmetry-forbidden, can be observed experimentally because of vibronic coupling due to nuclear motion ("zero motion") at each temperature, partially negating the prohibition.

2) Electron motion in their orbits (orbital angular momentum)

It is related to the preservation of orbital symmetry during the transition from one molecular orbital to another (orbital forbiddenness) and to the sufficient spatial overlap of the orbitals participating in the transition (overlap forbiddenness). Orbital prohibitions are relatively weak and can be overcome by mixing appropriate orbitals, for example, through out-of-plane vibrations, allowing the observation of the transition spectroscopically.

3) Electron spin self-rotation (spin angular momentum)

It is directly related to the conservation of momentum, as transitions between states of different spin multiplicities are not allowed. For example, intersystem crossing (ISC) and phosphorescence are usually forbidden processes, as the participating states are of different multiplicities (triplet → singlet). It should be noted that, according to the Pauli principle, two electrons in the same orbital must have opposite spins. An immediate consequence is that the fundamental state must be a singlet, so that each orbital has paired (antiparallel) spins. However, in the excited state, the two electrons are in different orbitals, so their spins do not necessarily have to be parallel. Cancelling this prohibition occurs through the coupling of orbital angular momentum with spin angular momentum (spin-orbit coupling, SOC). During SOC, the conservation principle of total angular momentum holds for the overall angular momentum, not just for spin angular momentum. Therefore, phosphorescence emission is eventually observed. To achieve strong SOC and thereby increase the probability of intersystem crossing (ISC) and emission from the triplet state, the following parameters need to be considered:

(i) The type of orbitals participating in the transition. The coupling of orbital angular momentum with spin (SOC) involves the "exchange" of angular momentum. Therefore, an s orbital with spherical symmetry cannot participate in such a process since it cannot change the orientation of its electron's orbit, whereas a p orbital can change orientation (e.g., from p_x to p_y).

(ii) The atomic number, Z (nuclear charge). From the solution of quantum mechanical equations, it is found that the Hamiltonian operator of SOC and, therefore, the strength of SOC is proportional to the atomic number Z raised to the fourth power.[3]

$$H_{SO} \sim \frac{Z^4}{n^3(l+1)(l+1/2)l} \qquad (14)$$

where n is the principal quantum number and l is the azimuthal (angular momentum) quantum number. A direct consequence is that atoms with a large atomic number will enhance the SOC. This phenomenon is called the "heavy atom effect" and is distinguished into internal and external heavy atom effects, depending on whether the

heavy atom is part of the molecule or added independently as a moiety, compound, or included in the solvent to enhance ISC and subsequently phosphorescence.

(iii) One-center effect. In addition to (i), where it is mentioned that the orbitals participating in the transition must be able to undergo a simultaneous change in their angular momentum with the spin change, this rule is directly related to the well-known "El-Sayed Rule"[2]. According to this rule, "internal conversion (ISC) from the lowest singlet excited state (S_1) to the isoenergetic vibrational level of the nearest triplet state (T_n) is favored, provided that this transition occurs between different types of orbitals." Thus, for example, ISC from a simple singlet state $^1(\pi, \pi^*)$ to a triplet state $^3(n, \pi^*)$ is favored but not to a triplet $^3(\pi, \pi^*)$, and vice versa. This can be represented using Dirac notation (with matrix elements) as follows[2]:

$$\langle S_1|H_{SO}|T_n\rangle^2 \rightarrow \left\langle {}^1\pi\middle|H_{SO}\middle|{}^3n\right\rangle^2 \gg \left\langle {}^1\pi\middle|H_{SO}\middle|{}^3\pi\right\rangle^2 \quad (15)$$

4.2 Photophysics of Semiconducting Polymers

In addition to the electrical properties of conjugated polymers discussed above, the expansion of their technological application fields was significantly influenced by the fascinating optical properties of certain semiconducting polymers, namely their spectroscopic characteristics related to light absorption and emission. For example, the high absorptivity of certain polymers across a wide range of wavelengths within the visible spectrum (e.g., polythiophenes) prompted the development of organic photovoltaic cells (OPVs), while the ability of some polymers to emit light at various wavelengths with high quantum efficiency (e.g., polyphenylenes, polyphenylenevinylenes, polyfluorenes) (Image 17) facilitated the rapid growth of products based on organic light-emitting diodes.

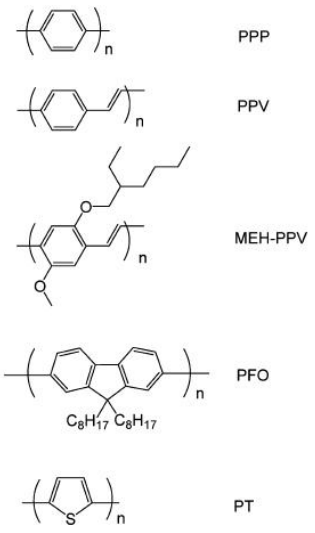

Image 17: Conjugated polymers with technologically interesting optical properties.

4.2.1 Nature of Excited States

Understanding the photophysics of certain polymers entails studying the nature of the excited state responsible for light emission. A comprehensive description of the excited state requires considering not only the interactions between electrons themselves, which fundamentally determine the transition's permissibility, but also the interaction of the electron with the lattice. This latter aspect indicates the strong correlation of the electronic structure of polymers with their respective geometry. Thus, the excitation of a polymer, whether optically (with light) or electrically (by injecting carriers), leads to the formation of two opposing charges (polarons) in the lattice, which subsequently "relaxes" to a lower energy state (lattice relaxation). These opposite charges recombine to form a neutral excited state, known as a "neutral polaron exciton," which upon de-excitation results in light emission.[4]

4.2.2 Excitons and Band Models

Until the late 1980s and early 1990s, the following two models aimed to explain the spectroscopic characteristics of conjugated polymers[5]:

1) The *semiconductor band model* assumes strong coupling between excited states, resulting in the formation of uncorrelated electron-hole pairs. According to this model, photoluminescence spectra are explained within the framework of the electron-hole recombination process, while the Stokes shift between absorption and emission spectra is perceived as evidence of polaron formation prior to recombination.

2) In contrast, the *excitonic model* posits weak coupling combined with low dielectric constants favoring the creation of strongly correlated electron-hole pairs, i.e., excitons, upon light absorption. According to this model, photoluminescence spectra are explained within the framework of the transfer of neutral excitations between segments of the polymer chain differing in excitation energy.

The latter model eventually prevailed over the former and successfully interpreted experimental results (e.g., optical absorption anisotropy). Specifically, when a photon is absorbed by a segment of the polymer chain, it creates a singlet exciton, which can then migrate to another segment of the same or a neighboring chain with lower excitation energy. At the end of this random walk, which includes only a few hops at low temperatures, the exciton will end up on a recipient segment where it will de-excite with or without radiation emission, as there are no other available segments with lower or equal energy to further migrate to.

4.2.3 Exciton Binding Energy

The exciton binding energy (E_b) is defined as the difference between the energy of formation of two independent, separated opposite charges, namely a positive and a negative polaron, and the energy of a neutral exciton polaron, including the energy due to electron-electron and electron-lattice interactions. The value of this energy in conjugated polymers is on the order of several tenths of electron volts (≈ 0.1-0.4 eV), in contrast to the excitons in inorganic semiconductors, where the corresponding energy is on the order of several millielectron volts. The small exciton binding energy of conjugated polymers is attributed to the mutual cancellation of the contributions from electron-electron and electron-lattice interactions, through the indirect effect that these interactions have on the wavefunction of the excited state. Thus, while on one

hand there exists the electrostatic Coulomb attraction between the electron and hole, simultaneously, the lattice relaxation in the exciton polaron is reduced compared to the isolated polaron.

4.2.4 Singlet/Triplet Ratio

When an organic molecule is electrically excited, the probability of forming a singlet exciton (S_1) is 25%, while the probability of forming a triplet exciton (T_1) is 75% [6]. This arises from considering that the recombination of an electron and a hole, both having spin 1/2, can occur in four different spin combinations, leading to a singlet state with parallel spins and three degenerate triplet states. Generally, these four states are considered equiprobable, resulting in a statistical ratio of singlet/triplet exciton formation of 1:3. It has been found that this does not hold true in coupled polymers, where the probability of forming a singlet exciton is much greater than that of forming a triplet exciton. Some of the theories proposed to explain the experimental results are discussed below:

- Application of molecular orbital theory in calculating the probability of singlet or triplet exciton formation in a polymer chain consisting of an electron and a hole located in two neighboring chains concludes that in the description of the recombination process, factors such as (a) the probability of the electron hopping from one chain to another and (b) the electronic repulsion between electron densities around a bond in one chain and an area of the second chain need to be considered. This latter factor differentiates the wavefunction corresponding to the simple excited state from that of the triplet. Specifically, it has been found that the wavefunction of the singlet state is more delocalized, thus resulting in better overlap with the initial state, where the carriers were separated in the two chains, and consequently a higher probability of singlet exciton formation.[7,8]

- Singlet excitons have an ionic character, while triplets have a covalent character. Since the initial polarons (positive-hole and negative-electron) are ionic species, their recombination will most likely yield another ionic species, namely a singlet

exciton. Their ratio depends on the material and is connected to it through the energy gap, which shapes the degree of ionization of the polymer.[9]

- The probability of singlet or triplet exciton formation depends on the energy exchange, i.e., the energy difference between the singlet and triplet states, Δ(S-T): if this difference is small, the energy transfer from the triplet to the singlet is faster than the de-excitation of the triplet, whereas if T_2 is large, it will preferentially transfer its energy to the nearest S rather than to T_1, thus ultimately reducing the probability of triplet exciton formation.[10] Additionally, the percentage of finally formed singlets can also be contributed by those generated from the mutual annihilation of two triplets (triplet-triplet annihilation, TTA).[11]

4.3: Electroluminescence and EL Spectroscopy in OLEDs

Organic Light-Emitting Diodes (OLEDs) have gathered significant attention due to their potential applications in various fields including display technologies, lighting, and sensing. Central to the operation of OLEDs is the phenomenon of electroluminescence (EL), where the device emits light in response to an electric current passing through it. Understanding the mechanisms of electroluminescence and employing spectroscopic techniques to analyze the emitted light spectrum are crucial for optimizing OLED performance and developing new functionalities.

This chapter aims to provide a comprehensive overview of electroluminescence in OLEDs, elucidating the underlying principles, mechanisms, and factors influencing EL efficiency. Additionally, it explores the application of electroluminescence spectroscopy (EL spectroscopy) as a powerful tool for characterizing OLED devices, analyzing their emission spectra, and gaining insights into their operational characteristics.

4.3.1: Electroluminescence in OLEDs

Electroluminescence in OLEDs occurs through the recombination of charge carriers (electrons and holes) within the organic layers of the device. When a voltage is applied across the OLED structure, electrons and holes are injected from the cathode

and anode, respectively, and transport through the organic layers. Upon reaching the emissive layer, these charge carriers undergo radiative recombination, resulting in the emission of photons.

The radiative recombination process in OLEDs involves several steps, including exciton formation, exciton diffusion, and exciton decay. Excitons are transient bound electron-hole pairs that are generated upon electron-hole recombination. Depending on the nature of excitons (singlet or triplet), different emission mechanisms such as fluorescence and phosphorescence can occur, influencing the overall electroluminescence efficiency of the device.

Several factors influence the efficiency of electroluminescence in OLEDs, including:

- Material Properties: The choice of organic materials, their molecular structure, and energy levels significantly impact the efficiency of charge injection, transport, and exciton formation.

- Device Architecture: OLED device structure, including the arrangement of organic layers, thicknesses, and electrode materials, affects charge injection, transport, and exciton confinement, thereby influencing electroluminescence efficiency.

- Charge Balance: Maintaining a balanced distribution of electrons and holes within the device is crucial for efficient electroluminescence. Imbalances can lead to non-radiative processes such as quenching and exciton annihilation.

- External Factors: External parameters such as temperature, voltage, and environmental conditions can also influence electroluminescence efficiency by altering charge carrier mobility, exciton formation rates, and device stability.[12-17]

4.3.2: Electroluminescence Spectroscopy

Electroluminescence spectroscopy is a powerful technique used to analyze the emission spectrum of OLED devices under operating conditions. EL spectroscopy involves collecting and analyzing the emitted light from the OLED device as a

function of wavelength, providing valuable information about the device's emission characteristics, spectral distribution, and efficiency.

In EL spectroscopy, a photodetector or spectrometer is used to measure the intensity of light emitted by the OLED device across a range of wavelengths. By analyzing the EL spectrum, researchers can determine the peak emission wavelength, spectral linewidth, and relative intensity of different emission peaks, providing insights into the radiative processes occurring within the device.

EL spectroscopy finds widespread applications in OLED research and development, including:

- Device Characterization: EL spectroscopy enables the characterization of OLED devices, providing information about their emission properties, spectral purity, and efficiency. By comparing EL spectra under different operating conditions, researchers can optimize device performance and identify factors limiting electroluminescence efficiency.

- Material Analysis: EL spectroscopy is used to study the properties of organic materials used in OLEDs, including their emission spectra, quantum efficiency, and energy transfer mechanisms. This information aids in the selection and design of materials with improved electroluminescence properties.

- Lifetime Assessment: Monitoring changes in the EL spectrum over time allows researchers to assess the stability and degradation mechanisms of OLED devices. By tracking variations in emission intensity, peak wavelength, and spectral shape, insights into device lifetime and reliability can be gained.

Electroluminescence and electroluminescence spectroscopy play integral roles in understanding the operational principles and optimizing the performance of OLED devices. By elucidating the mechanisms of electroluminescence and employing spectroscopic techniques to analyze emission spectra, researchers can advance the development of efficient, stable, and versatile OLED technologies for various applications. Continued research in this field holds promise for further enhancing the performance and expanding the capabilities of OLED devices in the future.[18-21]

References

[1] D. A. Dimotikali, Βασικές Αρχές Φωτοχημείας (Ε.Μ.Π., Αθήνα, 1995).

[2] N. J. Turro, Modern Molecular Photochemistry (University Science Books, 1991).

[3] A. Köhler and H. Bässler, Materials Science & Engineering R-Reports 66, 71 (2009).

[4] J. L. Bredas, J. Cornil, and A. J. Heeger, Advanced Materials 8, 447 (1996).

[5] U. Rauscher, H. Bässler, D. D. C. Bradley, and M. Hennecke, Physical Review B 42, 9830 (1990).

[6] M. A. Baldo, D. F. O'Brien, M. E. Thompson, and S. R. Forrest, Physical Review B 60, 14422 (1999).

[7] Z. Shuai, D. Beljonne, R. J. Silbey, and J. L. Bredas, Physical Review Letters 84, 131 (2000).

[8] D. Beljonne, Z. Shuai, J. Cornil, J. P. Calbert, and J. L. Bredas, Journal of Photochemistry and Photobiology A-Chemistry 144, 57 (2001).

[9] M. Wohlgenannt, K. Tandon, S. Mazumdar, S. Ramasesha, and Z. V. Vardeny, Nature 409, 494 (2001).

[10] T. M. Hong and H. F. Meng, Physical Review B 63, 75206 (2001).

[11] B. H. Wallikewitz, D. Kabra, S. Gélinas, and R. H. Friend, Physical Review B 85, 45209 (2012).

[12] Adachi, C. (2014). Third-generation organic electroluminescence materials. Springer.

[13] Baldo, M. A., O'Brien, D. F., You, Y., Shoustikov, A., Sibley, S., Thompson, M. E., & Forrest, S. R. (1998). Highly efficient phosphorescent emission from organic electroluminescent devices. Nature, 395(6698), 151-154.

[14] Friend, R. H., Gymer, R. W., Holmes, A. B., Burroughes, J. H., Marks, R. N., Taliani, C., Bradley, D. D., Dos Santos, D. A., Bredas, J. L., & Lögdlund, M. (1999). Electroluminescence in conjugated polymers. Nature, 397(6715), 121-128.

[15] Reineke, S., Lindner, F., Schwartz, G., Seidler, N., Walzer, K., Lüssem, B., & Leo, K. (2009). White organic light-emitting diodes with fluorescent tube efficiency. Nature, 459(7244), 234-238.

[16] Brütting, W., Fröbel, M., & Schmidt, T. D. (2007). Electroluminescence from triplet states in organic light-emitting diodes: A review. Materials Science and Engineering: R: Reports, 58(1-6), 1-61.

[17] Chondroudis, K., & Mitzi, D. B. (1999). Electroluminescence from an organic semiconductor heterojunction diode. Science, 283(5408), 804-806.

[18] Gather, M. C., & Reineke, S. (2013). Recent advances in light outcoupling from white organic light-emitting diodes. The Journal of Physical Chemistry Letters, 4(9), 1532-1543.

[19] Wong, W. Y., & Ho, C. L. (2010). Materials for light-emitting devices: LEDs, OLEDs, and smart pixels. John Wiley & Sons.

[20] Reineke, S., Baldo, M. A., & Forrest, S. R. (2009). Reduced efficiency roll-off in phosphorescent organic light emitting diodes containing a host material of high triplet energy. Applied Physics Letters, 94(16), 163306.

[21] Kalinowski, J., Cocchi, M., Virgili, D., Ulanski, J., Grzegorczyk, W., & Zassowski, P. (2007). Charge transport and recombination in organic light-emitting diodes. Journal of Physics D: Applied Physics, 40(2), R1.

5. Deep Electron Traps in OLEDs

Organic light-emitting diodes (OLEDs) have emerged as a promising technology for next-generation displays and lighting applications due to their high efficiency, flexibility, and low power consumption, as stated before. However, despite significant progress in OLED research and development, certain challenges persist, including device degradation over time and limited operational lifetime. One of the key factors contributing to these challenges is the presence of deep electron traps within the organic layers of OLED devices.

Deep electron traps in OLEDs can originate from various sources, including impurities introduced during material synthesis, defects at the interfaces between organic layers and electrodes, and structural imperfections within the organic semiconductor materials themselves. These traps possess energy levels located deep within the bandgap of the organic materials, making them highly effective at capturing and immobilizing electrons. As a result, they act as nonradiative recombination centers.

The presence of deep electron traps in OLEDs can have detrimental effects on device performance, leading to reduced efficiency, accelerated degradation, and non-uniform luminance. When electrons become trapped within these deep states, they are effectively removed from the charge transport and recombination processes, resulting in a decrease in the number of excitons generated and emitted photons. This phenomenon not only lowers the device's external quantum efficiency but also increases the risk of exciton-polaron quenching and exciton annihilation, further exacerbating device degradation.

Several strategies have been proposed to mitigate the adverse effects of deep electron traps in OLEDs and improve device performance and operational stability. These include material engineering approaches such as the development of trap-free organic semiconductors with minimal defect densities, the optimization of interface properties to minimize charge injection barriers and interfacial traps, and the incorporation of trap-passivating additives or dopants into the organic layers to reduce trap-mediated charge recombination. In this study, the differences between devices that have various elecrton transport layers incorporated will be shown.[1-6]

References

[1] Kondakov, D. Y., & Sandifer, J. R. (2008). Trap-assisted tunneling in organic semiconductors: II. Theoretical modeling of dark current and tunneling-limited electroluminescence in single-carrier devices. Journal of Applied Physics, 104(11), 114513.

[2] Kondakov, D. Y., & Sandifer, J. R. (2005). Transient electroluminescence from organic light emitting diodes: Bimolecular versus trap-assisted recombination. Journal of Applied Physics, 98(6), 064503.

[3] Hertel, D., Neher, D., & Meerholz, K. (2004). Charge carrier transport and trap-limited recombination in organic light-emitting diodes. Physical Review B, 69(3), 035328.

[4] Nüesch, F., & Ruhstaller, B. (2004). Charge carrier mobility and trap density in light-emitting diodes based on polyfluorene copolymers. Physical Review B, 69(12), 125203.

[5] Köhnen, A., & Reineke, S. (2019). Impact of trap-assisted and trap-free recombination on the efficiency and stability of organic light-emitting diodes. Physical Review Applied, 12(3), 034056.

[6] Kondakov, D. Y., Sandifer, J. R., Tang, C. W., & Young, R. H. (2007). Nonradiative recombination centers and electrical aging of organic light-emitting diodes: Direct connection between accumulation of trapped charge and luminance loss. Journal of Applied Physics, 101(2), 024512.

6. Fabrication Processes

The fabrication processes play a crucial role in determining the performance, efficiency, and cost-effectiveness of OLED devices. In this chapter, we delve into the key fabrication techniques employed in the production of OLEDs, including roll-to-roll manufacturing, spin coating, laser printing, vacuum thermal evaporation, and inkjet printing, among others. Each technique offers unique advantages and challenges, which are essential to understand for optimizing OLED fabrication processes.[1,2]

- *Roll-to-Roll (R2R) Manufacturing:* Roll-to-roll manufacturing is a high-throughput, continuous production process that involves depositing and patterning thin organic layers onto flexible substrates, typically using a series of rollers. In R2R OLED fabrication, flexible substrates such as plastic films are cleaned and coated with conductive materials like indium tin oxide (ITO) to serve as the anode electrode. Organic layers comprising hole transport, emissive, and electron transport materials are then sequentially deposited onto the substrate via vapor deposition or inkjet printing. Subsequently, the deposited layers are patterned by means of laser ablation or photolithography to define the pixel structure. Finally, a protective encapsulation layer is applied to prevent degradation of organic layers from exposure to moisture and oxygen. R2R manufacturing offers advantages such as high throughput, scalability, and compatibility with flexible substrates, making it suitable for large-area OLED production.[3]

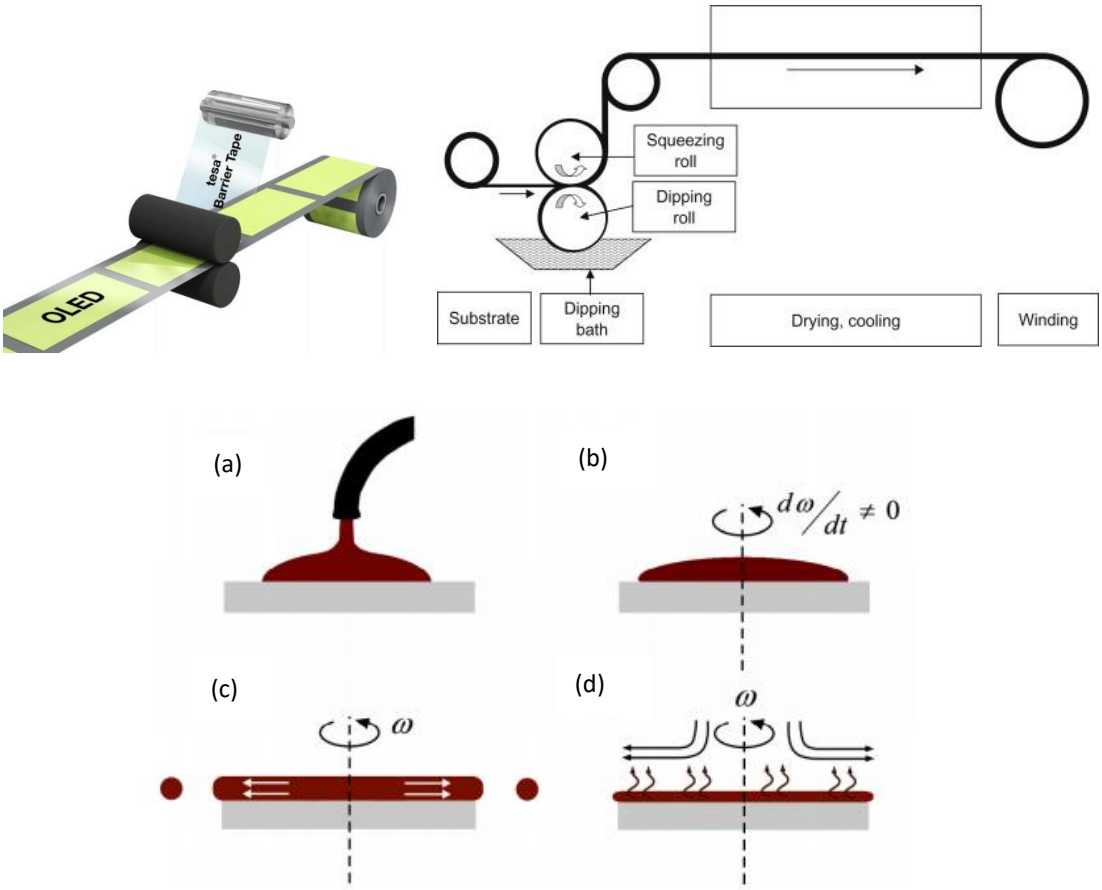

Image 18: Roll to roll technique (up) and the stages of spin coating: a) deposition of the solution, b) circular acceleration, c) uniform distribution of the material due to centrifugal force, and d) evaporation of the solvent (down).

- *Spin Coating:* Spin coating is a widely used technique for depositing uniform thin films of organic materials onto flat substrates. The process involves spinning the substrate at high speeds while dispensing a solution containing the organic material onto its surface. Organic materials are first dissolved in a suitable solvent to form a homogeneous solution. The solution is then dispensed onto the substrate, which is spun at high speeds to spread the solution uniformly across its surface. The spinning process causes the solvent to evaporate, leaving behind a thin film of the organic material on the substrate. Spin coating offers simplicity, cost-effectiveness, and versatility in depositing a wide range of organic materials, making it a preferred choice for laboratory-scale OLED fabrication and research.[4]

- *Laser Printing:* Laser printing, also known as laser-induced thermal imaging (LITI), is an additive manufacturing technique that enables precise patterning of organic layers in OLED devices. The process involves coating substrates with a

photosensitive organic material. A laser beam is then selectively applied to the photosensitive layer, inducing localized thermal or chemical reactions that define the desired pattern. Subsequently, the substrate is developed to remove the unexposed areas, leaving behind the patterned organic layers. Laser printing offers high resolution, fine feature control, and compatibility with various substrates, making it suitable for fabricating high-resolution OLED displays and microdevices.[5]

- *Vacuum Thermal Evaporation:* Vacuum thermal evaporation is a widely used technique for depositing organic thin films in OLED fabrication. In this process, organic materials are heated in a vacuum chamber, causing them to vaporize. The vaporized molecules then condense onto a cooled substrate, forming a thin film. By controlling parameters such as deposition rate, temperature, and substrate positioning, precise control over the film thickness and uniformity can be achieved. Vacuum thermal evaporation offers advantages such as high purity, excellent film quality, and compatibility with a wide range of organic materials, making it suitable for industrial-scale OLED production.[6,7]

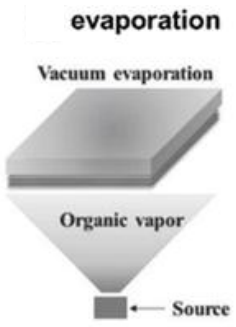

Image 19: Vacuum thermal evaporation process.

- *Inkjet Printing:* Inkjet printing is an additive manufacturing technique that involves depositing small droplets of liquid organic materials onto a substrate to form patterns or layers. In OLED fabrication, inkjet printing offers advantages such as high precision, reduced material wastage, and compatibility with flexible substrates. By optimizing ink formulations and printing parameters, inkjet printing enables the deposition of organic materials with precise control over layer thickness and composition. This technique is particularly suitable for

producing OLED displays with custom designs or patterns and holds potential for low-cost, large-area manufacturing.[8,9]

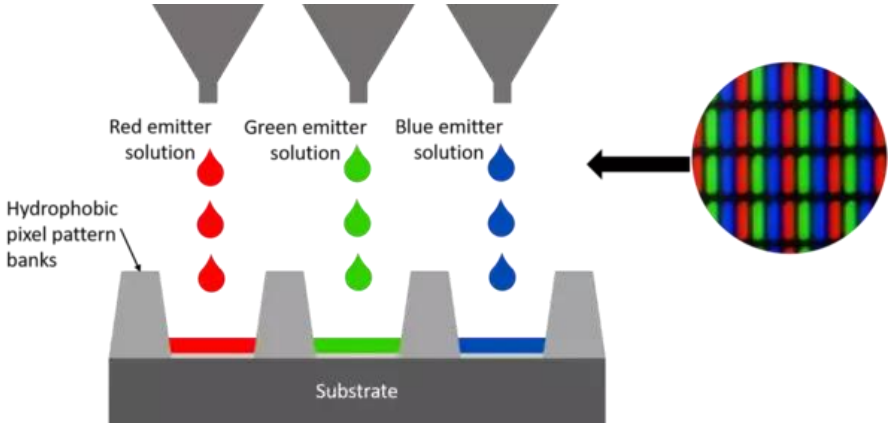

Image 20: Inkjet printing process.

Each technique has unique advantages and challenges as they are tailor made to different application requirements and production scales. Understanding these processes is essential for optimizing OLED device performance, efficiency, and cost-effectiveness, thereby advancing their widespread adoption in diverse technological applications.

References

[1] Krebs, F. C. (2009). Fabrication and processing of polymer solar cells: A review of printing and coating techniques. Solar Energy Materials and Solar Cells, 93(4), 394-412.

[2] Kaltenbrunner, M., White, M. S., Głowacki, E. D., Sekitani, T., Someya, T., & Sariciftci, N. S. (2012). Ultrathin and lightweight organic solar cells with high flexibility. Nature Communications, 3(1), 770.

[3] Pardo, D. A., Malagón, J. J., Rueda, D. R., & Velasco, J. I. (2016). Roll-to-roll manufacturing of organic electronics: barriers, solutions, and opportunities. Journal of Materials Chemistry C, 4(44), 10458-10473.

[4] Tokito, S. (2009). Organic light-emitting diodes employing spin coated polymers. Polymer Journal, 41(12), 1038-1048.

[5] Kwon, J. H., & Kim, H. S. (2012). Laser thermal transfer printing for organic light-emitting diodes. Organic Electronics, 13(11), 2326-2330.

[6] Duan, L., Hou, L., & Qiao, J. (2019). A review on the development of vacuum thermal evaporation technology in organic electronic device fabrication. Frontiers in Chemistry, 7, 34.

[7] Fässler, F., Stadlober, B., Zirkl, M., & Haase, A. (2004). Vacuum evaporation and photolithography of small-molecule organic semiconductors for organic light-emitting devices. Journal of Vacuum Science & Technology B: Microelectronics and Nanometer Structures, 22(4), 1849-1853.

[8] Kim, J. S., Jeong, H. G., Park, J. H., Lee, H. J., Choi, J. H., Lee, C. W., ... & Lee, D. Y. (2006). Organic light emitting diodes with inkjet-printed polymer layers for flexible displays. Synthetic Metals, 156(15-16), 1019-1022.

[9] Seino, Y., Yano, S., Sugiura, H., & Tokito, S. (2009). Organic light-emitting diodes fabricated by inkjet printing: ITO-free and flexible devices. Journal of Display Technology, 5(10), 395-398.

Experimental Part

1. Materials

The samples used during the experimental measurements were provided by the research center NCSR Demokritos. The polymeric materials from which the organic light-emitting diodes (OLEDs) are constructed, available to us, are divided into the following categories:

1) Coupled/Semiconducting Polymers (PEDOT:PSS, F8BT):

PEDOT:PSS is a conducting polymer composed of the coupled polymer poly(3,4-ethylenedioxythiophene) [PEDOT], a derivative of polythiophene, doped with the anionic polyelectrolyte poly(styrene sulfonate) [PSS]. PSS serves as the charge-balancing counter-ion, maintaining electro-neutrality, but also contributes to the water-soluble nature of PEDOT:PSS. The membrane of PEDOT:PSS consists of acidic PSSH-rich surfaces, while the bulk of the membrane is in the form of granules, each comprising a core of PEDOT doped with PSS and acidic PSSH segments on the outer shell. It was used as the injection and hole transport layer, coated on glass/ITO substrates, to reduce the work function (PEDOT:PSS $E_F \approx 5.2$ eV) and thus the barrier between the electrode and the HOMO level of the polymer, which constitutes the emissive active layer. Additionally, it helps to reduce the roughness of the ITO surface to minimize leakage current.[1]

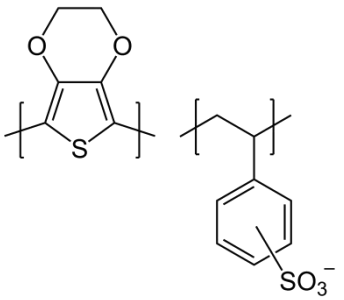

Image 21: Structure of PEDOT:PSS.

Fluorene-based copolymers, such as poly(9,9-dioctylfluorene-alt-benzothiadiazole) known as *F8BT*, are commonly utilized as the emission layer in organic light-emitting diodes (OLEDs) due to their high photoluminescence quantum yield and excellent

film-forming properties. F8BT emits light in the green to yellow spectral region, making it suitable for various display and lighting applications. As the emission layer, F8BT facilitates the generation and radiative recombination of excitons formed by the injection of charge carriers from the adjacent electron-transport and hole-transport layers. The efficient energy transfer and exciton confinement within the F8BT layer led to the emission of photons with high external quantum efficiency. Moreover, F8BT exhibits good thermal and morphological stability, contributing to the long-term performance and operational reliability of OLED devices.

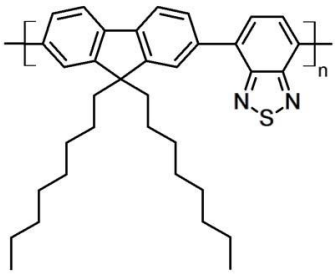

Image 22: Structure of F8BT.

2) Intermediate Layers:

I) C-Dots (Carbon Dots): Carbon dots are nanoparticles that have a quasi-spherical shape and consist of amorphous crystalline carbon. Carbon dots are considered zero-dimensional materials since the atoms of the nano-carbon do not exceed 10 nm.[2] In the samples used in this work, carbon dots acted as charge regulators to ensure charge balance and high performance. Carbon dots possess high electron affinity and work function, making them suitable for efficient charge injection and transport. By introducing carbon dots at interfaces between different functional layers, such as the electron transport layer and the emissive layer, device efficiency and stability can be improved. Carbon dots can help in reducing energy barriers for charge carrier injection and minimizing exciton quenching at the interfaces, leading to enhanced device performance. They are typically synthesized using low-cost precursors through solution-based methods, making them highly attractive for large-scale manufacturing of OLEDs. Their solution-processability enables the deposition of uniform and thin

carbon dot layers over large-area substrates using techniques such as spin-coating, inkjet printing, or spray coating. This makes them suitable for the fabrication of flexible and transparent OLED displays. Compared to traditional OLED materials that may contain heavy metals or rare earth elements, carbon dots are often considered more environmentally friendly. They are composed of carbon-based compounds and can be derived from sustainable sources, contributing to the development of greener optoelectronic technologies.[3]

II) NC-Dots (Nitrogen Carbon Dots): They were used for the same purpose as carbon dots and are the result of doping carbon dots with nitrogen. As a result, many pores were created, which ultimately were occupied by pieces of PEDOT:PSS or by inert air and/or nitrogen gases that hinder thermal conduction. Thus, these gases create additional layers besides those known to exist between the anode and cathode. The coupled structures, especially the π-electrons, break upon doping carbon with nitrogen thusimproving the electron mobility. Consequently, the heat transfer from moving electrons is reduced. These layers also induce phonon scattering, as their surface is not smooth and causes irregularities in the contact between PEDOT:PSS and F8BT. In addition, the incorporation of NC-Dots in OLEDs can also lead to enhanced device

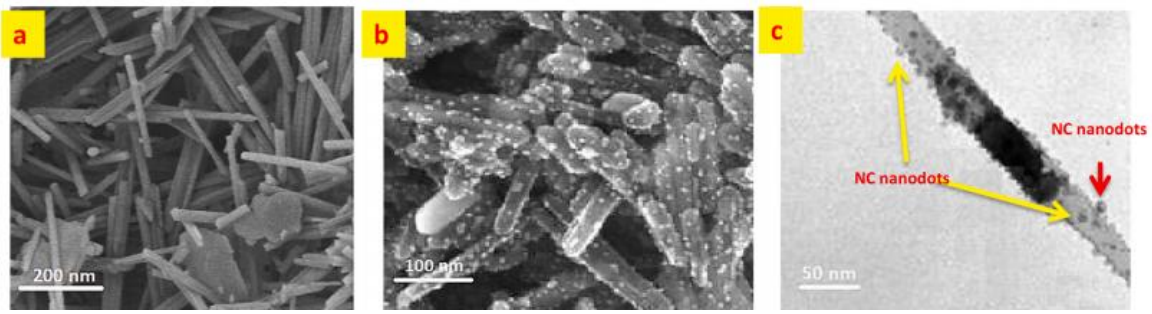

Image 23: NC-Dots aggregates under the microscope.

stability and efficiency. The introduction of nitrogen atoms into the carbon dots can alter their chemical and electronic properties, potentially resulting in better charge injection and transport characteristics within the OLED structure.[4] Moreover, the presence of nitrogen functionalities may contribute to the formation of stable interfacial layers, reducing the likelihood of device degradation over time. Furthermore, the precise control over the nitrogen doping level in NC-Dots offers opportunities for fine-tuning the OLED performance parameters, such as luminance, color purity, and operational lifetime. Overall, the utilization of NC-Dots holds

promise for advancing the development of high-performance and long-lasting OLED devices.

III) Cesium carbonate (Cs_2CO_3): Cesium carbonate also gained significant attention as a versatile material for electron transport layers (ETLs) in organic light-emitting diodes (OLEDs). Its suitability stems from a combination of favorable properties that contribute to enhanced device performance and stability. One key advantage of Cs_2CO_3 is its high electron mobility, which facilitates efficient electron transport through the ETL.[5]

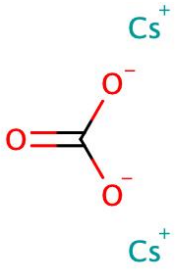

Image 24: Structure of Cesium Carbonate.

This property is crucial for ensuring rapid and uniform electron injection from the cathode into the emissive layer, thereby promoting balanced charge carrier transport and reducing charge accumulation at the electrode interfaces. Additionally, Cs_2CO_3 exhibits excellent film-forming properties, enabling the fabrication of smooth and uniform ETL films over large areas, which is essential for achieving uniform device performance and minimizing non-uniform luminance distribution. Furthermore, Cs_2CO_3 possesses a wide bandgap and a low-lying conduction band energy level, making it effective in blocking the injection of holes from the anode while facilitating electron injection. This feature contributes to improved charge balance and reduced exciton quenching at the interface between the ETL and the emissive layer, resulting in enhanced electroluminescence efficiency and color purity. Moreover, Cs_2CO_3 can act as a buffer layer, effectively aligning the energy levels at the electrode interfaces and reducing energy level barriers for charge injection and extraction. This property enhances device stability and operational lifetime by minimizing charge trapping and ensuring efficient charge carrier injection and extraction. Overall, the multifaceted advantages of Cs_2CO_3 make it a promising candidate for ETL materials in OLEDs,

with the potential to significantly enhance device performance, uniformity, and longevity in various optoelectronic applications.[6]

IV) Zinc Porphyrin amidine (ZnP-amidine) compounds, derived from zinc porphyrin and amidine moieties, have emerged as promising candidates for various roles in organic light-emitting diodes (OLEDs) owing to their unique chemical structure and advantageous properties. Porphyrins are aromatic macrocycles containing four pyrrole subunits interconnected by methine bridges. These structures possess π-conjugated systems, endowing them with excellent electronic properties, including high electron affinity and efficient charge transport capabilities. Amidines, on the other hand, are organic compounds characterized by the presence of an amidino group (-C(NH_2)=NH) bonded to a nitrogen atom. They exhibit strong electron-withdrawing properties and can act as Lewis bases, facilitating coordination interactions with metal ions such as zinc. ZnP-amidine compounds combine the beneficial attributes of both porphyrins and amidines.

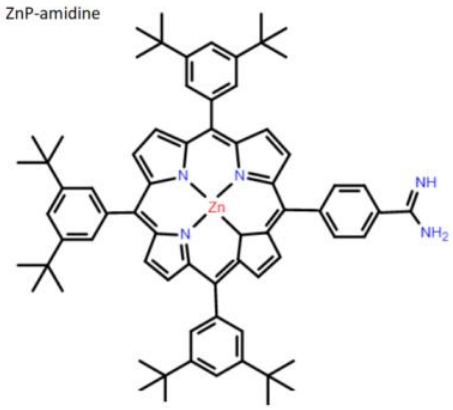

Image 25: Structure of ZnP-amidine.

As electron transport materials, ZnP-amidines exhibit high electron mobility, facilitating efficient charge injection and transport within the device. The conjugated framework of the amidine ligands allows for effective delocalization of π-electrons, ensuring rapid electron transfer from the cathode to the emissive layer. This characteristic promotes balanced charge transport and mitigates the formation of non-radiative recombination centers, thereby enhancing the electroluminescence efficiency and color purity of OLEDs. Additionally, ZnP-amidines possess favorable thermal and morphological stability, ensuring device integrity and longevity under operating

conditions. Their tunable electronic and optical properties enable precise control over device characteristics, including emission wavelength, intensity, and spectral purity. Furthermore, ZnP-amidines can serve as versatile host materials in OLED emissive layers, providing a stable and efficient matrix for guest emitter molecules. The ability to tailor molecular structures and functional groups offers opportunities for the design of customized OLED architectures with improved performance, stability, and functionality. Overall, ZnP-amidine compounds represent a promising class of materials with significant potential for advancing OLED technology and enabling the development of next-generation displays, lighting systems, and optoelectronic devices.[7]

During the experimental measurements, careful cleaning of the organic samples was required. The purpose of this procedure was to dissolve the upper layers of each OLED locally so that proper contact could be made between the needle and the ITO, as will be further explained in the next chapter. The solvents used to serve this purpose were acetone (CH_3COCH_3) and isopropyl alcohol ($CH_3CHOHCH_3$).

3) Anode and Cathode

Indium Tin Oxide (ITO) is widely utilized as a transparent conducting oxide (TCO) in organic light-emitting diodes (OLEDs) due to its excellent combination of optical transparency and electrical conductivity. As the anode material in OLED devices, ITO plays a crucial role in facilitating the injection of positive charge carriers (holes) from

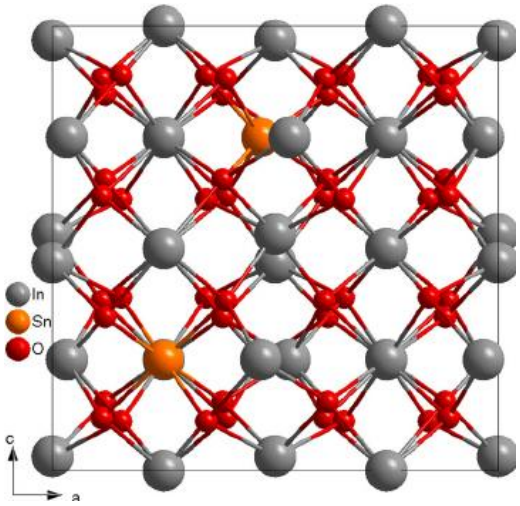

Image 26: Structure of ITO.

the anode into the organic layers, thus enabling efficient electron-hole recombination and light emission. Its high transparency allows emitted light to pass through the anode with minimal absorption, resulting in enhanced device efficiency and luminance. Moreover, ITO's compatibility with various organic semiconductors and stability under operating conditions make it a preferred choice for OLED fabrication. Furthermore, ITO's durability and resistance to oxidation make it a reliable choice for prolonged device operation, ensuring stable performance over time.[8-10]

Aluminum (Al) serves as a common choice for the cathode material in organic light-emitting diodes (OLEDs) due to its low work function (~4.16 eV) and good electron injection properties. As the cathode, aluminum facilitates the injection of negative charge carriers (electrons) from the cathode into the organic layers, promoting efficient electron-hole recombination and light emission. Its low work function ensures that electrons can easily flow from the cathode into the organic layers, leading to the formation of excitons and subsequent light emission. Aluminum's compatibility with organic materials and ease of deposition makes it a widely used material in OLED fabrication processes.[11]

References

[1] M. Gross, D. C. Müller, H. G. Nothofer, U. Scherf, D. Neher, C. Bräuchle, and K. Meerholz, Nature 405, 661 (2000).

[2] Lagonegro, P.; Giovanella, U.; Pasini, M. Carbon Dots as a Sustainable New Platform for Organic Light Emitting Diode. Coatings 2021, 11, 5.

[3] Georgiopoulou,Z.; Verykios, A.; Ladomenou, K.; Maskanaki, K.; Chatzigiannakis, G.; Armadorou, K.-K.; Palilis, L.C.; Chroneos, A.; Evangelou, E.K.; Gardelis, S.; et al. Carbon Nanodots as Electron Transport Materials in Organic Light Emitting Diodes and Solar Cells. Nanomaterials 2023, 13,169.

[4] El-Shamy A. G., The Role of Nitrogen-Carbon Dots (NC) Nano-particles in Enhancing Thermoelectric Power Functions of PEDOT:PSS/Te Nano-composite Films, Chemical Engineering Journal 417 (2021) 129212

[5] Han, T. H., Kim, J. H., Lee, K. H., & Han, Y. K. (2009). Enhanced electron injection by cesium carbonate: An effective approach for achieving high efficiency phosphorescent OLEDs. Advanced Materials, 21(26-27), 2747-2751.

[6] Park, J. S., Kim, K. H., Kim, K. H., Seo, J. H., Lee, S. H., Yoon, S. S., & Kim, J. J. (2010). Cesium carbonate as an efficient electron injection/transport layer for blue phosphorescent organic light-emitting diodes. Organic Electronics, 11(5), 920-924.

[7] Soultati, A., Verykios, A., Tsekouras, M., Georgiopoulou, Z., et al. A zinc porphyrin- amidine as a green carbon- based electron transportmaterial for organic- light emitting diodes. Applied Physics A (2024) 130:172.

[8] Kim, Y. H., Lee, J., & Kim, J. J. (2011). Transparent conducting oxides for organic light-emitting diodes. Chemistry of Materials, 23(14), 3414-3423.

[9] Lin, M. Y., & Chen, Y. T. (2009). Characteristics of organic light-emitting diodes with an ITO/Ag/ITO transparent electrode. Journal of Applied Physics, 106(8), 083104.

[10] Li, Z., Zhang, Z., Hu, H., Li, X., Qiao, J., Zhang, Y., ... & Yu, G. (2011). High-performance flexible organic light-emitting diodes fabricated on novel composite transparent conductive substrates. Advanced Functional Materials, 21(13), 2488-2494.

[11] So, F., & Kido, J. (2008). Organic light-emitting devices for solid-state lighting. MRS Bulletin, 33(7), 663-669.

2. Device Fabrication

OLED devices were fabricated on ITO coated glass substrates of sheet resistance of 20 Ω/sq, which served as anode bottom electrodes. Prior to the deposition of organic semiconductors, the substrates were successively sonicated for 10 min in acetone, 2-propanol and deionized water and then dried in nitrogen flow. Next, the substrates were subjected to oxygen plasma treatment for 10 minutes followed by deposition of a thin (~ 40 nm) layer of poly(3,4- ethylenedioxythiophene)-poly(styrenesulfonate) (PEDOT-PSS, 1.3 wt. % dispersion 15 in H_2O) (purchased from Sigma Aldrich) which was filtered using a 0.45μm PVDF filter and spin coated in ambient conditions at 7000 rpm for 40 sec and then annealed at 130 ^oC for 30 min. The emissive layer (F8BT, with a 9:1 F8:BT ratio, purchased from American Dyes Source, ADS 233 YE) was then spin coated from a 10 mg/mL solution in chloroform, filtered through a 0.22 μm pore size PTFE filter, at 1200 rpm for 40 sec to form a ~ 100 nm thick layer on top of PEDOT-PSS and then annealed at 95 ^oC for 10 min. In the control devices, a thin layer of ZnP-amidine/Cs_2CO_3/C-Dots/NC-Dots was deposited on top of F8BT via spin coating at 2000 rpm for 40 sec, from a methanol solution with a concentration of 5 mg/mL to serve as electron injection/transport layer. The devices were finally completed with a 150 nm aluminum cathode deposited through a shadow mask in a dedicated chamber.

3. Experimental set-up

In the Semiconductor Devices Research Laboratory (SDRL) of University of Ioannina there are two measuring probe stations where electrical and optical characterization experiments can be conducted simultaneously. We hereby assign different names i.e metallic and wooden station with respect to the box's material used. Both stations provide excellent shielding from external light, EM radiation while maintain a rather constant ambient temperature.

The experimental techniques conducted in both stations utilize measurement(s) of the following electro-optical quantities:

- Current intensity as a function of applied voltage (I-V)
- Luminance as a function of applied voltage (L-V)

- Current intensity as a function of time (I-T)
- Luminance as a function of time (L-T)
- Capacitance as a function of voltage (C-V)
- Capacitance as a function of frequency (C-f)
- Electroluminescence spectra (EL)

The metallic station was used for measurements obtained at longer time scales as compared to the same measurements taken in the wooden one. By taking measurements over a longer period of time, we can gather more information regarding reliability issues of the diodes under test. This is common in OLEDs as ambient temperature, humidity, oxygen present in atm as well as self-heating factors lead to optical and electrical degradation.

I) Metallic Station

The experimental set-up for the electro-optical measurements uses the following instruments (see Image 27):

- KEITHLEY 230 Programmable Voltage Source
- KEITHLEY 617 Programmable Electrometer
- HP 4140B pA Meter/DC Voltage Source

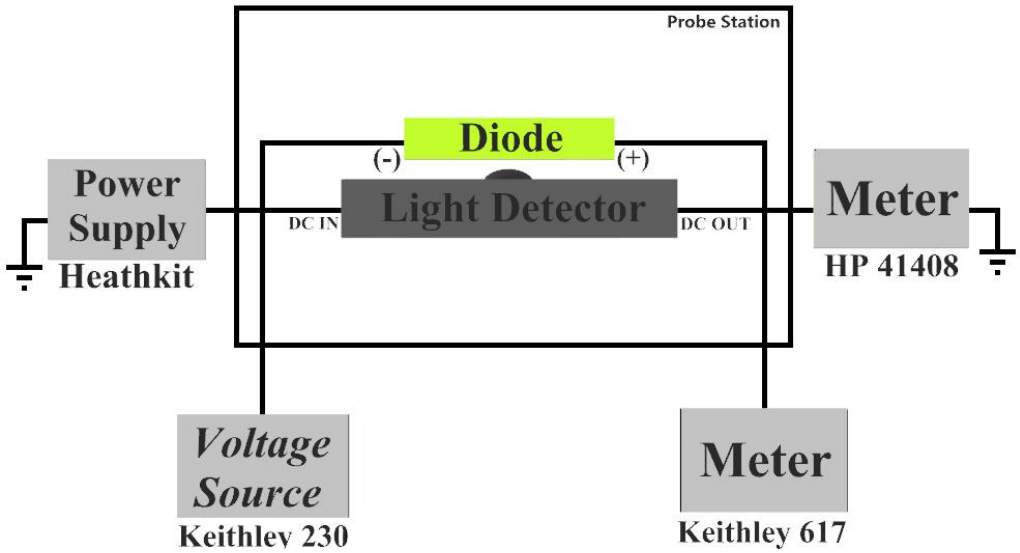

Image 27: Block diagram of the metallic measuring station.

All instruments are interconnected via GPIB cables so that, using the appropriate LabView program(s), experimental data are automatically obtained.

With the aim of achieving the best possible measurement, each OLED is carefully placed on the photodetector, and each diode is precisely aligned with it using a microscope (Image 28 (left)). The contact on the OLED is made with metallic tips. One tip has a spherical end, and thus a larger diameter, and is used to touch the cathode of the diode, namely the aluminum dot, without piercing or damaging it. Conversely, the other tip has a pointed end and is used to penetrate the OLED reaching the ITO electrode (Image 28 (right)).

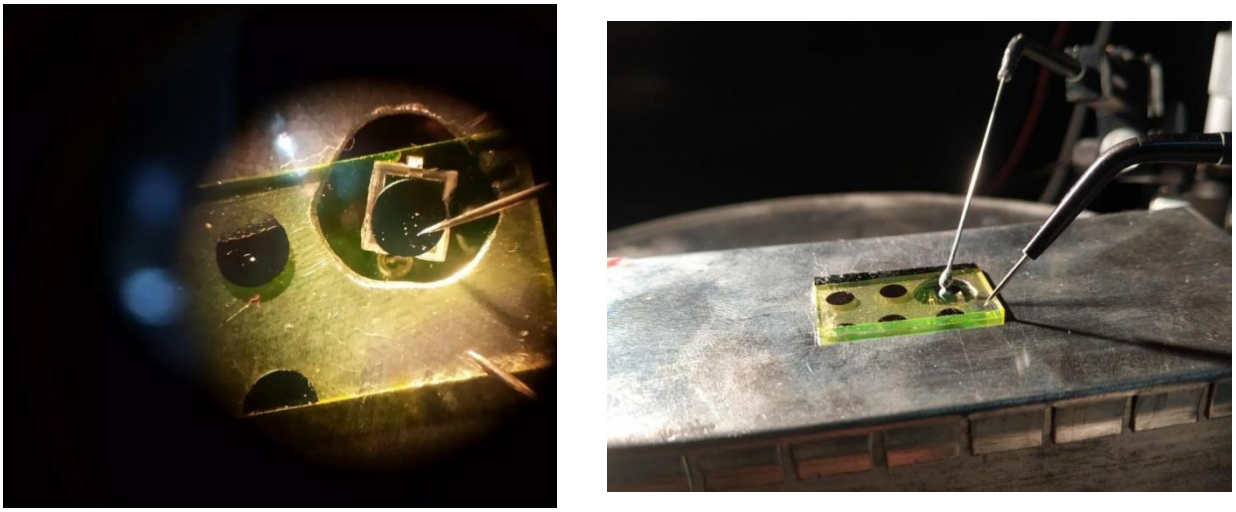

Image 28: OLED alignment with the photodetector under the microscope (left), spherical and pointy pins in contact with the device (right).

The photodetector is placed inside a dark box so that it exclusively measures the light emitted by the organic diodes. Consequently, absolute darkness conditions prevail inside the chamber to ensure that the measurement results are not affected. The photodetector of the circuit constitutes a separate circuit on its own, as depicted in the following diagram (Image 29), which is housed within the metallic box and is based on a a BPW34 type photodiode. The box carries sockets for BNC cables that connect the photodetector circuit with the rest of the experimental setup.

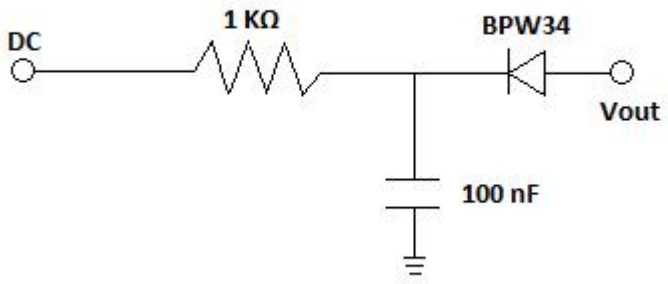

Image 29: Photodetector circuit diagram.

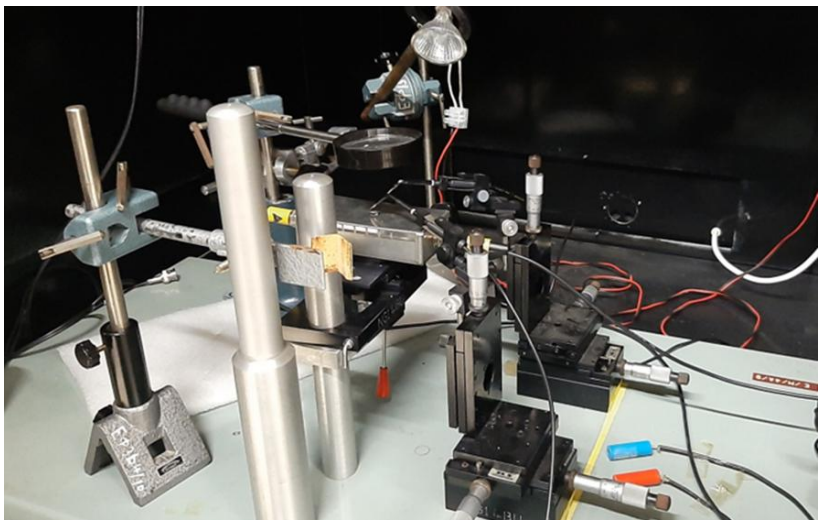

Image 30: Metallic measuring station.

Moreover, by adding an optical fiber (Image 31) the circuit is altered so as to measure

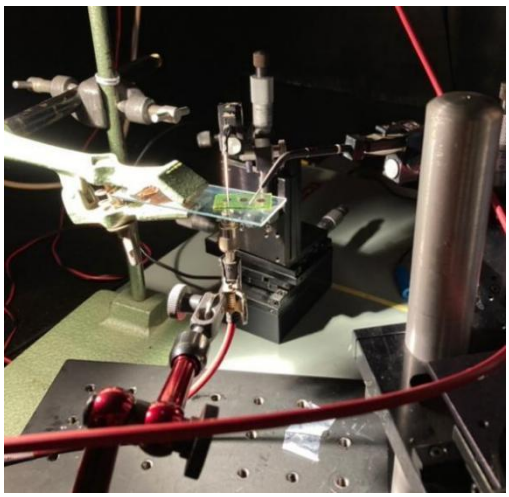

Image 31: Metallic measuring station with optical fiber added.

electroluminescence spectra, by using the corresponding software.

II) Wooden Station

The purpose of the experiments is to simultaneously measure the electric current passing through each photodiode and the luminous radiation it emits in relation to the applied potential difference. To perform current (I) - voltage (V) and luminance (L) - voltage (V) measurements, we use the program we created in the TSP environment.

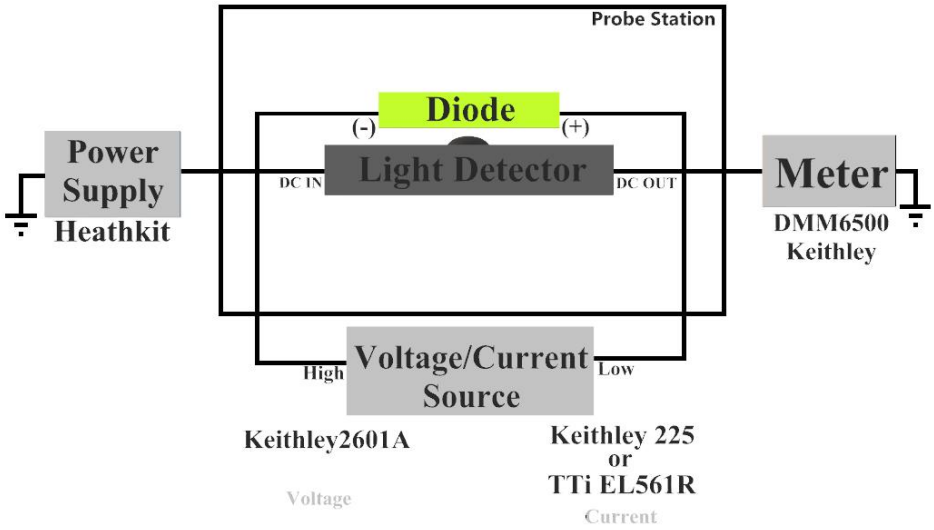

Image 32: Block diagram of the wooden measuring station.

As stated before, the measurements retrieved at this station are taken in a shorter time span in order to study transient processes or phenomena that only appear at the order of nanoseconds. At this station the utilized instruments are connected as shown below and include a voltage/current source, a multimeter and a power supply.

Similar to the metal station, the photodetector's circuitry is depicted in the following diagram (Image 33), which is also housed within a metallic box. This photodetector box is based on the FDS100 photodiode.

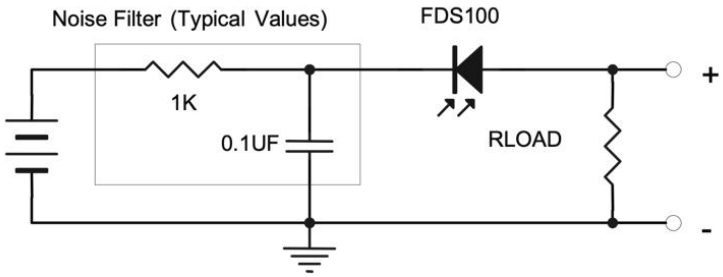

Image 33: Photodetector circuit diagram.

Image 34: Wooden measuring station.

4. Experimental Process

Current-Voltage (I-V) and Luminance-Voltage (L-V) curves were obtained simultaneously on fresh or electrically stressed devices to investigate both the current conduction mechanisms as well as the evolution of deep electron traps that affect the turn on voltage and the overall quality of the tested OLEDs. I-V and I-t measurements were conducted by using two separate stations; one suitable for shorter intervals of time (~100 ns) and one for longer ones (~100 ms) as previously described. Capacitance-Voltage (C-V) and Capacitance-Frequency (C-f) were employed in order to gain insights to the carrier dynamics of the devices.

The various OLEDs studied had a layered structure (Image 35), where the reference sample is ITO/PEDOT/F8BT, with no ETL, while all others have an additional

intermediate layer between F8BT and the Al electrode (F8BT/C-DOTS, F8BT/NC-DOTS, F8BT/Cs_2CO_3, and F8BT/ZnP-amidine). The main aim of this work is to compare the I-V and L-V obtained from each sample to determine whether any of these additional intermediate layers enhance the operational (i.e. optical/electrical) performance or the lifespan of the OLEDs and associate any differences to the physics of the corresponding carrier conducting mechanisms.

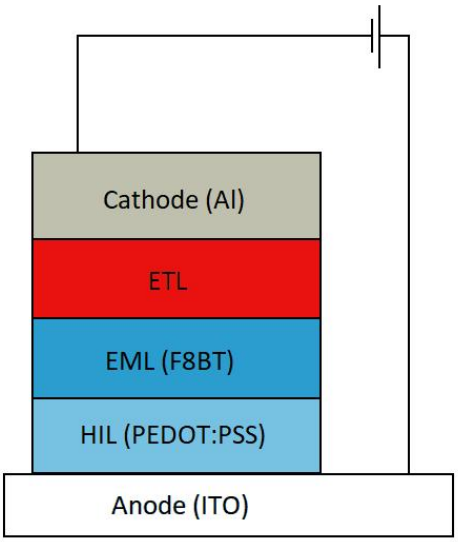

Image 35: OLED architecture of studied samples

Some of the OLEDs were circular with r = 2 mm while other were squares with a = 1 mm (Image 36). The differences between the regular sized and smaller devices shall

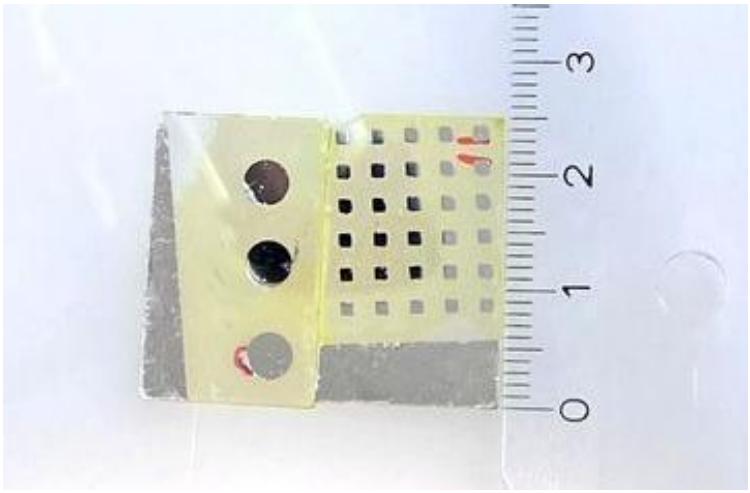

Image 36: Different sized diodes. Circular diodes with 2 mm radius (left) and square diodes with 1 mm side length (right).

be discussed in detail in a following chapter.

4.1 Sample Preparation

All samples are stored in vacuum chambers when not in use to prevent them from being affected by atmospheric air and humidity. Initially, the sample is removed from the vacuum conditions and is placed on a clean work surface. Then, using acetone (CH_3COCH_3, Acetone), a spot is carefully dissolved on the upper layers, aiming to reveal the clean ITO surface. This step is necessary in the process because the ITO serves as an electrode on which one measuring tip must make contact.

Finally, each sample undergoes annealing at ambient environment, in order to cure from moisture, OH^- and O_2 contamination. Therefore, each sample is placed on a hot plate for 10 minutes at 100°C. This step was found to improve the performance of the

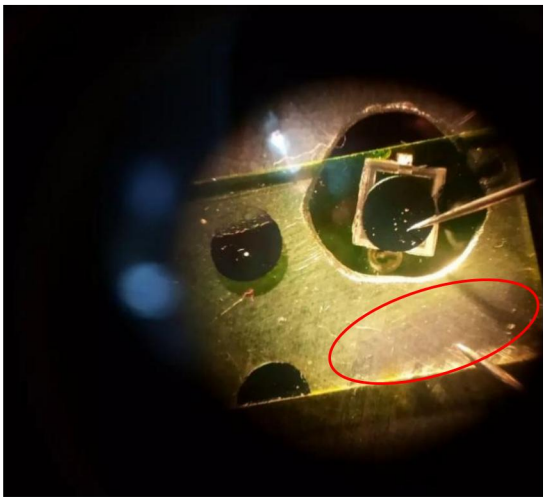

Image 37: OLED under the microscope aligned with the photodetector. Exposed ITO is visible (circled).

organic diodes considerably, resulting in clean samples, ready for transfer to the dark chamber and the initiation of the experimental procedures.

4.2 Measurements

After placing the sample in the metallic dark chamber, we carefully touch the pins on the electrodes and ensure that an ohmic contact is achieved. Then, using a LabView program, we select the minimum and maximum voltage (maximum voltage 15-18 V)

to be applied to each diode, as well as the step by which it will change (typical value for voltage step = 0.250 V). Additionally, we choose the number of measurements (number of measurements) to be taken, the average of which gives us the final measurement, along with the corresponding time (time of measurement). In this work, the number of measurements was set to 2, and the measurement time was set to 200 ms. Finally, we obtain a list of all measurements through the program, which gives us the I-V curves we need.

We follow the same procedure with reverse biasing,. As a result, this allows us to control the behavior of the organic diodes in the negative voltage region. Thus, we include the reversed measurements in the final graphs.

The HP 4140BpAMeter/DC Voltage Source, as mentioned above, measures the current flowing through the photodetector in amperes. To convert the units from radiometric to photometric, we need to convert the current flowing through the photodetector into irradiance. This is made possible thanks to the characteristics of the

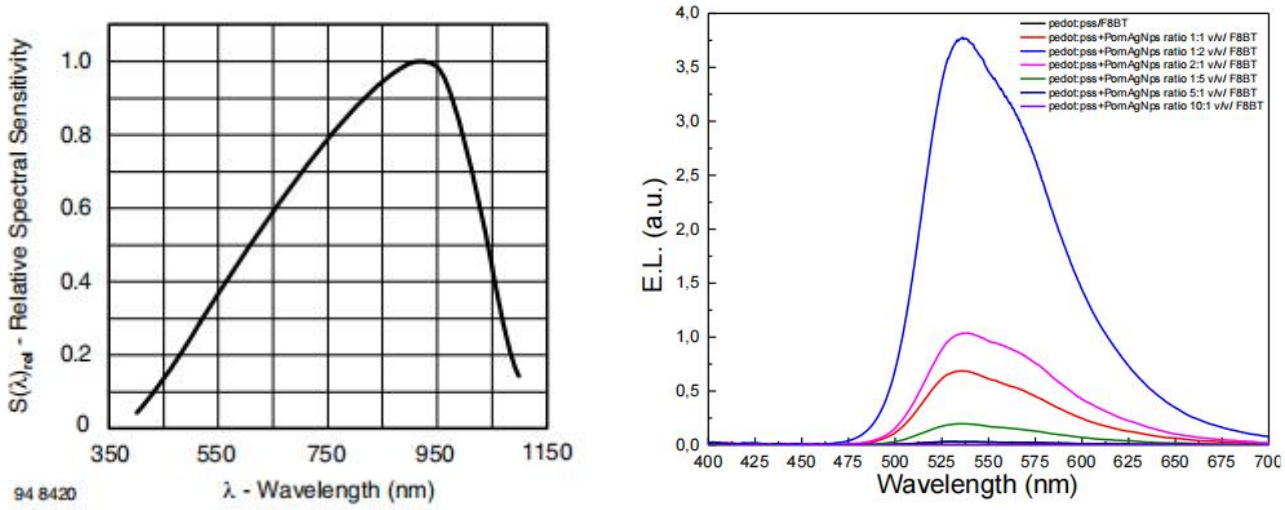

Image 38: (a) Relative Spectral Sensitivity vs Wavelength curve for BPW34, (b) EL spectrum of reference devices.

BPW34 diode located in the photodetector circuit, which are provided by the manufacturer. We will also use the graph Relative Spectral Sensitivity vs Wavelength (Image 38a), which shows us what factor to use depending on the wavelength emitted by the OLED we are interested in. In our case, our OLEDs emit a wavelength equal to 536 nm (Image 38b). Therefore, for this wavelength, the relative spectral sensitivity is 0.31, and we will multiply our relation by this factor.

Then we divide by the radiant sensitive area, which is the area of the photodiode that is sensitive to light, according to the manufacturer, which is: A = 7 mm². Finally, the irradiance will be:

$$(\text{irradiance})[\,{}^{\mu W}/_{mm^2}\,] = (\text{current})\ [\mu A] * \frac{1}{7mm^2 * 0.31\ [\,{}^{A}/_{W}\,]} \quad (16)$$

To convert from radiometric to photometric units, we finally use the following formula:

$$(\text{photometric unit}) = (\text{radiometric unit}) \times 683 \times V(\lambda) \,/\, (2\pi \times 100) \quad (17)$$

where V(λ) is the photopic response, which indicates how well the human eye can detect a specific wavelength. The photopic response is a function of the wavelength, so in order to find it, it is necessary to know the light source. In the present thesis, the light source is, of course, the organic light-emitting diodes. Therefore, the relation between the intensity of the electric current and the intensity of radiation alone is not enough. We also need the wavelength emitted by the OLEDs (ITO/PEDOT:PSS/F8BT), which we extract from the electroluminescence spectrum, as mentioned earlier, and the wavelength is equal to 536 nm.

In order to calculate the photopic response, the following approximation, derived from experimental data, is used:

$$V(\lambda) = 1.019\ e^{-285.4(\lambda - 0.559)^2} \quad (18)$$

Where λ is the wavelength in micrometers. Substituting λ = 0.536 μm into the above equation, we obtain V(λ) = 0.876. Therefore, now we are able to convert the intensity of the electric current obtained from the HP 4140B pAMeter / DC Voltage Source instrument into irradiance (radiation intensity) and from that into luminance or luminous flux.

Lumens (lm) are the photometric equivalent of watts, "weighted" to match the sensitivity of the observer's eyes. Yellow-green light has more weight, as it stimulates the eye more than blue or red light. The number 683 in the formula arises from the

definition of lumens, as 1 Watt = 683.0 lumens at 555 nm, the wavelength at which the human eye exhibits maximum sensitivity.

On the other hand, candela is a unit of luminous intensity, which is the amount of light emitted in a particular direction per unit solid angle. Converting from lumens (lm) to candela (cd) involves a solid angle factor, which is the angle at which the light is emitted. To convert lumens (lm) to candela (cd), we must consider the solid angle under which the light is emitted. The total solid angle around a source is 4π, which is the solid angle of a sphere, but we are only interested in the portion of the sphere from which the OLEDs emit light. In our case, the samples emit light over half of a sphere, so the formula for conversion is:

$$(\text{luminous intensity})[\text{cd}] = (\text{luminous flux})[\text{lm}]/(\text{solid angle})[\text{sr}]$$

$$\rightarrow \ \text{cd} = {}^{\text{lm}}/_{\pi} \qquad (19)$$

Finally, the factor 1/100 arises from converting irradiance from [$\mu W/mm^2$] to [W/m^2].

For the I-t and L-t measurements, in addition to the BPW34 diode, we use the FDS100 photodiode, resulting in a change in the process of converting luminous radiation into photometric units. Initially, we place our sample in the wooden dark chamber and then adjust the probes to properly touch it. Depending on the duration we want a measurement to last, with the help of the TSB program, we select the time and simultaneously the voltage that will flow through the sample. After selecting the commands related to the characteristics with which the measurement will be performed, either manually or from the TSB program environment, we obtain all the experimental values we need.

For the case of the FDS100 diode, we use the Responsivity (A/W) vs Wavelength graph (Image 39), which indicates a spectral sensitivity of 0.33 for the wavelength equal to 536 nm, emitted by the OLEDs. Since the diode has an internal resistance of 100 KΩ, in order to perform the conversion, the voltage recorded by the instrument for each measurement must first be divided by the diode's resistance.

$$\text{I(A)} = \frac{\text{V(V)}}{10^5} \qquad (20)$$

Then, we divide by the radiant sensitive area, which is not that of the photodiode but rather according to the manufacturer, which is: A = 13 mm^2.

Finally, we get:

$$(irradiance)[{}^{\mu W}/_{mm^2}] = (current)[\mu A] * \frac{1}{13\ mm^2\ x\ 0{,}33[{}^{A}/_{W}]} \qquad (21)$$

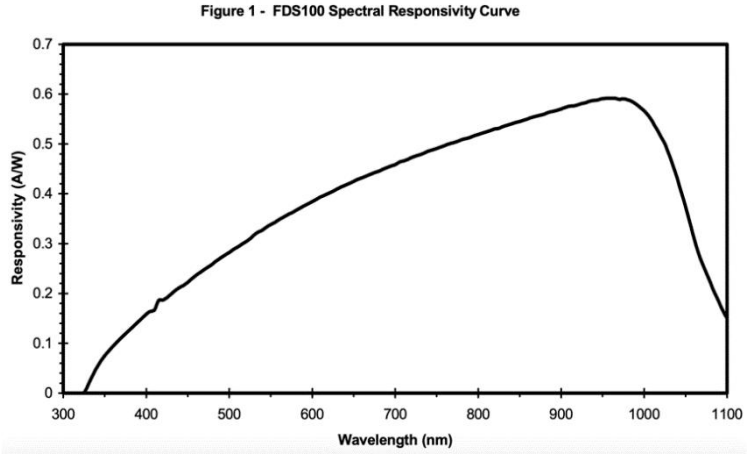

Image 39: Spectral Responsivity vs Wavelength curve for FDS100.

After retrieving the radiometric values, we can then convert them in photometric by using the relation we examined before (Eq. 17).

Electroluminescence spectra were also retrieved from reference and ZnP-amidine devices in order to compare them and check for ant differences. Electroluminescence (EL) spectroscopy differs from photoluminescence (PL) spectroscopy in terms of the excitation source, which in this case is electrical rather than optical. Thus, by applying a voltage across the ends of two electrodes, electron and hole injection occurs in the organic layer sandwiched between them, thereby creating an excited state (exciton) that emits light upon de-excitation.

The emitted light is collected via an optical fiber, which has a diameter larger than the diameter of the setup, ensuring the collection of all emitted light in the vertical direction. The optical fiber was an added feature to the metallic station described earlier. Spectra were measured with a step of 0.5s, but in the diagrams for the reference and ZnP-amidine, which were obtained through measurements, they are presented every 10s. The study of electroluminescence spectra was conducted using

the normalization process. Subsequently, the analysis of the overall spectra was performed through fitting, where the average value was calculated from the spectra, removing the noise that appears in the results.

4.3 Results and Discussion

4.3.1 Thin Film Characterization

Some other techniques that were utilized for thin film characterization include X-Ray Diffraction (XRD), Atomic Force Microscopy Topography (AFM) and contact angle measurements regarding the hydrophobicity of the materials.

The hydrophobic nature of ZnP-amidine slightly improves the hydrophobicity of the F8BT film, as observed by the contact angle measurements (Image 40), which may influence the device stability.

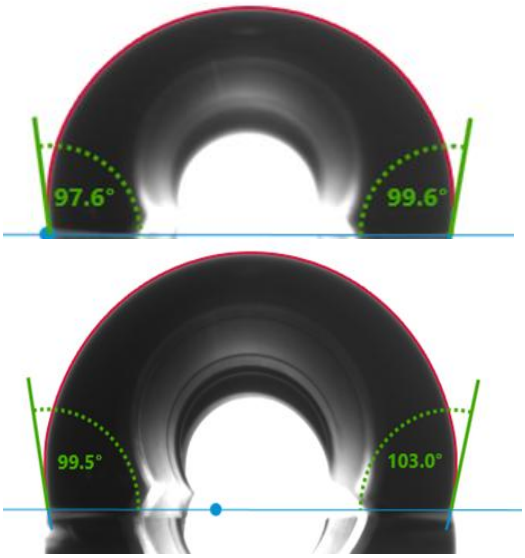

Image 40: Contact angle measurements of F8BT (top) and F8BT/ZnP-amidine (down).

From XRD measurements it is retrieved that in the case of the F8BT/ZnP-amidine the

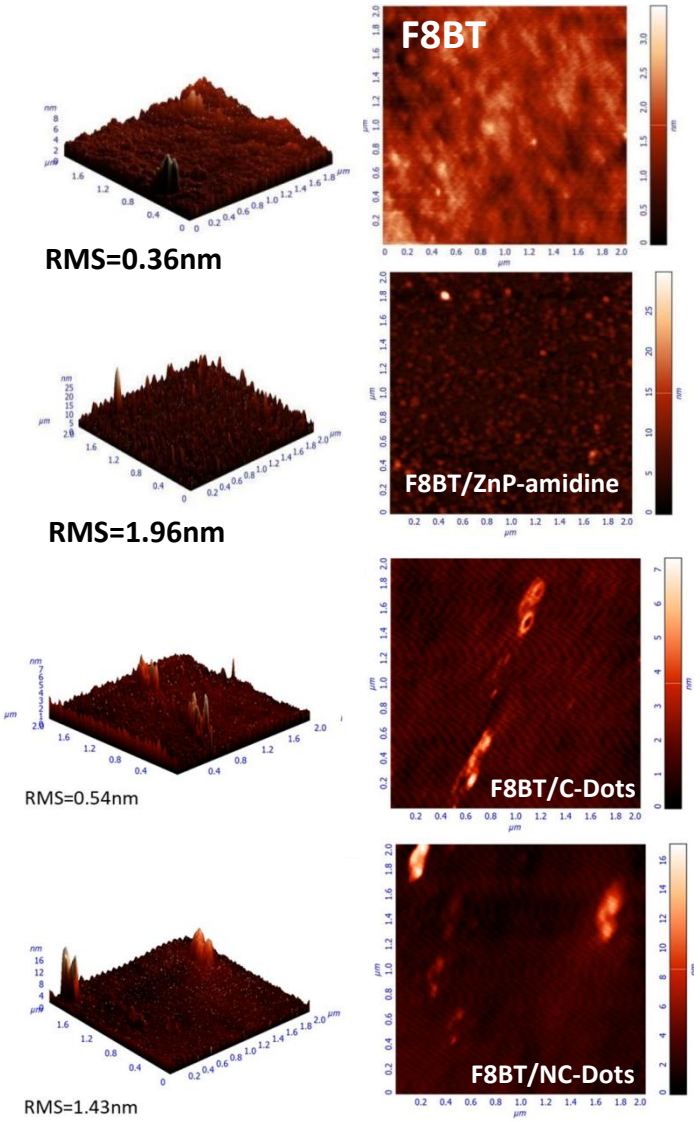

Image 42: AFM topographies of F8BT, C-Dots, NC-Dots and F8BT/ZnP-amidine.

FWHM of the peak is larger compared to that of the F8BT sample, indicating smaller crystalline size, 43.26 nm for the F8BT and 36.75 nm for the F8BT/ZnP-amidine sample. The decrease in the crystalline size of the emitter, F8BT, may enhance exciton confinement in the EML leading to improved radiation probability.

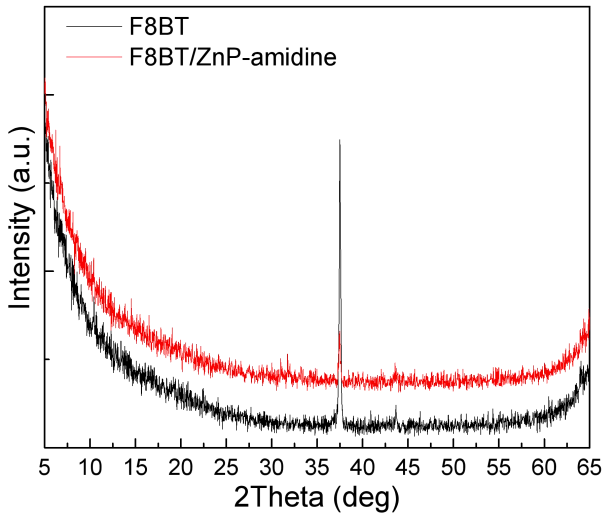

Image 41: XRD graph of F8BT and F8BT/ZnP-amidine.

From these 2D and 3D topographies, it can be noticed that ZnP-amidine forms a nano-aggregated layer on the F8BT film, which may facilitate electron injection from the ETL to the EML resulting in enhancement of the OLEDs performance (Image 42).

References

[1] M. Vasilopoulou, A.M. Douvas, D.G. Georgiadou, V. Constantoudis, D. Davazoglou, S. Kennou, L.C. Palilis, D. Daphnomili, A.G. Coutsolelos, P. Argitis, Nano Res. 7 679–693 2014.

[2] Peng Zhang, Yee Sin Ang, Allen L. Garner, Ágúst Valfells, J. W. Luginsland, and L. K. Ang, J. Appl. Phys. 129, 100902 (2021)

[3] Ahn, J.-H., Chung, D.-H., Lee, J.-U., Song, M.-J., Han, W.-K., & Kim, T. W., J. Korean Phys. Society (Vol. 46, Issue 2) 2005

4.3.2 Electrical Characterization

The structure ITO/PEDOT:PSS/F8BT was used as a reference device, while devices with C-Dots, NC-Dots, Cs_2CO_3 and ZnP-amidine as electron transport layers were also employed. Each diode underwent annealing before each measurement in order to achieve the best possible results. Current-Voltage/Luminance-Voltage and Current-Time/Luminance-Time graphs are presented below for each of the diodes. Capacitance-Voltage and Capacitance-Frequency measurements were also conducted,

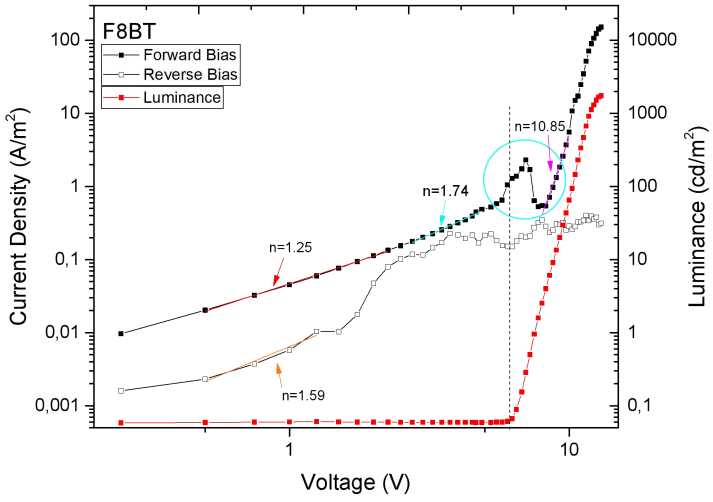

Figure 1: Reference OLED I-V (forward and reverse bias) and L-V in semi-log (left) and log-log (right). The bump is visible in forward bias.

as well as electroluminescence spectra were retrieved for a reference device and a ZnP-amidine device. For each diode, we took at least two I-V measurements, one at the beginning of the measurements and one at the end, one to five I-T measurements, and C-V/C-f measurements.

While studying the I-V measurements, a 'bump' at biases just prior to the onset of light emission was observed in some of the devices. In Figure 1, an I-V/L-V of a reference device is plotted where the bump is clearly visible both in semi-log and log-log axes. In all cases shown hereafter, such a phenomenon is not observed in reverse biased diodes. As a result, we can link the presented bump with the injection of electrons into the emission layer (i.e. F8BT).

After examining the devices with different materials used as an ETL, most of them were found to present smoother I-V curves (Figure 3). OLEDs with Cs_2CO_3, NC-Dots and ZnP-amidine as ETLs did not present bumps in most measurements. As discussed previously, holes have larger mobility than electrons. When electrons are injected, it is obvious that the conduction mechanism changes (Figure 1). Such a thing, however, is not observed in most of the devices that contain Cs_2CO_3. Those devices were found to give a fully symmetrical curve both in forward and reverse bias, meaning that the carrier conduction mechanism is the same (Figure 2). Of course, that is not actually

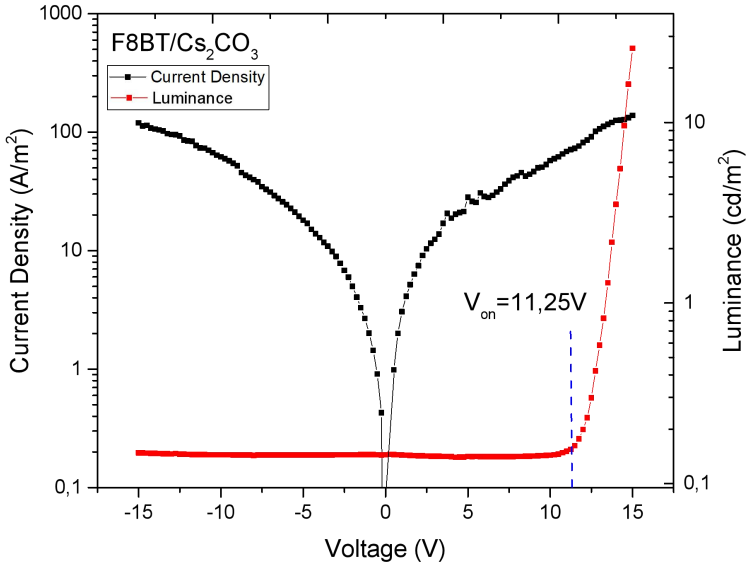

Figure 2: Cs_2CO_3 OLED I-V (forward and reverse bias) and L-V. The curves are symmetrical.

true. Electrons are indeed injected in the emission layer and thus emitted light is detected. What seems to be happening is that hole transport mechanisms dominate over the electron ones and, as a result, there is not an apparent difference between the forward bias that concerns both holes and electrons and the reverse bias that concerns only the holes.

We shall discuss about forward bias only from now on, since the reverse bias has not presented any other interesting phenomena. The existence of a bump in the various devices could be associated with charge traps that need to be filled with carriers in order for them to pass onto the next layer and finally recombine and emit light. Since there is an observed difference regarding that bump in reference devices and devices with an ETL, it is plausible to say that these traps seek electrons and not holes. By

adding an ETL, those electron traps are eliminated and, therefore, there is no need for them to be charged for the light emission process to be initiated. As a result, a bump is no longer observed.

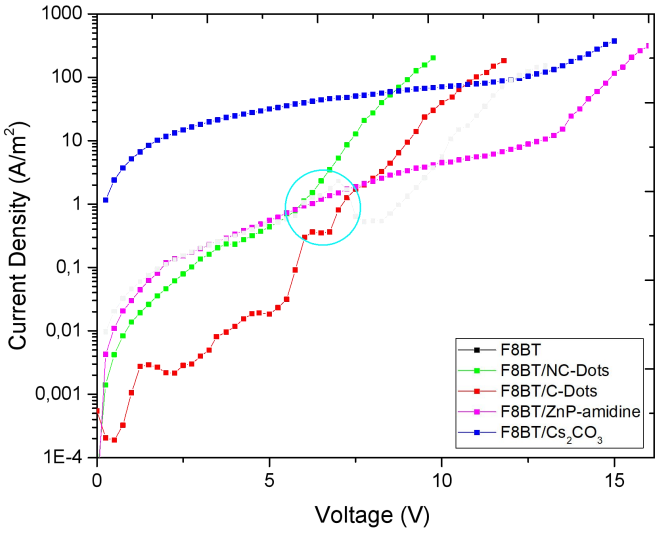

Figure 3: Comparison of I-V (forward bias) for all materials used as an ETL. Cs_2CO_3, NC-Dots and ZnP-amidine present smooth curves.

A very important obstacle to verifying whether the electron traps are eliminated by using an ETL is that we are unable to identify their exact position or depth between the interlayers. Since the bump disappears when using an ETL, it is safe to say that the electron traps are generated between the cathode (Al) and the emission layer (F8BT)[1]. In order to verify this statement, we studied smaller square diodes (a = 1 mm) rather than the circular ones we studied before (r = 2 mm) (Image 40). As a perfect monolayer of ETL can not be formed, the materials used are forming islands/clusters on the F8BT and as a result they do not cover the whole surface, leaving gaps in which the cathode is directly in touch with the EML. Using a smaller cathode would decrease the possibilities of having an island of ETL right below it and if that happened, the diode would give results similar to a reference device.

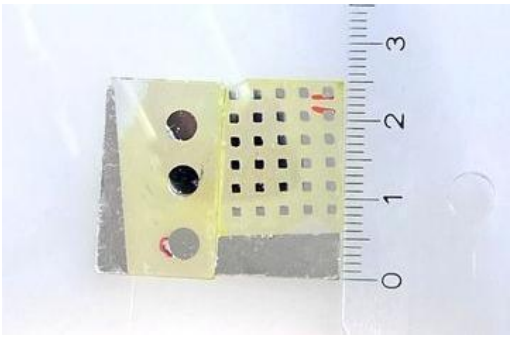

Image 40: Different sized diodes. Circular diodes with 2 mm radius (left) and square diodes with 1 mm side length (right)

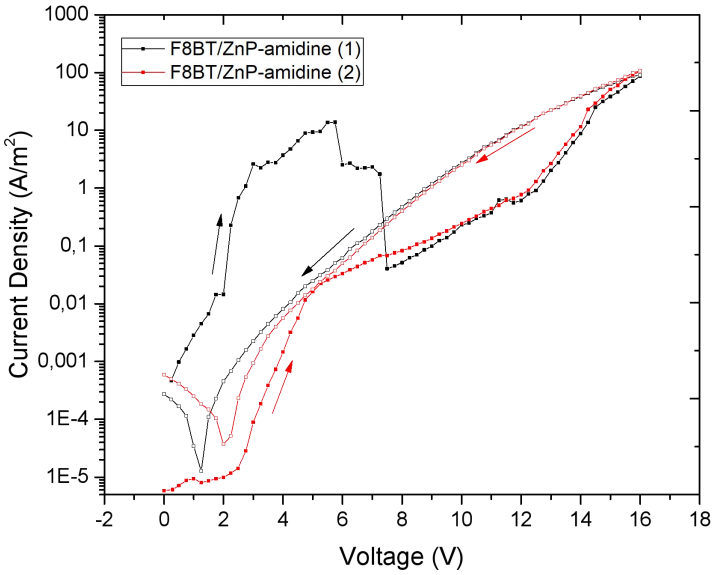

Figure 4: Comparison of two ZnP-amidine diodes on the same substrate. Each measurement was taken as a loop; from 0V to 16V to 0V.

After studying smaller diodes, we observed two different kinds of curves; one with a bump and a smooth one (Figure 4). Such plots were retrieved for all different materials used as ETLs. Here, we present a graph that refers to two different small diodes that were fabricated on the same glass substrate. The black curve shows a big bump while the voltage increases, while the red one does not. Supposedly, the black curve comes from a diode that happens to not have an island below its cathode, while the red curve responds to a diode that does. It is worth mentioning that these I-V measurements include both 0 to 16 V and 16 to 0 V routes. The fact that the return route for the black curve does not present a bump is a rather rational outcome, since the bump is attributed to the electron traps being charged while the voltage increases. As the voltage decreases the traps remain charged and a bump is no longer observed.

It is also shown that both curves are very similar after the bump, so the same mechanisms are involved after the traps are charged. This also applies to the returning routes (16 to 0 V).

It is also worth mentioning that, in order to identify the conduction mechanisms, one has to find the relation between the current density and the applied voltage ($J \sim V^n$). If $J \sim V^2$, the mechanism is known as space charge limited conduction (SCLC)[2]. By using proper fitting, we are able to define the exponent *n* in $J \sim V^n$ for all of the retrieved curves. During solely hole injection, we can see that *n* approaches 2, as in SCLC. When electron injection begins, the exponent increases dramatically (Figure 5). That is not the case in devices containing Cs_2CO_3, because as mentioned before the mechanism is slightly changed (Figure 6).

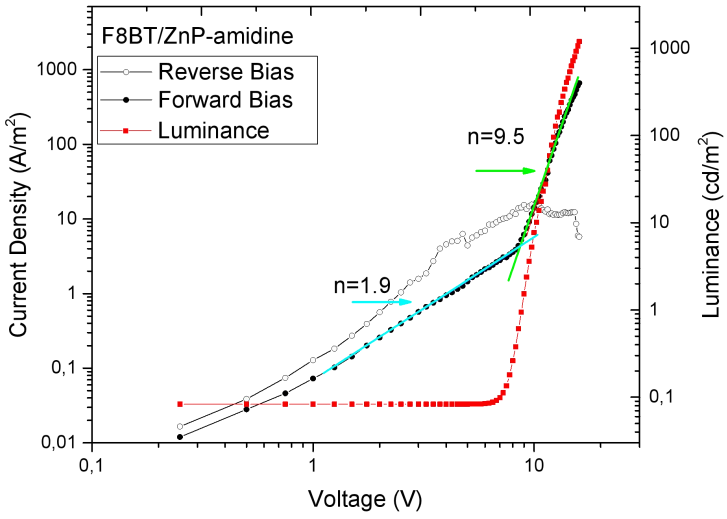

Figure 5: F8BT/ZnP-amidine I-V and L-V (log-log). The exponent increases when electrons are injected.

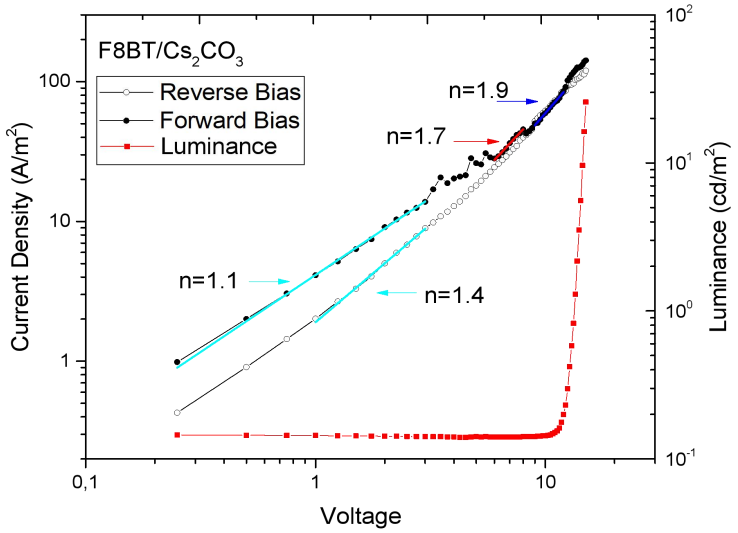

Figure 6: F8BT/Cs_2CO_3 OLED I-V and L-V (log-log). The exponent changes slightly.

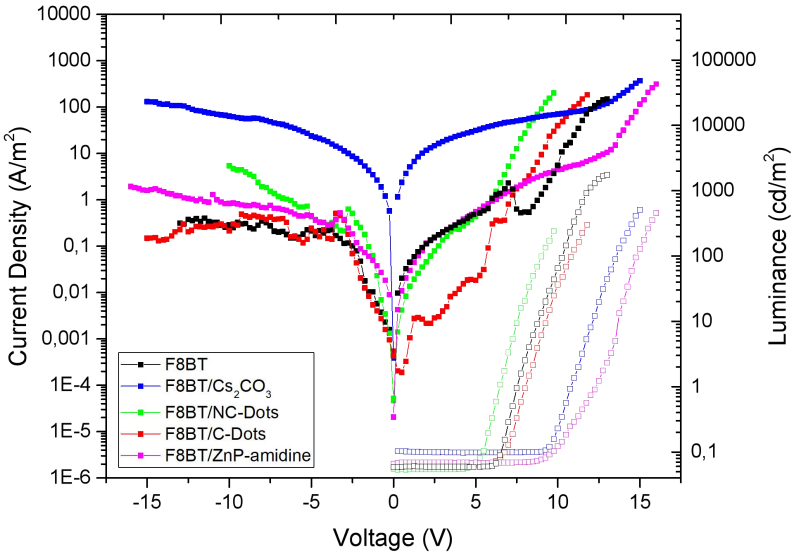

Figure 7: I-V (closed symbol), L-V (open symbol) comparison of all materials used as ETLs.

Finally, another interesting result that came up after our measurements was retrieved from an I-V characteristic (Figure 8) in which the device was measured for voltage from 0 to 14 V, each step 0.25 V and time interval 10 s for each voltage value taking 10 measurements per second. As a result, we can identify the voltage value that needs to be applied in order to charge all electron traps. The arrow points to the step that the mechanism of light emission changes. For the specific device measured, this value corresponds to 12.5 V.

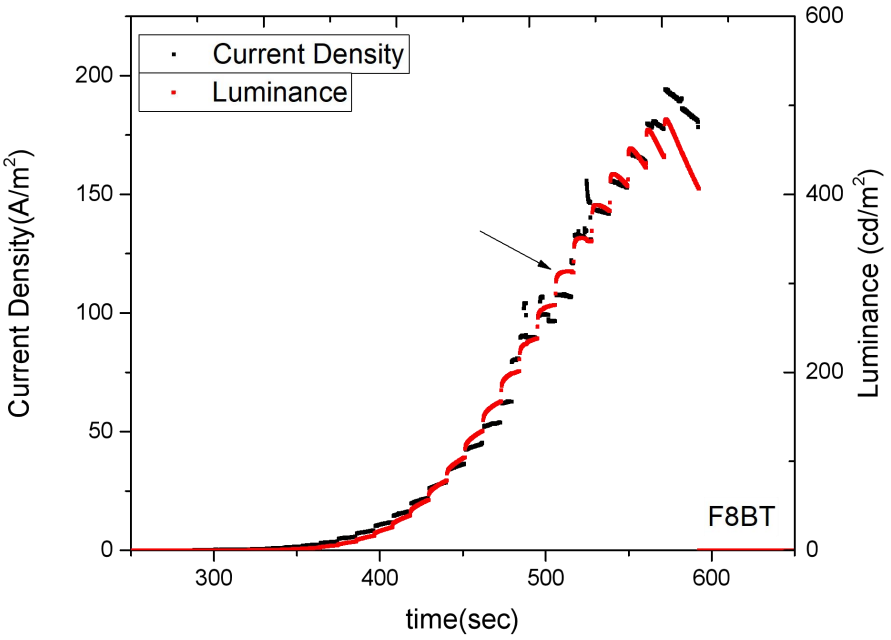

Figure 8: I-V with 10 s interval time/step. The light emission mechanism changes at 12.5 V.

After the I-V/L-V analysis, we conducted Capacitance - Voltage (C-V) and Capacitance - Frequency (C-f) measurements. The C-V characteristics of the devices serve as a crucial tool for investigating the dynamic behavior of mobile charges[3]. Figure 9 illustrates the capacitance-voltage (C-V) characteristics of the reference device. The measurements were conducted at a constant frequency of 10 kHz and four distinct bias conditions can be identified.

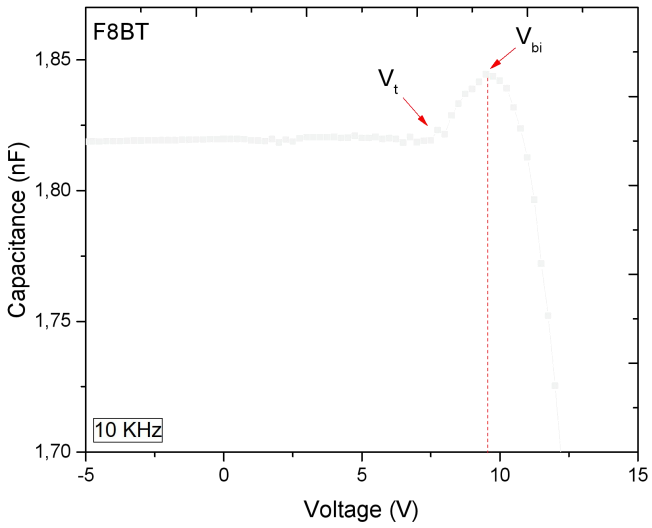

Figure 9: Capacitance – voltage (C-V) measurements obtained for the reference sample at a frequency of 10 kHz.

When the applied bias (V_0) is less than the threshold bias (V_t) ($V_0<V_t$), there is not injection of charge carriers. Consequently, the capacitance remains constant, and the value corresponds to the device's geometric capacitance:

$$C_0 = \frac{\varepsilon_0 \varepsilon_R A}{d} \qquad (22)$$

where here ε_R, is the relative dielectric constant of the polymer, ε_0 the permittivity of the free space, A the area of the device and d the thickness of the polymer film, respectively. As V_0 surpasses V_t but remains lower than the built-in voltage (V_{bi}) ($V_t<V_0<V_{bi}$), holes are introduced into the device, leading to a gradual increase in capacitance due to hole accumulation. The capacitance continues to rise with increasing V_0 until it reaches V_{bi} ($V_0=V_{bi}$). For $V_0>V_{bi}$, electron injection takes place, leading to electron-hole recombination and a subsequent decrease in capacitance. In order to compare the built-in voltage between the reference sample and the OLED with an inserted electron transport layer (ETL), Figure 10 illustrates both configurations at a fixed frequency of 100 kHz. The capacitance-voltage (C-V) plot is normalized to the geometric capacitance of the samples. A noteworthy observation is that the reference sample exhibits a built-in voltage (V_{bi}) at 10.6 volts, whereas the samples incorporating ZnP-amidine as an electron transport layer (ETL) display a decreased built-in voltage, indicating that the device is now activated at lower voltages. The addition of ZnP-amidine as an ETL has effectively reduced the built-in

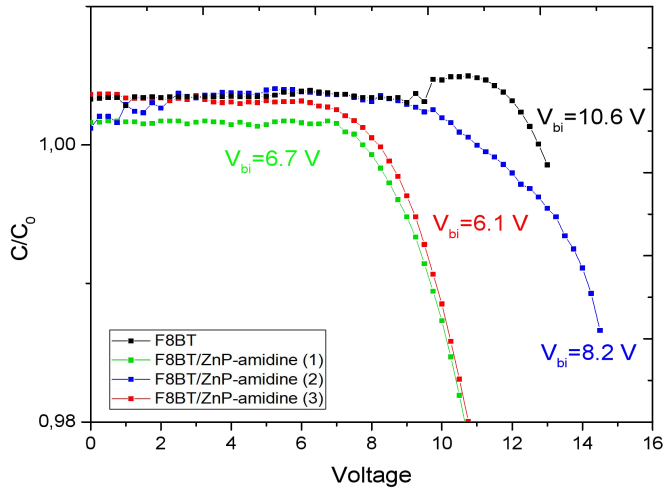

Figure 10: The normalized capacitance – voltage characteristics of the reference (black) and the ZnP-amidine devices.

voltage of the device, as the presence of the ETL diminishes the potential barrier that electrons must surmount to access the light-emitting layer.

The C-f measurements were conducted in parallel mode in order to calculate the complex impedance:

$$Z = \sqrt{{G_p}^2 + {B_p}^2} \qquad (23)$$

Where, G_p is the parallel conductance ($G_p = 1/R_p$), B_p is the parallel susceptance ($BC = C_p$) and $\omega = 2\pi f$.

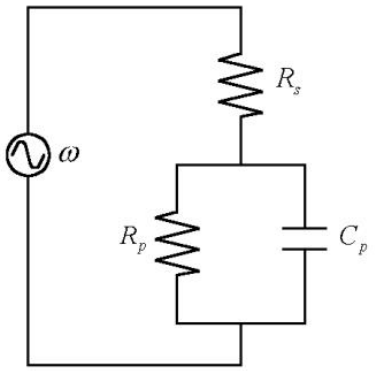

Image 41: Equivalent-circuit model of an OLED comprised of a contact resistance R_s in series with a parallel combination of a resistance R_p and a capacitance C_p.

The investigated device does not conform to a simple resistor or capacitor model, necessitating the use of an equivalent model to describe the underlying phenomena. Presented in Image 41 is the equivalent model that consists of the real and imaginary parts of the complex impedance described by the following equations:

$$Z' = R_s + \frac{R_p}{1 + (\omega\tau)^2} \qquad (24)$$

$$Z'' = \frac{\omega\tau R_p}{1 + (\omega\tau)^2} \qquad (25)$$

In the reference sample, interfacial states are present, representing defects at the interface between the metal and the emissive layer. These imperfections create a localized charge deficit, leading to a loss of symmetry and the formation of dipoles.

Under the influence of an external electric field, these dipoles tend to align their dipole moments with the direction of the field. Consequently, when these dipoles respond to the AC signal, some of the signal energy is dissipated as a result of the dipole movement, leading to energy losses. The energy losses are represented by the imaginary part of the complex impedance and depicted in Figure 11 at a constant bias of 12 V.

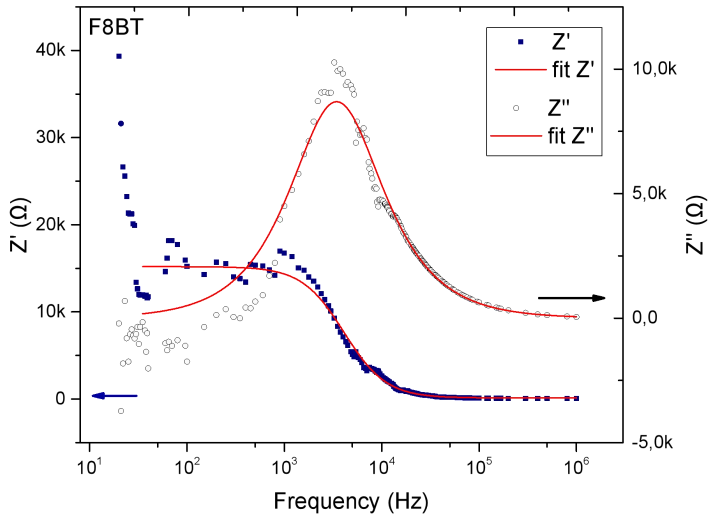

Figure 11: The real Z' (open symbol) and imaginary Z'' (blue symbol) parts of the complex impedance Z for the reference sample along with the fitting of the experimental data (red line) to the equivalent circuit.

Notably, in the reference sample, losses are observed at a frequency of f = 3 kHz due to the presence of interfacial defects between the metal and organic films. Additionally, at very low frequencies, it appears that another peak emerges, likely attributed to large macromolecules of the polymer. Illustrated in Figure 12 is the fitted data for the ZnP-amidine device with the fitting discussed above.

The resonance frequency in the analyzed device exhibits an increase from 3 kHz to 23 kHz, resulting in a lengthening and broadening of the curve compared to the reference sample. This suggests a higher density of defects in the system, causing faster response times. Moreover, the introduction of another material has led to the incorporation of additional electrically active defects between the ETL and the EML. It is yet to be understood whether those defects are linked to the deep electron traps that cause the bump that we analyzed earlier while studying the I-V characteristics.

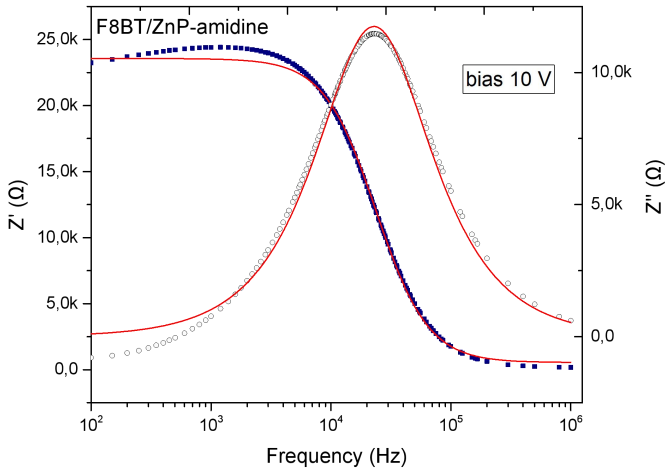

Figure 12: The real Z' (open symbol) and imaginary Z'' (blue symbol) parts of the complex impedance of the ZnP-amidine device along with the fitting of the experimental data (red line) to the equivalent circuit.

The Cole-Cole plot presented in Figure 13 represents the imaginary part of impedance as a function of the real part, and it typically exhibits a semi-circular shape. The chosen model, initially proposed to describe the circuit, demonstrates a good fit to our experimental layout, accurately capturing the observed electrical behaviour and characteristics.

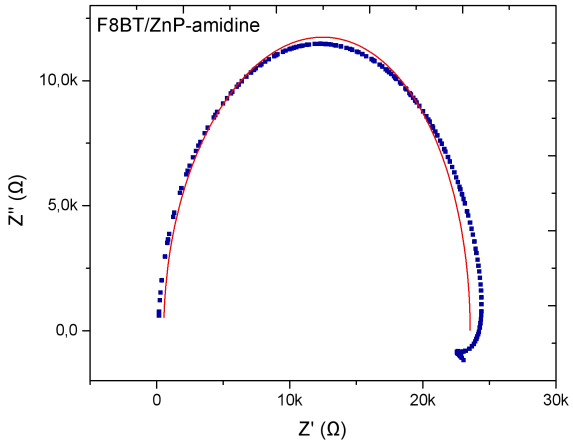

Figure 13: The Cole – Cole plot of the complex impedance Z for the ZnP-amidine device.

As more diodes with an ETL layer were measured noteworthy findings emerged. Specifically, we observed that the frequency of the enriched with ETL devices is approximately ten times higher than that of the reference sample. This substantial increase in frequency was consistently observed in all samples featuring the extra

ETL layer. Consequently, each of these samples exhibited a distinct peak at higher frequencies in their respective measurements.

Further analysis regarding the charge of the carrier traps lies in studying the results retrieved from the Current - Time and Luminance - Time (I-t/L-t) plots, under constant voltage. It is shown that the curve we retrieve depends on the applied voltage. If the applied voltage is very near V_{on}, which is the voltage that the device begins to emit light, the current density remains constant, and the luminance increases during the whole measurement without reaching a maximum value. On the other hand, if the applied voltage is greater than V_{on} (i.e. V_{op}), a maximum value is reached within a few seconds and then degradation mechanisms take over (Figure 14). These phenomena are observed in both reference devices and devices that contain an ETL.

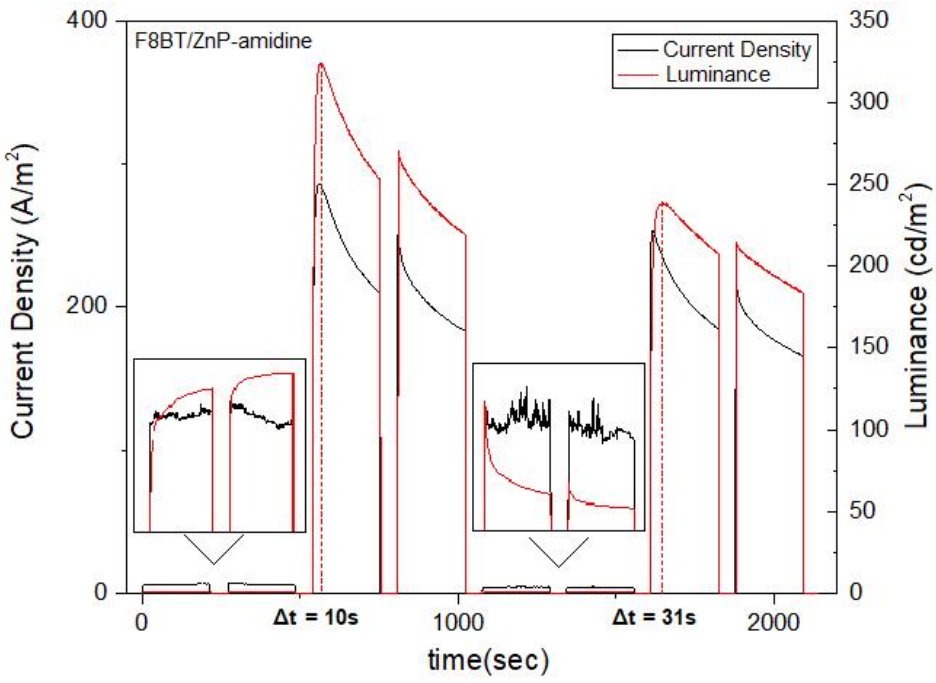

Figure 14: ZnP-amidine I-t measurement with 8 steps taken in pairs with V_{on} and V_{op} applied alternately.

Another interesting observation is the fact that when a V_{op} is applied the current density and luminance peaks do not occur simultaneously. The time difference between these maxima is at the order of seconds. We can see that in Figure 14, there are eight steps, four of which were retrieved by applying V_{on} and four of them by applying V_{op}, taken in pairs, alternately. After each step, there was a 50 second period of time, when the applied voltage was 0 V. During the third and the seventh step a

time difference between the peaks is observed. At the third step that Δt is 10 seconds long and at the seventh the time difference is 31 seconds long. It is also shown that during the first two steps a luminance maximum is not reached as the electron traps were not fully charged. On the contrary, during all upcoming steps, a peak is observed followed by degradation mechanisms of the device. Steps 5 and 6, despite having been measured with the same voltage as steps 1 and 2, are not similar to the first pair. This is attributed to the electron traps being already charged from the previous steps. What seems to be the most interesting phenomenon observed at this graph is the fact that after all that electrical stressing the device went through steps 1-6, at step 7 the time difference between the current density and luminance maxima is three times longer than the time difference in step 3. This observation probably lies in the discharging of the electron traps that need to be charged again, since electrical aged OLEDs have generated deep interface states and as a result the interfaces need more time to charge. It is also worth mentioning, that if a V_{op} is applied to two or more consecutive steps, only during the first one a time we observe a time difference between the current density and luminance maxima (Figure 15).

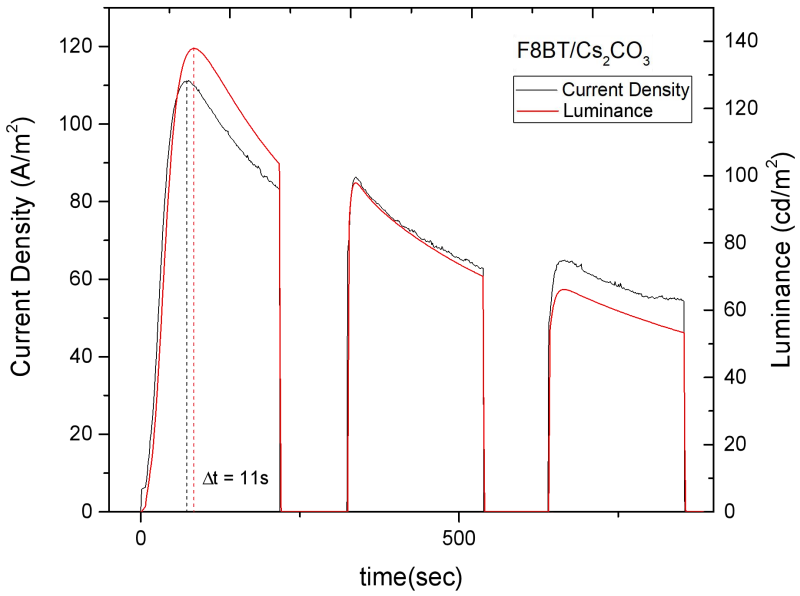

Figure 15: Cs_2CO_3 I-t measurement with three steps. Time difference between current density and luminance maxima is observed only in the first step.

Such a time difference is not observed at the reference device since it reaches a maximum current density value almost immediately after applying V_{on}, but it does not

reach a maximum value of luminance. If V_{op} is applied on a reference device, a luminance maximum is quickly reached, but degradation is far more severe here than in other devices that have ETLs incorporated. It is shown that devices with ZnP-amidine incorporated as ETL reach maximum values of current density and luminance sooner in comparison to devices with Cs_2CO_3 (Figure 16).

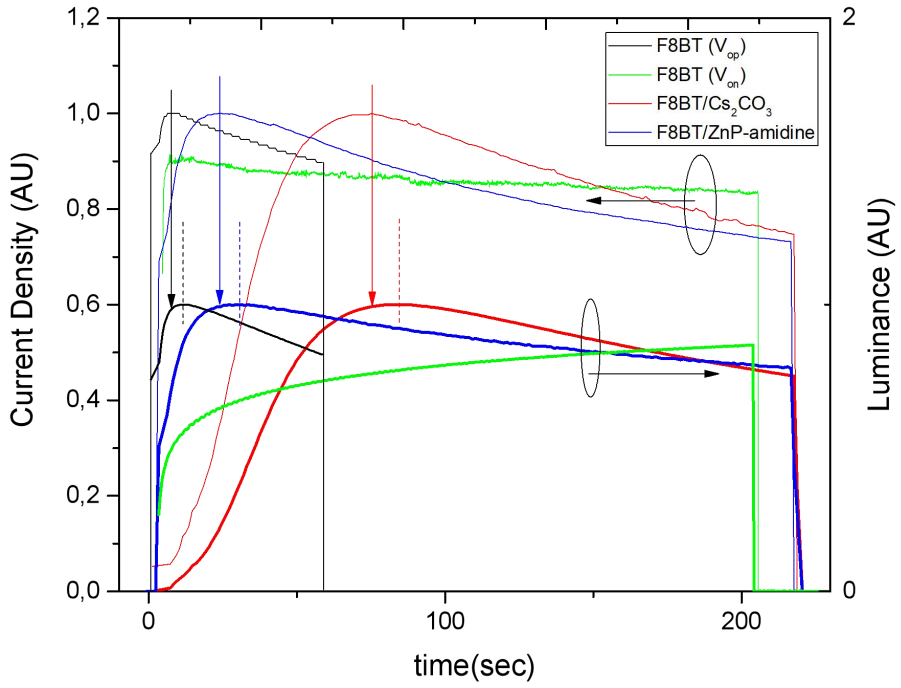

Figure 16: Comparison of I-t, L-t measurements between devices with various ETLs.

4.3.3 Optical Characterization

By adding an optical fiber to the circuit of the metallic measuring station we were able to retrieve electroluminescence spectra of various devices, as mentioned before. Particularly, we collected spectra regarding the reference device and the ZnP-amidine device. The electroluminescence spectra are presented as a function of wavelength and time for the reference configuration and for ZnP-amidine respectively, in 3-D and 2-D format. The spectra were recorded with a 10s step. Specifically, they simulate the Current-Luminance/Time measurements analyzed earlier (Figure 16), and it is evident that there is degradation of the spectrum over time. It is also important to note that the maximum emission remains stable, indicating that the emission characteristics are independent of operating time. From Figures (17) and (19), for both materials, a

maximum emission peak is observed at approximately 538 nm, corresponding to the energy difference between the HOMO and LUMO levels of F8BT. Additionally, at longer wavelengths, a smaller peak is observed in both graphs at around 567 nm, attributed to the presence of an excited triplet state. Specifically, the intersystem crossing (ISC) mechanism takes place, where the created singlet excitons transition to the triplet state due to the difference in excitations, reflected as peaks in the graphs.

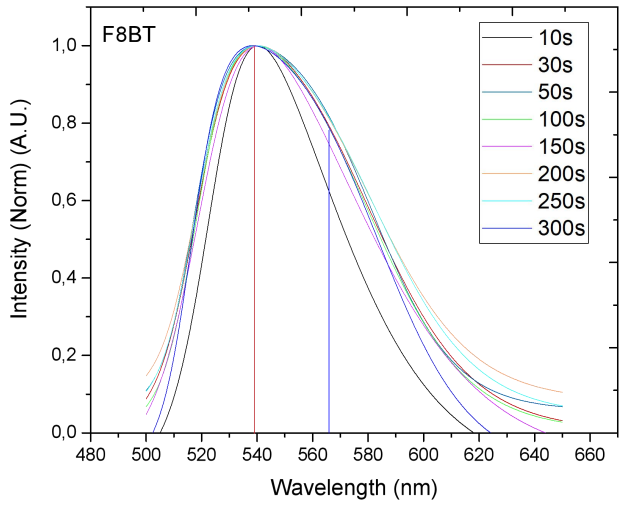

Figure 17: Electroluminescence spectra of reference device.

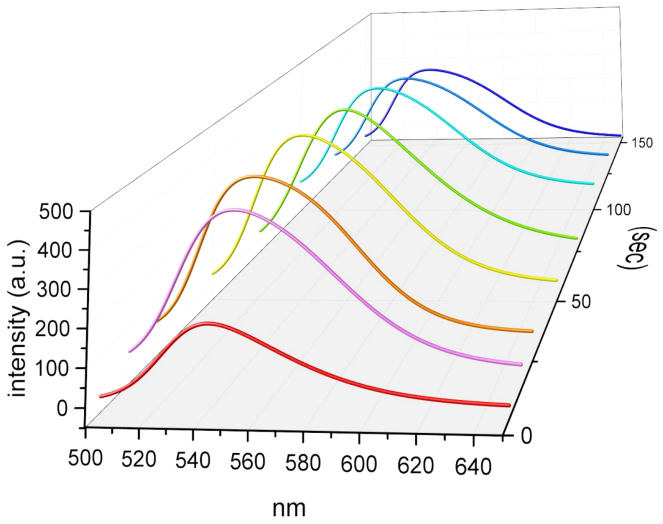

Figure 18: Electroluminescence spectra of reference device (3D version).

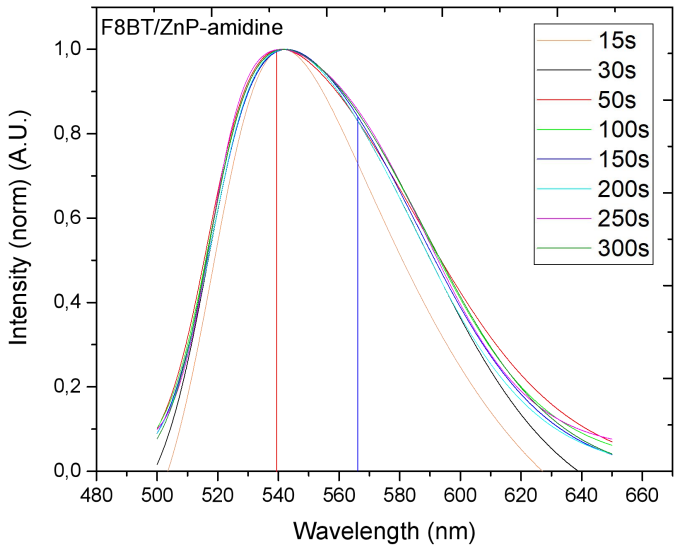

Figure 19: Electroluminescence spectra of ZnP-amidine device.

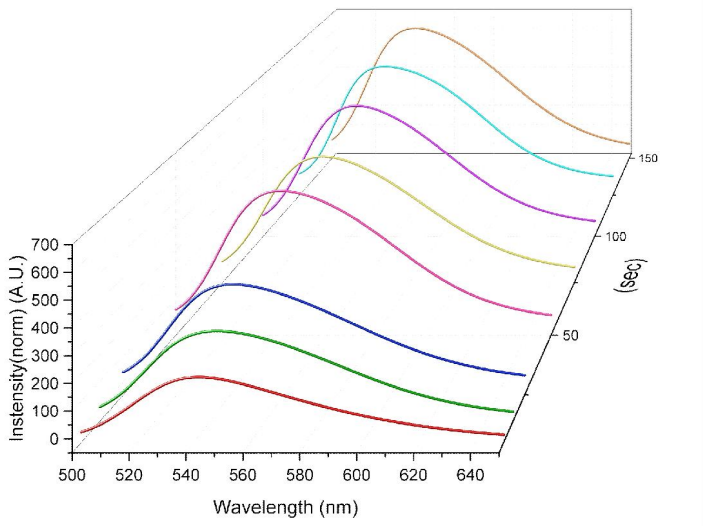

Figure 20: Electroluminescence spectra of ZnP-amidine device (3D version).

In order to identify the most efficient material used as an ETL, a Luminous Efficiency - Voltage graph is presented that compares all materials. It is shown that devices with ZnP-amidine as ETL seem to present significantly higher values of luminous efficiency in lower voltages compared to other materials (Figure 21).

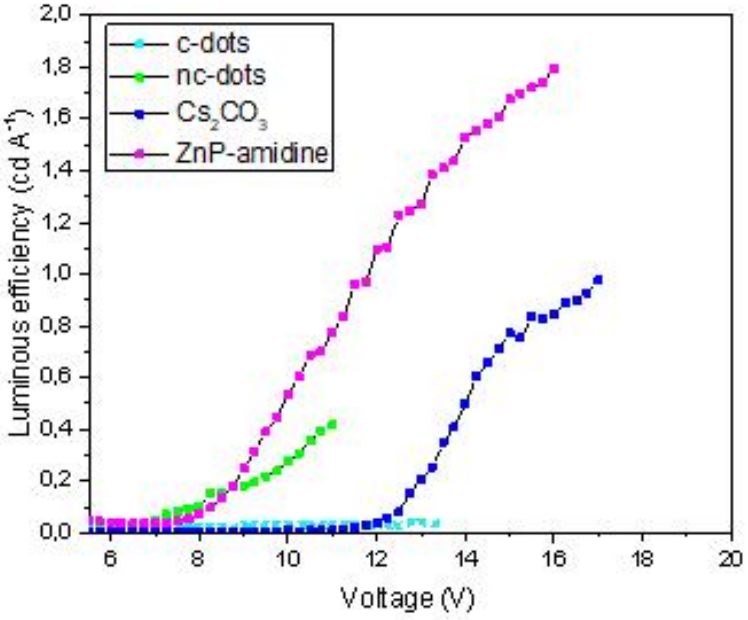

Figure 21: Luminous efficiency - Voltage plot. ZnP-amidine presents higher luminous efficiency in lower values of voltage.

Conclusions & Future Work

In order to improve the performance of OLEDs it is vital to incorporate carrier transporting interlayers thus reducing the charge energy barrier at the selected electrode/organic emissive layer. Characteristic curves were obtained simultaneously on fresh or electrically stressed devices to investigate both the current conduction mechanisms as well as the evolution of deep electron traps that affect the turn on voltage and the overall quality of the tested OLEDs.

In conclusion, electron traps deteriorate the quality of OLEDs. We performed several measurements which showed that an electron transport layer significantly reduces the deep electron traps that are generated between the aluminum cathode and the emission layer (F8BT), and, as a result, the corresponding devices are improved. By calculating the exponent *n* in the relation $J \sim V^n$, it is shown that the hole injection is described by space charge limited conduction (SCLC). On the other hand, when electron injection is initiated, the exponent *n* increases dramatically, thus another mechanism takes over. It is shown that ZnP-amidine is the most promising material among all the others.

Through C-V analysis it is observed that the incorporation of an ETL affects the way that electrons move in the device and leads to more defects and faster response times. The effects of electrical stressing are also studied since electrical aged OLEDs have generated deep interface states and as a result the interfaces need more time to charge. That is retrieved from I-t graphs which show that in higher voltage values the current density and luminance maxima do not occur simultaneously, but rather with a time difference at the order of seconds. The main obstacle presented during this study is that it is impossible to know the exact position and depth of the electron traps formed between the interlayers.

Incorporating various materials as ETLs significantly improves the luminance values of the devices, but due to the difficulty of these materials being applied as a uniform layer more electron traps are generated between the interfaces at points where the ETL is non-existent. As a result, those traps need more time to charge, as stated before.

In the future, more materials used as injection, transport or emission layers could be studied in order to find the most efficient ones. Further analysis on I-t measurements would be vital to comprehend in depth the conduction and degradation mechanisms that occur in OLEDs.

It is understood that the electron traps can be discharged. Figuring out how this is possible and whether it can affect the deterioration, or not, of the diodes would be a huge step to understand further these complicated devices. High energy photons incident to the OLEDs may be able to discharge the electron traps.

OLEDs are known to be sensitive to air and moisture. As a result, it would be interesting to perform measurements in vacuum chambers, in order to inspect whether the devices' efficiency is affected.

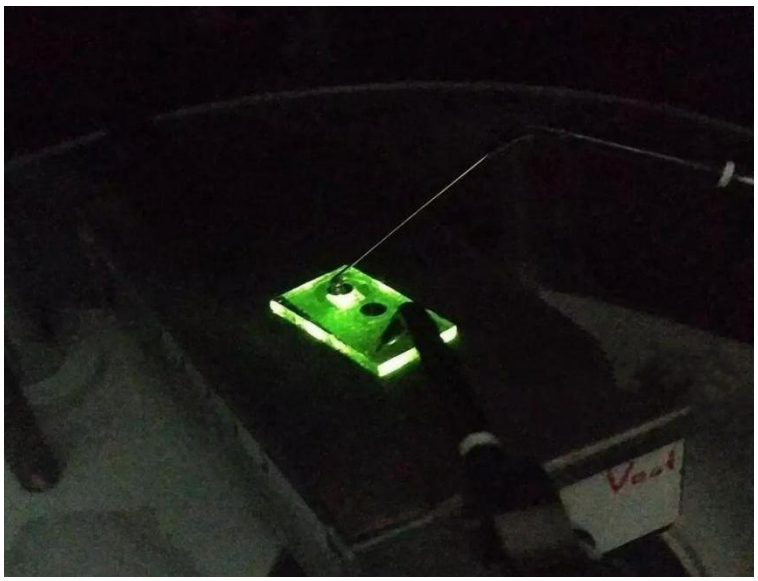

Image 54: OLED emitting light.

Appendices

I. Experimental Set-up

Metallic Station

- ***HEATHKIT Regulated Power Supply Model IP-2***

  A constant voltage source at 5 V is used, which is applied across the terminals of the circuit's photodetector to activate it.

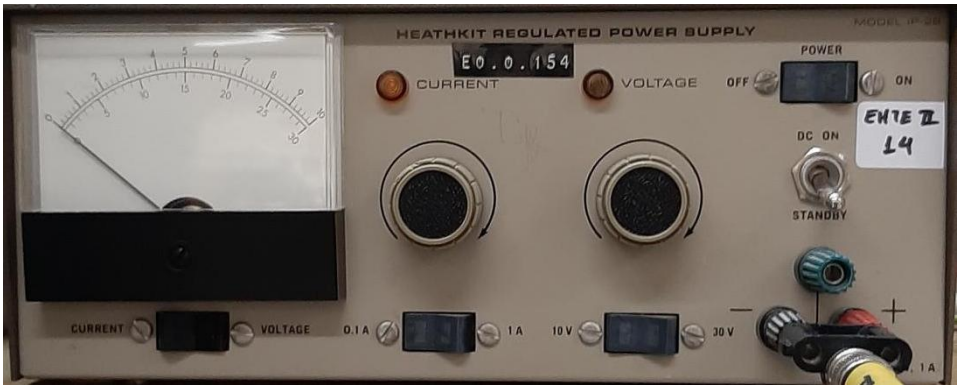

Image I: HEATHKIT Regulated Power Supply Model IP-2.

- ***KEITHLEY 230 Programmable Voltage Source***

It is used to apply voltage values to the OLED under test. The applied voltage ranges from -20 V to 20 V.

Image II: KEITHLEY 230 Programmable Voltage Source.

- ***KEITHLEY 617 Programmable Electrometer***

It is used as a multimeter. It has the ability to measure voltage, electric current intensity, and ohmic resistance values. In our experimental setup, it is used as an ammeter, aiming to measure the intensity of the electric current passing through the OLED. The range of current values that can be measured is from 2 pA to 20 mA.

Image III: KEITHLEY 617 Programmable Electrometer.

- ***HP 4140B pA Meter/DC Voltage Source***

It is used as a voltage source as well as a current measuring instrument. In our experimental setup, it serves as an electric current meter as it is connected to the photodetector, which is penetrated by current due to the photons emitted by the photodiode. We subsequently convert the values of current intensity into luminous flux values (from amperes to lumens).

Image IV: HP 4140B pA Meter/DC Voltage Source.

The range of current values that can be measured is from 10^{-15} A to 10^{-2} A.

- ***AGILENT 4284A Precision LCR Meter***

It is used as a multimeter that measures capacitance, inductance, and resistance values as a function of frequency of the AC signal. In our experimental setup, it functions as a capacitance meter. It is used to perform C-V and C-f measurements.

Image V: AGILENT 4284A Precision LCR Meter.

The above instruments are connected to the experimental setup via BNC cables.

Wooden Station

The instruments used at this station are:

- ***HEATHKIT IP2718 Tri-power Supply***

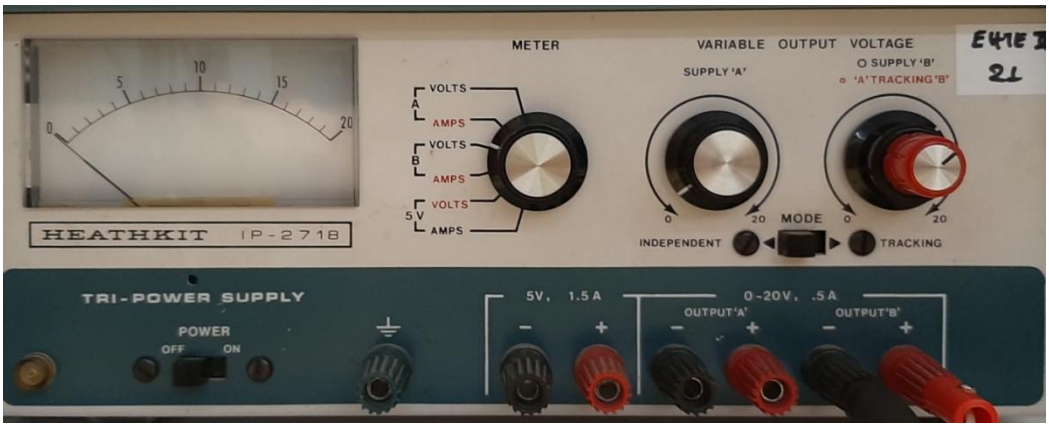

Image VI: HEATHKIT IP2718 Tri-power Supply.

It is used as a stable voltage source, which is applied across the terminals of the circuit's photodetector to activate it.

- ***KEITHLEY DMM6500 6 ½ Digit Multimeter***

It is used as a multimeter as it can measure voltage and current intensity. In this specific experimental setup, it is used to measure the voltage across the photodiode. It is not connected to the computer. The measurement process is displayed on the instrument's screen, and the measurement data are extracted from the instrument via USB. The process is initiated by triggering.

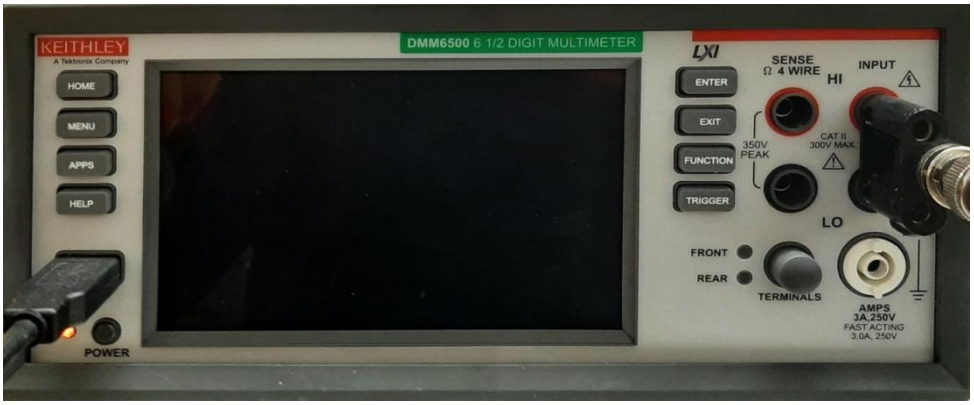

Image VII: KEITHLEY DMM6500 6 ½ Digit Multimeter.

- ***KEITHLEY 2601A System Source Meter***

It is used as a meter for the current intensity passing through the photodiode and also for applying potential difference across the diode. It should be connected to the computer via LAN cables so that, using the appropriate program that we create in a TSP code writing environment, we can conduct the experimental procedure and automatically obtain the measurements.

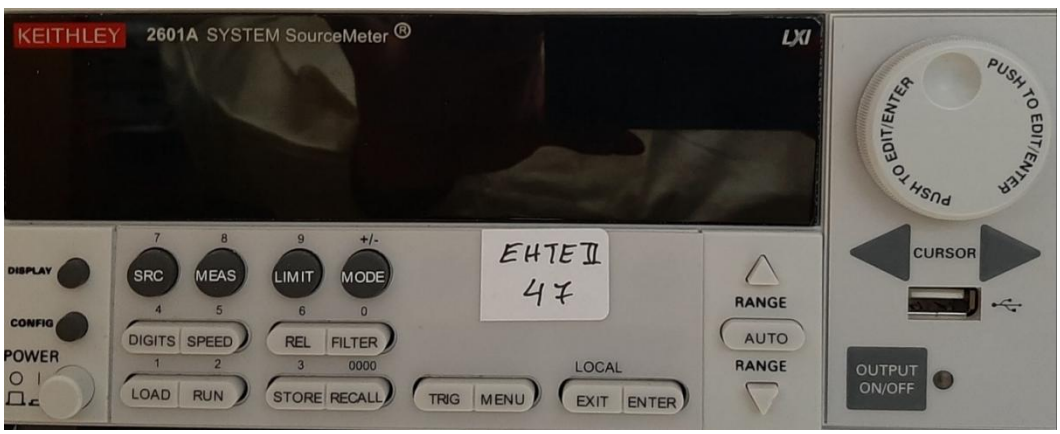

Image VIII: KEITHLEY 2601A System Source Meter.

- ***One of the following instruments, depending on whether we want to provide voltage or current to the photodiode:***

  - ***TTi EL561R Power Supply***

    It is used to apply voltage values to the photodiode.

Image IX: TTi EL561R Power Supply.

  - ***KEITHLEY 225 Current Source***

    It is used to apply Constant Current values to the device under test.

Image X: KEITHLEY 225 Current Source.